



HHS Public Access

Author manuscript

J Med Chem. Author manuscript; available in PMC 2023 April 28.

Published in final edited form as:

J Med Chem. 2022 April 28; 65(8): 6287–6312. doi:10.1021/acs.jmedchem.2c00195.

Discovery of Potent Orally Bioavailable WD Repeat Domain 5 (WDR5) Inhibitors Using a Pharmacophore-Based Optimization

Kevin B. Teuscher,

Department of Biochemistry, Vanderbilt University School of Medicine, Nashville, Tennessee 37232-0146, United States

Kenneth M. Meyers,

Department of Biochemistry, Vanderbilt University School of Medicine, Nashville, Tennessee 37232-0146, United States

Qiangqiang Wei,

Department of Biochemistry, Vanderbilt University School of Medicine, Nashville, Tennessee 37232-0146, United States

Jonathan J. Mills,

Department of Biochemistry, Vanderbilt University School of Medicine, Nashville, Tennessee 37232-0146, United States

Jianhua Tian,

Molecular Design and Synthesis Center, Vanderbilt Institute of Chemical Biology, Vanderbilt University, Nashville, Tennessee 37232-0142, United States

Joseph Alvarado,

Department of Biochemistry, Vanderbilt University School of Medicine, Nashville, Tennessee 37232-0146, United States

Jiqing Sai,

Department of Biochemistry, Vanderbilt University School of Medicine, Nashville, Tennessee 37232-0146, United States

Corresponding Author Stephen W. Fesik – Phone: +1 (615) 322-6303, Stephen.fesik@vanderbilt.edu; Fax: +1 (615) 875-3236.

Author Contributions

K.B.T., K.M.M., Q.W., J.J.M., J.T., and J.A. designed and synthesized compounds. J.S., M.V.M., and T.M.S. obtained the biochemical and cell-based data in Tables 1–4. T.A.R. and B.Z. performed X-ray crystallography studies of complexes. W.J.M. and G.M.S. helped design experiments. W.P.T., T.L., and S.W.F. designed and directed experiments. K.B.T., T.L., and S.W.F. contributed to the manuscript. All authors have given approval to the final version of the manuscript.

The authors declare the following competing financial interest(s): K.B.T., K.M.M., J.J.M., J.T., J.A., T.L., and S.W.F. are inventors on a patent application that was filed to protect this series of WDR5 inhibitors. All other authors declare no competing interest.

ASSOCIATED CONTENT

Supporting Information

The Supporting Information is available free of charge at <https://pubs.acs.org/doi/10.1021/acs.jmedchem.2c00195>.

Experimental procedures and characterization of **58**, **S18**, and **S19**; X-ray data collection and refinement statistics; and LCMS traces for **1**, **34**, **36**, **37**, **38**, **40**, and **41** (PDF)

SMILE table of compound structures (CSV)

Accession Codes

Atom coordinates and structure factors for WDR5–ligand complexes can be accessed in the PDB via the following accession codes: 7U9Y, compound **20**; 7UAS, compound **37**. The authors will release the atomic coordinates upon article publication.

Complete contact information is available at: <https://pubs.acs.org/doi/10.1021/acs.jmedchem.2c00195>

Mayme Van Meveren,

Department of Biochemistry, Vanderbilt University School of Medicine, Nashville, Tennessee 37232-0146, United States

Taylor M. South,

Department of Biochemistry, Vanderbilt University School of Medicine, Nashville, Tennessee 37232-0146, United States

Tyson A. Rietz,

Department of Biochemistry, Vanderbilt University School of Medicine, Nashville, Tennessee 37232-0146, United States

Bin Zhao,

Department of Biochemistry, Vanderbilt University School of Medicine, Nashville, Tennessee 37232-0146, United States

William J. Moore,

Leidos Biomedical Research, Frederick National Laboratory for Cancer Research, Frederick, Maryland 21701-4907, United States

Gordon M. Stott,

Leidos Biomedical Research, Frederick National Laboratory for Cancer Research, Frederick, Maryland 21701-4907, United States

William P. Tansey,

Department of Biochemistry and Department of Cell and Developmental Biology, Vanderbilt, University School of Medicine, Nashville, Tennessee 37232-0146, United States

Taekyu Lee,

Department of Biochemistry, Vanderbilt University School of Medicine, Nashville, Tennessee 37232-0146, United States

Stephen W. Fesik

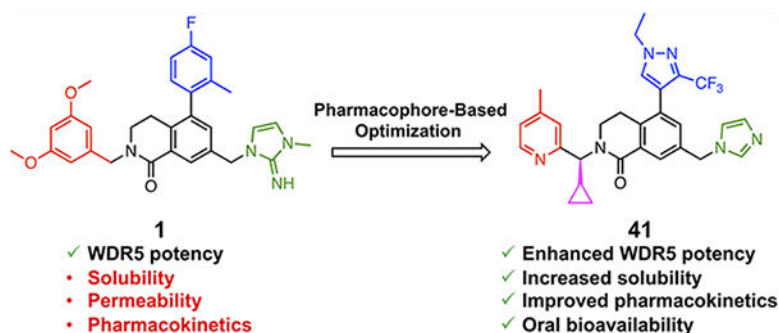
Department of Biochemistry and Department of Pharmacology, Vanderbilt University School of Medicine, Nashville, Tennessee 37232-0146, United States

Department of Chemistry, Vanderbilt University, Nashville, Tennessee 37232-0142, United States

Abstract

WD repeat domain 5 (WDR5) is a nuclear scaffolding protein that forms many biologically important multiprotein complexes. The WIN site of WDR5 represents a promising pharmacological target in a variety of human cancers. Here, we describe the optimization of our initial WDR5 WIN-site inhibitor using a structure-guided pharmacophore-based convergent strategy to improve its druglike properties and pharmacokinetic profile. The core of the previous lead remained constant while a focused SAR effort on the three pharmacophore units was combined to generate a new *in vivo* lead series. Importantly, this new series of compounds has picomolar binding affinity, improved cellular antiproliferative activity and selectivity, and increased kinetic aqueous solubility. They also exhibit a desirable oral pharmacokinetic profile with manageable intravenous clearance and high oral bioavailability. Thus, these new leads are useful probes toward studying the effects of WDR5 inhibition.

GRAPHICAL ABSTRACT



INTRODUCTION

WD repeat domain 5 (WDR5) is a highly conserved member of the WD40-repeat protein family with a characteristic circular barrel-shaped 7-bladed β -propeller structure.^{1–3} WDR5 is a core scaffolding component that contains two major binding interfaces, the WDR5 binding motif (WBM) and WDR5 interaction motif (WIN) sites, on opposite sides to accommodate a large variety of partner proteins to form multiple protein complexes that are essential in a wide range of biological activities, most of which occur in the nucleus.^{4–12} WDR5 has been extensively studied for its role in the activity of MLL1 histone methyltransferase (HMT) complexes, in which MLL1 binds on the WIN site using a conserved arginine in the MLL/SET proteins as an anchor.^{7–9,11,13–17} The complex also contains at least three other evolutionarily conserved proteins (retinoblastoma binding protein 5 (RBBP5), ASH2L, and DPY30) binding through WIN-site-independent interactions and catalyzes histone H3 lysine 4 (H3K4) di- and tri-methylation (H3K4me2, me3).^{8,14} All other MLL/SET (MLL2–4, SETd1A, and SETd1B) family proteins can form similar assemblies by engaging WDR5 on the WIN site through the same interactions but are less dependent on this interaction for catalytic activity than MLL1.^{7,14–17} In addition, WDR5-containing nonspecific lethal (NSL) and Ada2-containing (ATAC) histone acetyltransferase (HAT) complexes carry out acetylation of histone H4 at lysine 16 (H4K16).¹³

WDR5 is also an essential cofactor for the MYC family of oncoprotein transcription factors. WDR5 is tethered to chromatin via the WIN site and recruits MYC to chromatin at tumor-critical target genes via a direct interaction of the WBM site of WDR5 with the conserved MYC Box IIIb element of MYC.^{18–20} A MYC mutant, with impaired binding to WDR5, thus exhibits reduced binding of MYC to chromatin and loss of oncogenic potential *in vivo*, further supporting the role of WDR5 as a critical cofactor for MYC proteins in malignant gene expression programs.²⁰ In addition, aberrant overexpression of WDR5 can be found in a variety of aggressive cancers including bladder,²¹ breast,²² colorectal,²³ gastric,²⁴ pancreatic,²⁵ prostate,^{26,27} neuroblastoma,²⁸ head neck squamous cell carcinoma,²⁹ liver,³⁰ and various leukemias,^{31,32} and is often associated with poor prognoses.^{22,29,32} Therefore, inhibition of WDR5's multifaceted role in human malignancies has emerged as an attractive potential anticancer therapy.^{4,10,18,33} The activity of WDR5 WIN site inhibition is mediated by displacement of WDR5 from chromatin at ribosomal

protein genes (RPGs), which leads to an induction of nucleolar stress and activation of p53-dependent apoptosis.^{34,35} The small-molecule-mediated displacement of WDR5 also displaced the oncoprotein transcription factor MYC at these same RPGs, highlighting that MYC proteins may be one source of multi-factorial vulnerability to these agents.^{34,35}

Structurally diverse WDR5 WIN-site inhibitors have been discovered (Figure 1), and their binding interactions at the WIN site have been confirmed by X-ray co-crystal structures.³⁴⁻⁴¹ The mechanistic proof of concept was demonstrated by MM-589, a first-generation macrocyclic guanidine side chain containing peptidomimetic, that mimics MLL-WDR5 interactions within the WIN site.³⁶ The probe was reported to exhibit subnanomolar binding affinity at the WIN site, potent functional inhibitory activity with a low nanomolar IC₅₀ in the MLL1 HMT assay, and antiproliferative activities in MLL-fusion cancer cell lines.³⁶ OICR-9429 was the first nonpeptide WIN-site inhibitor with a reported K_d of 30 nM, which was discovered from a high-throughput screen hit.^{37,38} The X-ray co-crystal structure of OICR-9429 bound to WDR5 revealed the methyl-piperazine moiety occupied the arginine pocket of the WIN site by mimicking the guanidine side chain of R3765 in the MLL peptide.^{37,38} Because OICR-9429 exhibits druglike properties, its scaffold has become a platform for further optimization of on-target potency and physicochemical properties by several groups. DDO-2093³⁹ and DDO-2213⁴⁰ are recent examples in this class that exhibit antiproliferative activities in MV4:11 cancer cells with reported GI₅₀ values of ~10 μ M. These compounds were also tested in an MV4:11 mouse xenograft model and showed marginal *in vivo* tumor growth inhibition by intraperitoneal injection (ip) and oral (po) dosing, respectively, despite their limited cellular potency.^{39,40} In addition, several WDR5 proteolysis-targeting chimeras (PROTACs) were designed by linking known WIN-site ligands to E3 ligase binding moieties, pomalidomide (CRBN) or VHL.^{42,43} These PROTACs caused reduction of the WDR5 protein expression level in cancer cells via E3 ligase mediated selective WDR5 degradation. The most advanced WDR5 PROTAC MS67 also demonstrated *in vivo* tumor growth inhibition in mouse models.⁴³

We have also discovered a series of highly potent WDR5 inhibitors using fragment-based methods and structure-based design.^{34,35,41} Compound **1** contains a novel conformationally rigid 3,4-dihydroisoquinolin-1(2*H*)-one core that elicits a hydrogen-bond interaction with the backbone NH of C261 and provides ideal vectors to access key binding subsites in the WIN site.³⁵ Compound **1** occupies the MLL peptide residue binding subsites, S₂, S₄, and S₇, with the P₂ imidazole-imine to mimic the guanidine side chain, 4-fluoro-2-methylphenyl P₄, and 3,5-dimethoxybenzyl P₇ pharmacophore units, respectively.³⁵ This small-molecule probe exhibits a binding affinity below the theoretical detection limit of our binding assay ($K_i < 20$ pM) and potent antiproliferative activity in MV4:11 cells (GI₅₀ = 38 nM) with 210-fold cellular selectivity assessed by the GI₅₀ ratio between WDR5 insensitive K562 and sensitive MV4:11 cell lines.³⁵ Compound **1** also caused the displacement of the WDR5 protein from chromatin and triggered transcriptional repression of WDR5 bound genes leading to p53 induction at a significantly lower concentration compared to the previous lead.³⁵

Despite **1** having the highest *in vitro* on-target potency among the reported WDR5 WIN-site inhibitors, it is not an ideal chemical probe to demonstrate the therapeutic potential

of WDR5 inhibitors in *in vivo* models due to its suboptimal physicochemical properties. Compound **1** contains three hydrophobic phenyl moieties, which limit its aqueous solubility. In addition, the probe shows very low systemic exposure in mice by oral dosing, and the imidazole-imine “warhead” that mimics the guanidine side chain is suspected to be a main contributor to poor permeability. Our cellular assay protocol requires 3–5 days of incubation with WIN-site inhibitors to deliver an antiproliferative effect, which suggests repeated doses of a WIN-site inhibitor are required to maintain a pharmacologically relevant WDR5 occupancy to be efficacious *in vivo*. Therefore, the discovery of a potent WDR5 WIN-site inhibitor with high oral bioavailability is critical to develop an effective and practical therapeutic agent. Here, we report our continued efforts toward that objective, building upon our recently reported compound **1**. Our efforts led to the discovery of a new class of WDR5 inhibitors with enhanced potency and physicochemical properties using a pharmacophore-based convergent SAR strategy and X-ray structure-guided modifications. The new series of inhibitors exhibit significantly enhanced selective antiproliferative activity in WDR5 sensitive cells, aqueous solubility, and high oral bioavailability in mice.

RESULTS AND DISCUSSION

Compound **1** Profile and Pharmacophore-Based Convergent Optimization Strategy.

The physicochemical properties of our previous chemical probe **1** were profiled by *in vitro* assays and showed marginal kinetic aqueous solubility (29 μM at pH 7.4, 1% DMSO) and poor passive permeability ($P_e < 0.6 \times 10^{-6}$ cm/s) in the parallel artificial membrane permeability assay (PAMPA). Compound **1** also exhibited a suboptimal pharmacokinetic (PK) profile in mice including high intravenous (iv) clearance (78 mL/min/kg at 3 mg/kg) and an oral exposure below the limit of quantitation when dosed orally (3 mg/kg). In addition, signs of severe acute toxicity, such as reduced locomotive activity, lowered body temperature, and lethality, were observed when compound **1** was dosed (3 mg/kg) by an iv route. These data suggest that future WDR5 inhibitors would require significant improvement in druglike properties, *in vivo* PK and safety profiles from compound **1** while maintaining its high on-target potency to be used as an effective *in vivo* probe and a potential therapeutic agent.

The structure of compound **1** can be divided into four subunits (P₂, P₄, P₇, and core) according to their binding subsite alignments with residues 3764–3773 (ARAEVHLRKS) of MLL1 in the WDR5 WIN site.⁴⁴ The X-ray co-crystal structure of **1** bound to WDR5 (Figure 2) revealed that the conformationally rigid 3,4-dihydroisoquinolin-1(2*H*)-one core was positioned vertically in the center of the WIN site and provided the appropriate exit vectors for the P₂, P₄, and P₇ pharmacophore units to extend to the S₂, S₄, and S₇ binding subsites, respectively.³⁵ The binding pose of the core unit was stabilized through a hydrogen-bond interaction between the core carbonyl oxygen and the backbone NH of C261 and a T-shaped π – π stacking interaction between the core phenyl moiety and the side chain of F133 as shown in Figure 2A,B. The P₂ imidazole-imine “warhead” is the most critical element for binding affinity and selectivity by mimicking the guanidine side chain of R3765 in the MLL peptide.³⁵ The imidazole portion of P₂ is positioned between the two benzyl side chains of F133 and F263 to elicit a sandwiched π – π stacking interaction. In addition, the

imine moiety is located within a hydrogen-bond distance to the backbone carbonyl of C261, and the interaction will be further strengthened by the formation of the positively charged iminium ion at physiological pH (calculated $pK_a = 11$).³⁵ The 4-fluoro-2-methylphenyl P₄ moiety adopts an orthogonal conformation to the core unit to fully occupy the hydrophobic S₄ subsite (Figure 2D). Conversely, the S₇ binding site is a small hydrophobic cavity that can accommodate only half of the 3,5-dimethoxyphenyl P₇ group (Figure 2E).

Based on the above structural information of the binding interactions of each subunit at the corresponding binding site, a pharmacophore-based convergent optimization strategy was devised as shown in Figure 3. The 3,4-dihydroisoquinolin-1(2*H*)-one core served as a chemically stable scaffold that provided proper vectors to nearby binding subsites and was kept constant throughout the study. Efficient convergent synthetic methodologies were developed to facilitate SAR efforts, and a focused structure-guided SAR development was performed on each subunit. All optimized subunits were then combined into a single molecule to retain all desirable attributes.

The S₂ subsite in the WDR5 WIN site was evolved to accommodate the positively charged guanidinium side chain of the R3765 residue.¹⁴ The corresponding P₂ moiety would be the most important anchor unit for the binding potency and may tolerate only a small subset of chemical matter that can maintain the critical binding interactions at the site. For this reason, OICR-9429 mimicked the electronic character of the natural ligand specificity with the methyl-piperazinium P₂ moiety expecting similar binding interactions at the site. However, the WIN site surface representation of the MLL1 peptide 3764–3773 (ARAEVHLRKS) and OICR-9429 bound WDR5 X-ray structures showed the binding site assumed different bound conformations (Figure 4A,B). Inspection of both co-crystal structures revealed that the side chains of F133 and F263 in the S₂ subsite and F149 in the S₇ subsite of the OICR-9429 bound structure underwent significant conformational changes from the MLL1 peptide-binding pose to accommodate the chair shaped methyl-piperazinium P₂ moiety shown in Figure 4C. The conformational change of F149 appeared to be synchronized with the conformational rearrangement of F133 to relieve steric strain. Conversely, the P₂ imidazole-imine of compound **1** mimicked the flat geometry and electronic character of the guanidinium side chain to preserve the original protein conformation in the WIN site (Figure 4D). These structural analyses suggest that the S₂ subsite may be conformationally flexible, and its changes may redefine the shape of the entire WIN site. Considering the results of our previous reports^{34,35} we would conduct a focused SAR effort using P₂ moieties that could mimic the interactions of the imidazole-imine of **1**.

Compared to the narrow derivatization requirements of the S₂ subsite, the S₄ and S₇ subsites present a greater opportunity to optimize the druglike properties of WDR5 WIN-site inhibitors. The S₄ and S₇ subsites are more exposed with higher conformational flexibility than the S₂ subsite allowing a range of chemical matter to be used as potential pharmacophore units in each site. Therefore, broad derivatization of the P₄ and P₇ units would be better suited to optimize the physicochemical properties as well as the binding affinity of WDR5 inhibitors. All three pharmacophore units of **1** are responsible for the suboptimal physicochemical and PK properties of the compound. The P₂ imidazole-imine is suspected to be the main contributor to the poor PAMPA permeability of **1** due to its

pH-dependent basicity profile and its replacement with a neutral pharmacophore is expected to improve the passive permeability of WDR5 inhibitors. The hydrophobic P₄ and P₇ phenyl moieties of **1** contribute to its limited aqueous solubility and can be replaced with more druglike heterocycles.

On-target potency of all newly prepared WDR5 inhibitors was profiled initially using a time-resolved fluorescence energy transfer (TR-FRET) assay to determine the competitive binding affinity (K_i) against the MLL1 derived FITC-peptide probe.^{34,35} WDR5 inhibition-mediated cellular efficacy was assessed in MLL-fusion cancer cell lines MV4:11 and MOLM-13, which express wild-type p53. The K562 leukemia cell line, which is null for p53 and refractory to WIN site inhibition, was used as an insensitive control. The half-maximal growth inhibition (GI₅₀) ratio between K562 and MV4:11 serves as a cellular selectivity measure to ascertain primary cellular selectivity.^{34,35} Following optimization of the three pharmacophore units, druglike properties of select compounds were further profiled by kinetic aqueous solubility assays and *in vivo* PK studies in mice. The results of these studies led to the discovery of a new lead series of WDR5 inhibitors.

Optimization of the P₄ Pharmacophore for Imidazole-Imine Series WDR5 Inhibitors.

The 4-fluoro-2-methylphenyl P₄ moiety of **1** is the most hydrophobic pharmacophore unit and contributes to its limited aqueous solubility. Therefore, we searched for new effective P₄ moieties by employing more desirable heteroaryl groups with reduced hydrophobicity in **1**. For rapid SAR development, we developed a new synthetic route (Scheme 1), in which the P₄ moieties were installed in the last step of the synthesis. We used the calculated partition coefficient (cLogP) to monitor the predicted hydrophobicity of the compounds as substitutions were made to the P₄ unit. The binding affinity of **1** to WDR5 was below the theoretical detection limit of the TR-FRET assay ($K_i < 20$ pM) and substitutions to the P₄ unit maintained the tight picomolar binding affinity to WDR5 (Table 1). Compound **1** had a cLogP of 4.8, and substitution of the 2-methyl for the 2-methoxy group in **2** lowered the hydrophobicity of the compound. However, with the 2-methoxy group a 5-fold loss in antiproliferative activity was observed in both the MV4:11 and MOLM-13 cell lines. The phenol of **3** was tolerated better than methoxy but resulted in a 2-fold loss in cellular activity compared to **1**. A series of 3-pyridyl P₄ units with desirable substitutions from the phenyl series were then investigated to determine the effect of a heteroaryl group with increased hydration potential on the cellular potency of the compounds. The significant loss of binding and cellular activity for **4** served as a benchmark for the new series. The increased size of the P₄ group using the 2-methoxy and 2,5-dimethyl substitutions for **5** and **6** recovered the cellular activity by 2-fold from compound **4**. Introduction of the strong electron-withdrawing 2-trifluoromethyl group exhibited 10-fold enhanced cellular potency compared to **4**, but compound **7** still had 3-fold weaker activity compared to **1**. The 4-pyridyl P₄ units in **8** and **9** improved the cellular activity by 5- and 3-fold compared to regioisomers **4** and **6**, respectively. However, the expected activity boost was not observed for **9** compared to **8**. The lack of improved cellular activity for the pyridyl series led to the investigation of other heterocycles for the P₄ unit.

A series of five-membered heterocycles were profiled as WDR5 inhibitors keeping the similar substitution pattern as the previous series. Compound **10** with the 3-methylisoxazol-4-yl P₄ served as a benchmark for this new series. The 1,3-dimethyl-1*H*-pyrazol-4-yl P₄ of **11** contributed to the observed 2-fold increase in binding affinity and 4-fold increase in cellular activity. The additional methyl substitution for **12** was not tolerated and disrupted the binding of the compound to WDR5. Compound **13** with the 1,3-dimethyl-1*H*-pyrazol-5-yl P₄ had a similar binding affinity and a 2-fold increase in cellular activity compared to **11**. The trifluoromethyl in **14** and **15** gave a 5-fold increase in cellular activity compared to **11** and were comparable to the binding affinity and cellular activity of **1**. The cLogP and selectivity of **14** and **15** were both improved over **1**. The 1-methyl- and 1-ethyl-3-(trifluoromethyl)-1*H*-pyrazol-4-yl) P₄ units were good replacements for the 4-fluoro-2-methylphenyl P₄ unit and were kept in the further optimization of the compounds.

Optimization of the P₂ Pharmacophore with Nonbasic Warheads.

A few representative compounds in Table 1 were tested in the PAMPA permeability assay and showed no improvement from compound **1**, which suggests replacement of the P₂ imidazole-imine is necessary to improve the poor physicochemical properties of the compounds. Our optimization efforts on the P₂ moiety were then focused on five-membered heteroaryl groups that remain neutral at physiological pH to enhance the passive permeability while maintaining the flat geometry to form the key sandwiched π - π stacking interactions with F133 and F263 in the S₂ subsite to preserve the binding conformation of the WIN site and potency of **1**. We had previously discovered that N-linked imidazole was a hit in our early fragment screen.³⁴ A synthetic route was developed from common intermediate **42** to install the P₂ moiety in the last step of the sequence, which is depicted in Scheme 2. Compound **16** (Table 2) with the imidazole P₂ unit maintained good potency against WDR5 sensitive cell lines by exhibiting only a 2-fold loss in activity compared to **1** and **14** with the P₂ imidazole-imine. A series of N-linked azoles were investigated, and **17**–**19** showed significantly reduced binding affinity and cellular potency. This result suggests that the position of the nitrogen atoms and the electrostatic property of the heteroaryl groups were critical for engaging proper binding interactions in the S₂ subsite. The imidazole P₂ moiety was then further diversified by adding small hydrophobic substituents at the 2-position. The 2-methyl imidazole of **20** increased the cellular activity and was comparable to the potency of **1** and **14**. However, larger alkyl substituents at the 2-position of the imidazole P₂ unit in **21**–**23** were less tolerated in the S₂ subsite. Withdrawing electron density away from the imidazole ring with the 2-difluoromethyl group of **24** was also detrimental to the binding interaction. The imidazole and 2-methyl imidazole were found to be good replacements for the imidazole-imine and were used in the further optimization of the WDR5 inhibitors. Finally, compound **20** with the 2-methyl imidazole was profiled in the PAMPA assay and exhibited a 10-fold enhanced passive permeability ($P_c = 5.3 \times 10^{-6}$ cm/s) compared to **1** that further justified our optimization strategy.

The X-ray co-crystal structure of **20** bound to WDR5 was obtained to understand binding interactions of the new P₄ and P₂ units. Compound **20** was positioned in the WIN site in a similar manner as **1** by accessing all key binding subsites (Figure 5A). The

3,4-dihydroisoquinolin-1(2*H*)-one core maintained the same T-shaped π - π stacking with F133 and H-bond between the carbonyl oxygen and the backbone NH of C261 to provide stable exit vectors to the S₂, S₄, and S₇ subsites as previously described. The optimized 1-methyl-3-(trifluoromethyl)-1*H*-pyrazol-4-yl) P₄ unit bound tightly to the S₄ subsite within van der Waals close contacts. The electron-withdrawing and hydrophobic nature of the trifluoromethyl substituent may balance both the hydration potential and overall hydrophobicity of the polar pyrazole pharmacophore unit to avoid significant loss of binding affinity due to increased desolvation energy. Indeed, the 1-methyl-3-(trifluoromethyl)-1*H*-pyrazol-4-yl) P₄ unit of **14** reduced its cLogP by 1.3 without a loss of potency compared to the corresponding 4-fluoro-2-methylphenyl of **1**. The position of the *N*-methyl group showed that a slightly larger group may be accommodated, such as the *N*-ethyl group in **15**, without a steric clash. Overall, the binding conformation of **20** was nearly superimposable with **1** including the newly optimized P₄ and P₂ units (Figure 5B). The SAR of the *N*-linked azoles showed that only imidazole and 2-methyl imidazole were able to maintain comparable binding affinity and antiproliferative activity to the corresponding P₂ imidazole-imine of **14**. The X-ray structure revealed that the 2-methyl imidazole of **20** bound deeply in the S₂ subsite to maintain strong sandwiched π - π stacking interactions with F133 and F263 as denoted by the red dotted lines in Figure 5C, which was consistent with the P₂ imidazole-imine of compound **1**. Although the 2-methyl imidazole lacked the favorable direct H-bond found in the P₂ imidazole-imine to the backbone carbonyl of C261, the effect did not cause a loss of potency for **20**. Finally, the binding conformation of the three key phenylalanine residues, which defines the shape of the WIN site, was successfully preserved by **20** as shown in Figure 5D.

Optimization of the P₇ Pharmacophore Unit for 2-Methyl Imidazole WDR5 Inhibitors.

The next phase of optimization was for the P₇ unit. X-ray structures of both **1** and **20** bound to WDR5 suggested that the solvent-exposed portion of the P₇ unit can be modulated to optimize the physicochemical properties of the compound without a dramatic effect on the potency of the compound. To reduce the hydrophobicity of the P₇ unit the 3,5-dimethoxyphenyl of **1** was replaced by the pyridyl moieties in **25–33** (Table 3) using the synthetic route depicted in Scheme 3. The P₂ and P₄ units of **20** were kept constant while the *N*-methyl or *N*-ethyl group at the R³-position were both investigated. Depending on the substitution of the P₇ unit the cLogP values of **25–32** were reduced compared to **20** and supported our design of the new P₇ unit. The unsubstituted 2-pyridylmethyl containing compound **25** exhibited significantly reduced binding affinity and cellular potency compared to **20** due to improper binding in the S₇ subsite. We introduced a methyl group at various positions of the 2-pyridylmethyl group (**26–28**) to determine a positional preference of substitution for the S₇ subsite. The 6-methyl group of **26** was beneficial to enhance both binding affinity and cellular potency in the WDR5 sensitive cell lines by 6- and 9-fold from **25**, respectively. In addition, the 4-methyl substitution of **27** had an optimized interaction in the S₇ subsite to regain all lost activity of **25** and showed comparable on-target potency to **20** with a reduced cLogP. However, the 3-methyl group of **28** was not tolerated in the subsite and led to a weaker potency than **25**. The regioisomeric 3-methyl-4-pyridyl analog **29** showed that repositioning the nitrogen atom was unfavorable and the

4-methyl-2-pyridylmethyl group of **27** provided the best scaffold for the P₇ pharmacophore. We then expanded the SAR of the 4-methyl group of **27** by introducing slightly larger groups. Both 4-methoxy **30** and 4-ethyl **31** were well tolerated and exhibited similar binding affinity and cellular potency compared to the parent **27**. Compounds **32** and **33** containing the *N*-ethyl R³ group maintain a similar potency profile to **30** and **31**, and these groups can be interchanged as needed to modulate the properties or PK profiles of future compounds. It is also noteworthy that all potent WDR5 inhibitors in the series (**27**, **30–34**) exhibited enhanced cellular selectivity because each compound had significantly reduced antiproliferative activity in the WDR5 insensitive K562 cell line compared to the parent **20**. In summary, the 2-pyridylmethyl group properly substituted at the 4-position is an effective P₇ pharmacophore unit for both potency and druglike properties.

Optimization of the α -Substituted 2-Pyridyl Series WDR5 Inhibitors to Improve Metabolic Stability.

The final phase of optimization sought to take the WDR5 inhibitor with newly optimized P₂, P₄, and P₇ pharmacophore units and identify what elements were necessary to produce a compound that exhibited an improved PK profile. The metabolic stability of **30** was tested in rat liver microsomes (RLM) and the predicted clearance was $CL_{\text{int}} = 220 \mu\text{L}/\text{min}/\text{mg}$ with a half-life of $t_{1/2} = 3.2$ min. The benzylic position of the P₇ unit can be a potential metabolic soft spot. One possibility to improve the metabolic stability of the compound was to develop a series of inhibitors with α -substituted P₇ units. From the X-ray crystal structure of **20**, we predicted that substitution of the solvent-exposed benzylic position with small alkyl groups would be possible, and the (*S*)-enantiomer would maintain the optimal binding pose of **20**. To assess the effect of the size of the benzylic substitution, methyl and cyclopropyl groups were chosen, and all designed compounds showed acceptable cLogP values. Optically pure α -substituted pyridin-2-ylmethanamine P₇ units were prepared, and representative syntheses of **34–41** (Table 4) were shown in Scheme 4. The X-ray co-crystal structure of **37** determined its absolute configuration when bound to WDR5 (Figure 6). Compound **34** was observed to have a 3-fold improvement in cellular activity in the WDR5 sensitive cell lines compared to **32**. The metabolic stability of **34** was also tested in RLM and the predicted clearance was $CL_{\text{int}} = 60 \mu\text{L}/\text{min}/\text{mg}$ with a half-life of $t_{1/2} = 12$ min, nearly a 4-fold improvement in both parameters. As the X-ray structure predicted, the (*R*)-methyl enantiomer **35** showed a 5-fold weaker cellular activity compared to **34**. Compounds **36** and **37** featuring the (*S*)-cyclopropyl group were also tolerated and exhibited similar *in vitro* potency compared to **34**. The imidazole P₂ unit replaced the 2-methyl imidazole in **38** and maintained a similar cellular activity with a 2-fold enhanced metabolic stability in RLM ($CL_{\text{int}} = 31 \mu\text{L}/\text{min}/\text{mg}$ with a half-life of $t_{1/2} = 22$ min) compared to **34**. This may suggest that unsubstituted imidazole can be a preferred P₂ unit to deliver robust *in vivo* efficacy. Unsubstituted imidazole series compounds **38–41** also exhibited a parallel SAR pattern to corresponding 2-methyl-imidazole analogues **34–37**, suggesting same binding poses for both series. Finally, all (*S*)-enantiomers in Table 4 showed a 2- to 3-fold increase in kinetic solubility due to all modifications made throughout our study compared to the initial probe **1**. Consequently, future *in vivo* studies by oral dosing are more feasible with the improved aqueous solubility for these compounds.

To understand the binding mode of the α -substituted 2-pyridylmethyl P₇ unit, the X-ray co-crystal structure of compound **37** bound to WDR5 was obtained. Compound **37** bound to WDR5 using the same key binding interactions as **20** (Figure 6A). The (*S*)-1-cyclopropyl-1-(4-methylpyridine-2-yl)methyl P₇ unit bound in the S₇ subsite as predicted (Figure 6B). The (*S*)-cyclopropyl group pointed out of the binding interface. Conversely, the pro(*R*)-hydrogen pointed toward the protein surface; therefore, compounds containing the opposite enantiomer, such as **35** and **39**, would be forced to adopt a different binding conformation for the P₇ moiety to avoid a steric clash, which caused a loss of binding affinity for these compounds. The overlaid WDR5 bound confirmations of **20** and **37** in Figure 6C are nearly superimposable for all pharmacophore units including the new P₄ and P₇ units.

Pharmacokinetic Profile of WDR5 Inhibitors.

PK properties of representative new WDR5 inhibitors were profiled in CD-1 mice in preparation for studying the effect of WDR5 inhibition in an *in vivo* setting. The compounds were dosed in CD-1 mice at 3 mg/kg iv and 10 mg/kg po and the plasma concentrations of each compound were monitored for 24 h. To obtain a practical oral therapeutic agent, a compound would need to have sufficient oral exposure to reach a sustained pharmacologically relevant target occupancy during a dosing period. We focused on the structural modifications that improved the suboptimal physicochemical properties and poor PK profile (high iv clearance and no oral bioavailability) of compound **1** while maintaining its high on-target potency. The passive permeability of the series was greatly improved by replacing the troublesome P₂ imidazole-imine with an imidazole or 2-methylimidazole moiety. Optimization of P₄ and P₇ units also resulted in improved kinetic aqueous solubility and *in vitro* RLM stability. Consequently, we were gratified to observe oral bioavailability from all tested compounds, and **41** showed the highest oral exposure (AUC_{0,inf}) of the compounds (Table 5). In general, lower iv clearance was accompanied by an increase in oral exposure and may be due to lower first-pass metabolism. Compounds containing the (*S*)-cyclopropyl at the benzylic position of the P₇ unit (**36**, **37**, **40**, **41**) showed significantly reduced iv clearance compared to the corresponding (*S*)-methyl analogs (**34** and **38**). In addition, WDR5 inhibitors containing the unsubstituted imidazole P₂ unit (**38**, **40**, **41**) were superior oral agents to the corresponding 2-methyl-imidazole analogs (**34**, **36**, **37**) by achieving 4 to 7-fold higher oral exposures at the same dose level. Finally, all tested compounds were well tolerated in mice by both iv and po dosing and showed no clinical sign of abnormalities suggesting an enhanced safety profile for the series.

Chemical Synthesis.

Synthetic routes were designed around two objectives, each route would start from the same common intermediate **42**, and, where feasible, the route would be arranged to install the pharmacophore of interest in the final synthetic step. The preparation of compounds **2–15** (Scheme 1) began from hemiacetal **42**, which was prepared in three steps from a previously reported protocol.⁴⁵ Compound **42** underwent reductive amination with 3,5-dimethoxybenzyl-amine to form the bicyclic dihydroisoquinolinone **43**. Triflate **44** was synthesized using phenyl triflimide. The triflate was replaced by a bromide in two synthetic

steps to allow the Suzuki–Miyaura cross-coupling with R¹-boronic acids or R¹-pinacol boronate esters to take place in the final synthetic step. Boronate pinacol ester **45** was prepared through Miyaura borylation of triflate **44** and was converted to bromide **46** using copper(II) bromide. The methyl ester of **46** was reduced to benzyl alcohol **47**, which was brominated with phosphorus tribromide to yield alkyl bromide **48**. Nucleophilic substitution of **48** with 1-methyl-1*H*-imidazol-2-amine hydrochloride gave compound **49** in excellent yield (>99%). Compound **49** underwent Suzuki–Miyaura cross-coupling with R¹-boronic acids or R¹-pinacol boronate esters to yield **2–15**.

Based on the P₄ SAR results, 1-methyl-3-(trifluoromethyl)-1*H*-pyrazol was chosen as the replacement P₄ pharmacophore. The P₂ pharmacophore was optimized by investigating a series of nonbasic azole compounds **16–24** (Scheme 2). To reduce the number of synthetic steps triflate **44** underwent Suzuki–Miyaura cross-coupling with (1-methyl-3-(trifluoromethyl)-1*H*-pyrazol-4-yl)boronic acid to yield **50**. The methyl ester of **50** was reduced to benzyl alcohol **51** and was brominated to yield **52**. Compound **52** underwent nucleophilic substitution with R²-azoles to yield compounds **16–24**.

To optimize the P₇ pharmacophore, lactam intermediates **57** and **58** were alkylated with R⁴-pyridylmethyl halides in the final synthetic step to produce compounds **25–33** (Scheme 3). Triflate **53** was synthesized through a previously reported synthetic route³⁵ and underwent Suzuki–Miyaura cross-coupling with a pyrazole boronic acid to yield **54**. The 2,4-dimethoxybenzyl group was removed under acidic conditions to yield lactam **55**. The methyl ester of **55** was reduced and then brominated to yield **56**. Nucleophilic substitution of **56** with 2-methyl-1*H*-imidazole produced lactam **57**. Lactam **58** was synthesized using similar synthetic steps and is reported in the Supporting Information (Scheme S1). Compounds **57** and **58** were alkylated with R⁴-pyridylmethyl halides to yield **25–33**.

Chiral α -substituted **34**, **35**, **38**, and **39** (Scheme 4) were synthesized through the installation of chiral α -methyl benzylic amines **61** and **64** in the initial synthetic step. Enantiopure benzylic amines were synthesized in three steps beginning with the condensation of 4-methoxypicolinaldehyde with the appropriate Ellman's chiral auxiliary, (*S*)- or (*R*)- 2-methylpropane-2-sulfinamide, to yield sulfinimines **59** and **62**, respectively. The sulfinimines underwent diastereoselective addition with methyl magnesium bromide to yield sulfinamides **60** and **63**, which were purified by normal-phase chromatography. Chiral α -methyl benzylic amines **61** and **64** were obtained as hydrochloride salts following deprotection of the chiral auxiliary under acidic conditions. Hemiacetal **42** underwent reductive amination with chiral α -methyl benzylic amines **61** and **64** to yield **65** and **66**, respectively. Triflates **67** and **68** were synthesized using phenyl triflimide, and underwent Suzuki–Miyaura cross-coupling with (1-ethyl-3-(trifluoromethyl)-1*H*-pyrazol-4-yl)boronic acid to yield **69** and **70**. The methyl esters of **69** and **70** were reduced to benzyl alcohols **71** and **72** and were brominated to yield **73** and **74**. Compounds **73** and **74** underwent nucleophilic substitution with 2-methyl-1*H*-imidazole or 1*H*-imidazole to yield compounds **34**, **35**, **38**, and **39**. Compounds **36**, **37**, **40**, and **41** were synthesized by the same synthetic route and experimental details are reported in the Supporting Information (Scheme S2).

CONCLUSIONS

We describe the pharmacophore-based optimization of WDR5 inhibitors containing the 3,4-dihydroisoquinolin-1(2*H*)-one core. Compound **1** was previously discovered to have robust *in vitro* on-target potency against WDR5 sensitive cell lines; however, suboptimal physicochemical properties of specific pharmacophore units prevented the probe from having a desirable oral PK profile that would be expected to produce antitumor efficacy in an *in vivo* setting. To address the limitations of **1**, we used a pharmacophore-based convergent SAR and X-ray structure-guided modification strategy to discover a new class of WDR5 inhibitors with enhanced potency and physicochemical properties. We focused our SAR effort on individual P₂, P₄, and P₇ pharmacophore units and sequentially optimized each unit. The P₂ imidazole-imine was found to be the main contributor to the poor cellular permeability of **1** due to its pH-dependent profile. The P₂ imidazole-imine was replaced by the N-linked imidazole series. The X-ray structure of **20** confirmed that the 2-methyl imidazole P₂ unit maintained the critical binding interactions in the S₂ subsite that were originally observed with **1**, which were critical to preserving the original binding mode to the WDR5 WIN site. Although compound **30** with optimized P₂, P₄, and P₇ pharmacophores exhibited enhanced on-target potency, and improved physicochemical properties compared to the initial probe **1**, its poor RLM metabolic stability became a concern for further development. We recognized the benzylic position of the P₇ unit to be a metabolic soft spot and developed a series of α -substituted P₇ units to resolve the issue. This strategy turned out to be effective as the (*S*)-methyl enantiomer of **34** showed increased RLM metabolic stability and oral bioavailability in mice. However, additional optimization was needed to reduce the high iv clearance of **34**, which was unable to achieve a desired high oral exposure due to rapid first-pass metabolism. Finally, the (*S*)-cyclopropyl P₇ and unsubstituted imidazole P₂ in **40** and **41** significantly improved the PK profile including iv clearance and oral exposure and maintained potent *in vitro* on-target potency.

In summary, we have detailed the successful optimization of WDR5 inhibitors using a structure-guided and pharmacophore-based optimization strategy. The new *in vivo* leads **40** and **41** display potent *in vitro* potency and suitable PK profiles following oral dosing. Future studies will be aimed at optimizing potency and PK properties of a new lead series to demonstrate WDR5 inhibition-mediated *in vivo* efficacy in mouse xenograft tumor models by oral dosing and safety for the mechanism of action.

EXPERIMENTAL SECTION

General Chemistry.

All chemical reagents and reaction solvents were purchased from commercial suppliers and used as received. Proton nuclear magnetic resonance (¹H NMR) spectra were recorded on a Bruker AVIII-HD 400 MHz spectrometer and processed using Bruker TopSpin 3.6.1. For ¹H NMR spectra, chemical shifts are reported in parts per million (ppm) and are reported relative to residual nondeuterated solvent signals. Coupling constants are reported in hertz (Hz). The following abbreviations (or a combination, thereof) are used to describe splitting patterns: s, singlet; d, doublet; t, triplet; q, quartet; p, pentet; m, multiplet; br, broad. All

final compounds were of >95% purity as measured by analytical reversed-phase HPLC. Analytical HPLC was performed on an Agilent 1200 series system with UV detection at 214 and 254 nm, along with evaporative light scattering detection (ELSD). Low-resolution mass spectra were obtained on an Agilent 6140 mass spectrometer with electrospray ionization (ESI). LCMS experiments were performed with the following parameters. Method 1: Phenomenex Kinetex 2.6 μm XB-C18 100 Å LC column (30 mm \times 2.1 mm); 1.1 min gradient, 7–95% MeCN in H₂O, and 0.1% TFA. Method 2: Phenomenex Kinetex 2.6 μm XB-C18 100 Å LC column (50 mm \times 2.1 mm); 2 min gradient, 5–95% MeCN in H₂O, and 0.1% TFA. Analytical thin-layer chromatography (TLC) was performed on Kieselgel 60 F254 glass plates precoated with a 0.25 mm thickness of silica gel. TLC plates were visualized with UV light and iodine. Silica gel chromatography was performed using a Teledyne ISCO Combiflash Rf system, eluting with varying concentrations of EtOAc in hexanes or MeOH in CH₂Cl₂. Preparative reversed-phase HPLC was performed on a Gilson HPLC equipped with a Phenomenex Kinetex C18 column, using varying concentrations of MeCN in H₂O, and 0.1% TFA. Solvents for reactions, extraction, and washing were of ACS grade, and solvents for chromatography were of HPLC grade. Compounds **1**, **42**, and **53** were prepared according to previously reported protocols.^{35,45}

General Procedure A: Reductive Amination.

Dimethyl 2-hydroxy-2,3-dihydrobenzofuran-4,6-dicarboxylate **42** (1 equiv) and an amine (1.5 equiv) were dissolved in CH₂Cl₂ and stirred at 30 °C for 30 min. Then sodium triacetoxyborohydride (2 equiv) was added and the reaction was stirred at 30 °C for 3 h. The reaction mixture was concentrated and dissolved in 1,4-dioxane and heated at 110 °C overnight. Saturated aqueous NaHCO₃ was added, and the mixture was extracted with CH₂Cl₂. The combined organic phases were dried over anhydrous Na₂SO₄ and concentrated under reduced pressure. The compound was used without further purification.

General Procedure B: Triflation of Phenol.

Phenyl triflimide (1.2 equiv) was added to a solution of phenol (1 equiv) and an amine (2.5 equiv) in THF/CH₂Cl₂ (5:1) at 23 °C and stirred for 14 h. Saturated aqueous NaHCO₃ was added, and the mixture was extracted with CH₂Cl₂. The combined organic phases were dried over anhydrous Na₂SO₄ and concentrated under reduced pressure. The residue was purified by flash chromatography (Combi-flash Rf, EtOAc/hexanes = 0–50% gradient).

General Procedure C: Reduction of Methyl Ester.

A solution of lithium triethylborohydride (1 M THF, 3 equiv) or lithium borohydride (2 M THF) was added dropwise to a solution of methyl ester (1 equiv) in THF at 0 °C. The reaction was stirred for 40 min, then quenched with saturated aqueous NaHCO₃. The mixture was extracted with EtOAc. The combined organic layers were dried over MgSO₄ and concentrated under reduced pressure. The residue was purified by flash chromatography (Combi-flash Rf, EtOAc/hexanes = 0–100% gradient).

General Procedure D: Bromination of Benzyl Alcohol.

PBr₃ (2 equiv) was added to a solution of benzyl alcohol (1 equiv) in CH₂Cl₂ at 0 °C. The reaction was stirred and slowly warmed to room temperature. Saturated aqueous NaHCO₃ was added, and the mixture was extracted with CH₂Cl₂. The combined organic layers were dried over MgSO₄ and concentrated under reduced pressure. The residue was purified by flash chromatography (Combi-flash Rf, EtOAc/hexanes = 0–30% gradient).

General Procedure E: Suzuki–Miyaura Cross-Coupling.

The representative aryl halide or aryl triflate (1 equiv), aryl boronic acid or pinacol ester (2 equiv), K₂CO₃ (2 equiv), and Pd catalyst (0.05 equiv) were dissolved in 1,4-dioxane/H₂O (4:1). The reaction mixture was placed under an argon atmosphere heated to 80–90 °C for 2–14 h and then cooled to room temperature. The reaction mixture was diluted with water and extracted with CH₂Cl₂. The combined organic layers were washed with brine, dried over MgSO₄, filtered, and concentrated under reduced pressure. Intermediate compounds were purified by flash chromatography (Combi-flash Rf, EtOAc/hexanes = 0–100% gradient). Final compounds were purified by preparative reversed-phase HPLC (Phenomenex Gemini C18, MeCN/H₂O = 15–70%, 0.1% TFA) followed by neutralization with saturated aqueous NaHCO₃.

General Procedure F: Displacement of Benzyl Bromide with Amine.

R²-azole (3–4 equiv) was added to a solution of benzyl bromide (1 equiv) in acetonitrile at 23 °C. The reaction mixture was stirred for 12 h at 50 °C, then cooled to ambient temperature, filtered, and concentrated. Intermediate compounds were purified by flash chromatography (Combi-flash Rf, MeOH/CH₂Cl₂ = 0–10% gradient). Final compounds were purified by preparative reversed-phase HPLC (Phenomenex Gemini C18, MeCN/H₂O = 15–70% gradient, 0.1% TFA) followed by neutralization with saturated aqueous NaHCO₃.

General Procedure G: Lactam Alkylation.

Lactam (1 equiv) was dissolved in DMF and cooled to 0 °C. Sodium hydride (1.2 equiv) was added, and the reaction was stirred for 15 min. R⁴-halide (1.2 equiv) was added. The reaction was stirred and allowed to warm to room temperature and then water was added, and the aqueous layer was extracted with EtOAc. The combined organic layers were washed with brine, dried over MgSO₄, and concentrated under reduced pressure. The residue was purified by reversed-phase HPLC (Phenomenex Gemini C18, MeCN/H₂O = 15–70% gradient, 0.1% TFA) followed by neutralization with saturated aqueous NaHCO₃.

2-(3,5-Dimethoxybenzyl)-5-(4-fluoro-2-methoxyphenyl)-7-((2-imino-3-methyl-2,3-dihydro-1H-imidazol-1-yl)methyl)-3,4-dihydroisoquinolin-1(2H)-one (2).—General Procedure E was followed using **49** (50

mg, 0.1 mmol, 1 equiv), (4-fluoro-2-methoxyphenyl)-boronic acid (35 mg, 0.21 mmol, 2 equiv), potassium carbonate (36 mg, 0.26 mmol, 2.5 equiv), and PdCl₂(dppf)·CH₂Cl₂ (4.2 mg, 0.005 mmol, 0.05 equiv) to obtain the title compound (34 mg, 0.064 mmol, 62% yield). ¹H NMR (400 MHz, DMSO-*d*₆) δ 7.87 (d, *J* = 1.3 Hz, 1H), 7.31 (d, *J* = 1.7 Hz, 1H), 7.17 (dd, *J* = 8.3, 7.0 Hz, 1H), 7.02 (dd, *J* = 11.4, 2.4 Hz, 1H), 6.86 (td, *J* = 8.4, 2.4 Hz, 1H),

6.65 (s, 1H), 6.54 (s, 1H), 6.43 (d, $J = 2.2$ Hz, 2H), 6.40 (t, $J = 2.2$ Hz, 1H), 4.88 (s, 2H), 4.62 (s, 2H), 3.72 (s, 3H), 3.71 (s, 6H), 3.37–3.33 (m, 2H), 3.17 (s, 3H), 2.72–2.64 (m, 1H), 2.54–2.51 (m, 1H); LCMS (method 2, ESI): >95%, $R_t = 1.647$ min, $m/z = 531.1$ [M + H]⁺.

2-(3,5-Dimethoxybenzyl)-5-(4-fluoro-2-hydroxyphenyl)-7-((2-imino-3-methyl-2,3-dihydro-1H-imidazol-1-yl)methyl)-3,4-dihydroisoquinolin-1(2H)-one (3).—General Procedure E was followed using **49** (50 mg, 0.1 mmol, 1 equiv), (4-fluoro-2-hydroxyphenyl)-boronic acid (32 mg, 0.21 mmol, 2 equiv), potassium carbonate (36 mg, 0.26 mmol, 2.5 equiv), and PdCl₂(dppf)·CH₂Cl₂ (4.2 mg, 0.005 mmol, 0.05 equiv) to obtain the title compound (10.4 mg, 0.020 mmol, 20% yield). ¹H NMR (400 MHz, DMSO-*d*₆) δ 7.87 (d, $J = 1.2$ Hz, 1H), 7.40 (s, 1H), 7.07 (d, $J = 2.4$ Hz, 1H), 6.98 (t, $J = 7.9$ Hz, 1H), 6.92 (d, $J = 2.4$ Hz, 1H), 6.60 (d, $J = 11.7$ Hz, 1H), 6.44–6.38 (m, 5H), 5.11 (s, 2H), 4.61 (s, 2H), 3.69 (s, 6H), 3.42 (s, 3H), 3.34 (t, $J = 6.5$ Hz, 2H), 2.85–2.65 (brs, 2H); LCMS (method 2, ESI): >95%, $R_t = 1.576$ min, $m/z = 517.0$ [M + H]⁺.

2-(3,5-Dimethoxybenzyl)-7-((2-imino-3-methyl-2,3-dihydro-1H-imidazol-1-yl)methyl)-5-(2-methylpyridin-3-yl)-3,4-dihydroisoquinolin-1(2H)-one (4).—General Procedure E was followed using **49** (50 mg, 0.1 mmol, 1 equiv), (2-methylpyridin-3-yl)boronic acid (28 mg, 0.21 mmol, 2 equiv), potassium carbonate (36 mg, 0.26 mmol, 2.5 equiv), and PdCl₂(dppf)·CH₂Cl₂ (4.2 mg, 0.005 mmol, 0.05 equiv) to obtain the title compound (8.8 mg, 0.018 mmol, 17% yield). ¹H NMR (400 MHz, DMSO-*d*₆) δ 8.49 (dd, $J = 4.8, 1.7$ Hz, 1H), 7.94 (d, $J = 1.7$ Hz, 1H), 7.55 (dd, $J = 7.6, 1.7$ Hz, 1H), 7.35 (d, $J = 1.8$ Hz, 1H), 7.29 (dd, $J = 7.6, 4.9$ Hz, 1H), 6.61 (d, $J = 2.6$ Hz, 1H), 6.50 (d, $J = 2.6$ Hz, 1H), 6.44 (d, $J = 2.2$ Hz, 2H), 6.40 (t, $J = 2.2$ Hz, 1H), 4.90 (s, 2H), 4.62 (dd, $J = 40.8, 14.9$ Hz, 2H), 3.70 (s, 6H), 3.39 (t, $J = 6.6$ Hz, 2H), 3.16 (s, 3H), 2.67–2.59 (m, 1H), 2.49–2.44 (m, 1H), 2.22 (s, 3H); LCMS (method 2, ESI): >95%, $R_t = 1.252$ min, $m/z = 498.1$ [M + H]⁺.

2-(3,5-Dimethoxybenzyl)-7-((2-imino-3-methyl-2,3-dihydro-1H-imidazol-1-yl)methyl)-5-(2-methoxypyridin-3-yl)-3,4-dihydroisoquinolin-1(2H)-one (5).—General Procedure E was followed using **49** (50 mg, 0.1 mmol, 1 equiv), 2-methoxypyridine-3-boronic acid hydrate (35 mg, 0.21 mmol, 2 equiv), potassium carbonate (36 mg, 0.26 mmol, 2.5 equiv), and PdCl₂(dppf)·CH₂Cl₂ (4.2 mg, 0.005 mmol, 0.05 equiv) to obtain the title compound (36.8 mg, 0.072 mmol, 70% yield). ¹H NMR (400 MHz, DMSO-*d*₆) δ 8.23 (dd, $J = 5.0, 1.9$ Hz, 1H), 7.91 (s, 1H), 7.62 (dd, $J = 7.2, 1.9$ Hz, 1H), 7.38 (s, 1H), 7.11 (dd, $J = 7.2, 5.0$ Hz, 1H), 6.67 (s, 1H), 6.56 (s, 1H), 6.43 (d, $J = 2.2$ Hz, 2H), 6.40 (t, $J = 2.2$ Hz, 1H), 4.89 (s, 2H), 4.63 (s, 2H), 3.81 (s, 3H), 3.71 (s, 6H), 3.37 (t, $J = 6.5$ Hz, 2H), 3.18 (s, 3H), 2.75–2.65 (m, 2H); LCMS (method 2, ESI): >95%, $R_t = 1.507$ min, $m/z = 514.1$ [M + H]⁺.

2-(3,5-Dimethoxybenzyl)-7-((2-imino-3-methyl-2,3-dihydro-1H-imidazol-1-yl)methyl)-5-(2-(trifluoromethyl)pyridin-3-yl)-3,4-dihydroisoquinolin-1(2H)-one (6).—General Procedure E was followed using **49** (50 mg, 0.1 mmol, 1 equiv), (2-(trifluoromethyl)pyridin-3-yl)boronic acid (39 mg, 0.21 mmol, 2 equiv), potassium carbonate (36 mg, 0.26 mmol, 2.5 equiv), and PdCl₂(dppf)

·CH₂Cl₂ (4.2 mg, 0.005 mmol, 0.05 equiv) to obtain the title compound (8.5 mg, 0.015 mmol, 15% yield). ¹H NMR (400 MHz, DMSO-*d*₆) δ 8.82 (dd, *J* = 4.7, 1.3 Hz, 1H), 8.07 (d, *J* = 1.9 Hz, 1H), 7.96 (s, 1H), 7.94 (d, *J* = 1.1 Hz, 1H), 7.82 (dd, *J* = 7.8, 4.7 Hz, 1H), 7.41 (d, *J* = 1.5 Hz, 1H), 7.13 (d, *J* = 2.5 Hz, 1H), 7.06 (d, *J* = 2.5 Hz, 1H), 6.43 (d, *J* = 2.2 Hz, 2H), 6.41 (t, *J* = 2.2 Hz, 1H), 5.19 (dd, *J* = 20.2, 15.8 Hz, 2H), 4.63 (dd, *J* = 73.8, 14.9 Hz, 2H), 3.71 (s, 6H), 3.45 (s, 3H), 3.44–3.40 (m, 1H), 3.38–3.31 (m, 1H), 2.70–2.63 (m, 1H), 2.44–2.37 (m, 1H); LCMS (method 2, ESI): >95%, *R*_t = 1.543 min, *m/z* = 552.0 [M + H]⁺.

2-(3,5-Dimethoxybenzyl)-5-(2,5-dimethylpyridin-3-yl)-7-((2-imino-3-methyl-2,3-dihydro-1H-imidazol-1-yl)methyl)-3,4-dihydroisoquinolin-1(2H)-one (7).—

General Procedure E was followed using **49** (30 mg, 0.062 mmol, 1 equiv), (2,5-dimethylpyridin-3-yl)boronic acid (19 mg, 0.12 mmol, 2 equiv), potassium carbonate (21 mg, 0.15 mmol, 2.5 equiv), and PdCl₂(dppf)·CH₂Cl₂ (2.5 mg, 0.003 mmol, 0.05 equiv) to obtain the title compound (14.2 mg, 0.028 mmol, 45% yield). ¹H NMR (400 MHz, DMSO-*d*₆) δ 8.32 (s, 1H), 7.92 (s, 1H), 7.37 (s, 1H), 7.32 (s, 1H), 6.60 (d, *J* = 2.2 Hz, 1H), 6.50 (d, *J* = 2.2 Hz, 1H), 6.44 (d, *J* = 1.9 Hz, 2H), 6.40 (t, *J* = 2.0 Hz, 1H), 4.87 (s, 2H), 4.62 (dd, *J* = 45.4, 14.9 Hz, 2H), 3.71 (s, 6H), 3.39 (t, *J* = 6.6 Hz, 2H), 3.15 (s, 3H), 2.67–2.59 (m, 1H), 2.54–2.46 (m, 1H), 2.28 (s, 3H), 2.16 (s, 3H); LCMS (method 2, ESI): >95%, *R*_t = 1.271 min, *m/z* = 512.1 [M + H]⁺.

2-(3,5-Dimethoxybenzyl)-7-((2-imino-3-methyl-2,3-dihydro-1H-imidazol-1-yl)methyl)-5-(3-methylpyridin-4-yl)-3,4-dihydroisoquinolin-1(2H)-one (8).—

General Procedure E was followed using **49** (50 mg, 0.10 mmol, 1 equiv), (3-methylpyridin-4-yl)boronic acid (28 mg, 0.21 mmol, 2 equiv), potassium carbonate (36 mg, 0.26 mmol, 2.5 equiv), and PdCl₂(dppf)·CH₂Cl₂ (4.2 mg, 0.005 mmol, 0.05 equiv) to obtain the title compound (25 mg, 0.05 mmol, 49% yield). ¹H NMR (400 MHz, DMSO-*d*₆) δ 8.54 (s, 1H), 8.44 (d, *J* = 4.9 Hz, 1H), 7.94 (d, *J* = 1.8 Hz, 1H), 7.31 (d, *J* = 1.7 Hz, 1H), 7.17 (d, *J* = 4.9 Hz, 1H), 6.58 (d, *J* = 2.2 Hz, 1H), 6.47 (d, *J* = 2.4 Hz, 1H), 6.44 (d, *J* = 2.2 Hz, 2H), 6.40 (t, *J* = 2.2 Hz, 1H), 4.86 (s, 2H), 4.62 (dd, *J* = 34.2, 14.9 Hz, 2H), 3.70 (s, 6H), 3.39 (t, *J* = 6.6 Hz, 2H), 3.13 (s, 3H), 2.70–2.61 (m, 1H), 2.48–2.41 (m, 1H), 2.03 (s, 3H); LCMS (method 2, ESI): >95%, *R*_t = 1.224 min, *m/z* = 498.1 [M + H]⁺.

2-(3,5-Dimethoxybenzyl)-5-(2,5-dimethylpyridin-4-yl)-7-((2-imino-3-methyl-2,3-dihydro-1H-imidazol-1-yl)methyl)-3,4-dihydroisoquinolin-1(2H)-one (9).—

General Procedure E was followed using **49** (30 mg, 0.062 mmol, 1 equiv), (2,5-dimethylpyridin-4-yl)boronic acid (19 mg, 0.12 mmol, 2 equiv), potassium carbonate (21 mg, 0.15 mmol, 2.5 equiv), and PdCl₂(dppf)·CH₂Cl₂ (2.5 mg, 0.003 mmol, 0.05 equiv) to obtain the title compound (12 mg, 0.023 mmol, 38% yield). ¹H NMR (400 MHz, DMSO-*d*₆) δ 8.34 (s, 1H), 7.93 (s, 1H), 7.28 (s, 1H), 7.03 (s, 1H), 6.57 (s, 1H), 6.47 (s, 1H), 6.44 (s, 2H), 6.40 (s, 1H), 4.85 (s, 2H), 4.62 (dd, *J* = 38.8, 15.2 Hz, 2H), 3.71 (s, 6H), 3.39 (t, *J* = 6.6 Hz, 2H), 3.13 (s, 3H), 2.67–2.61 (m, 1H), 2.48–2.55 (m, 1H), 2.44 (s, 3H), 1.98 (s, 3H); LCMS (method 2, ESI): >95%, *R*_t = 1.274 min, *m/z* = 512.1 [M + H]⁺.

2-(3,5-Dimethoxybenzyl)-7-((2-imino-3-methyl-2,3-dihydro-1H-imidazol-1-yl)methyl)-5-(3-methylisoxazol-4-yl)-3,4-dihydroisoquinolin-1(2H)-one (10).—

General Procedure E was followed using **49** (30 mg, 0.062 mmol, 1 equiv), (3-methylisoxazol-4-yl)boronic acid (16 mg, 0.12 mmol, 2 equiv), potassium carbonate (21 mg, 0.15 mmol, 2.5 equiv), and PdCl₂(dppf)·CH₂Cl₂ (2.5 mg, 0.003 mmol, 0.05 equiv) to obtain the title compound (13.3 mg, 0.027 mmol, 44% yield). ¹H NMR (400 MHz, DMSO-*d*₆) δ 8.98 (s, 1H), 7.94 (s, 1H), 7.47 (s, 1H), 6.67 (s, 1H), 6.56 (s, 1H), 6.44 (s, 2H), 6.41 (s, 1H), 4.91 (s, 2H), 4.63 (s, 2H), 3.71 (s, 6H), 3.41 (t, *J* = 6.5 Hz, 2H), 3.18 (s, 3H), 2.81 (t, *J* = 6.4 Hz, 2H), 2.19 (s, 3H); LCMS (method 2, ESI): >95%, *R*_t = 1.472 min, *m/z* = 488.1 [M + H]⁺.

2-(3,5-Dimethoxybenzyl)-5-(1,3-dimethyl-1H-pyrazol-4-yl)-7-((2-imino-3-methyl-2,3-dihydro-1H-imidazol-1-yl)methyl)-3,4-dihydroisoquinolin-1(2H)-one (11).—General Procedure E was followed using **49** (50

mg, 0.10 mmol, 1 equiv), 1,3-dimethyl-4-(4,4,5,5-tetramethyl-1,3,2-dioxaborolan-2-yl)-1*H*-pyrazole (46 mg, 0.21 mmol, 2 equiv), potassium carbonate (36 mg, 0.26 mmol, 2.5 equiv), and PdCl₂(dppf)·CH₂Cl₂ (4.2 mg, 0.005 mmol, 0.05 equiv) to obtain the title compound (31.1 mg, 0.062 mmol, 60% yield). ¹H NMR (400 MHz, DMSO-*d*₆) δ 7.86 (d, *J* = 1.7 Hz, 1H), 7.71 (s, 1H), 7.36 (d, *J* = 1.7 Hz, 1H), 6.85 (s, 1H), 6.74 (s, 1H), 6.44 (d, *J* = 2.2 Hz, 2H), 6.41 (t, *J* = 2.2 Hz, 1H), 5.01 (s, 2H), 4.62 (s, 2H), 3.78 (s, 3H), 3.71 (s, 6H), 3.38 (t, *J* = 6.5 Hz, 2H), 3.30 (s, 3H), 2.81 (t, *J* = 6.2 Hz, 2H), 2.07 (s, 3H); LCMS (method 2, ESI): >95%, *R*_t = 1.433 min, *m/z* = 501.1 [M + H]⁺.

2-(3,5-Dimethoxybenzyl)-7-((2-imino-3-methyl-2,3-dihydro-1H-imidazol-1-yl)methyl)-5-(1,3,5-trimethyl-1H-pyrazol-4-yl)-3,4-dihydroisoquinolin-1(2H)-one (12).—General Procedure E was followed using **49** (50 mg,

0.10 mmol, 1 equiv), (1,3,5-trimethyl-1*H*-pyrazol-4-yl)boronic acid (32 mg, 0.21 mmol, 2 equiv), potassium carbonate (36 mg, 0.26 mmol, 2.5 equiv), and PdCl₂(dppf)·CH₂Cl₂ (4.2 mg, 0.005 mmol, 0.05 equiv) to obtain the title compound (7 mg, 0.01 mmol, 10% yield). ¹H NMR (400 MHz, DMSO-*d*₆) δ 7.95 (s, 1H), 7.92 (d, *J* = 1.9 Hz, 1H), 7.26 (d, *J* = 2.0 Hz, 1H), 7.19 (d, *J* = 2.5 Hz, 1H), 7.07 (d, *J* = 2.5 Hz, 1H), 6.44 (d, *J* = 2.2 Hz, 2H), 6.41 (t, *J* = 2.2 Hz, 1H), 5.17 (s, 2H), 4.63 (s, 2H), 3.71 (s, 6H), 3.69 (s, 3H), 3.46 (s, 3H), 3.39 (t, *J* = 6.5 Hz, 2H), 2.65 (t, *J* = 6.5 Hz, 2H), 2.00 (s, 3H), 1.92 (s, 3H); LCMS (method 2, ESI): >95%, *R*_t = 1.381 min, *m/z* = 515.1 [M + H]⁺.

2-(3,5-Dimethoxybenzyl)-5-(1,3-dimethyl-1H-pyrazol-5-yl)-7-((2-imino-3-methyl-2,3-dihydro-1H-imidazol-1-yl)methyl)-3,4-dihydroisoquinolin-1(2H)-one (13).—General Procedure E was followed using **49** (50

mg, 0.10 mmol, 1 equiv), (1,3-dimethyl-1*H*-pyrazol-5-yl)boronic acid (29 mg, 0.21 mmol, 2 equiv), potassium carbonate (36 mg, 0.26 mmol, 2.5 equiv), and PdCl₂(dppf)·CH₂Cl₂ (4.2 mg, 0.005 mmol, 0.05 equiv) to obtain the title compound (34.3 mg, 0.069 mmol, 67% yield). ¹H NMR (400 MHz, DMSO-*d*₆) δ 7.96 (d, *J* = 1.8 Hz, 1H), 7.42 (d, *J* = 1.8 Hz, 1H), 6.57 (d, *J* = 2.5 Hz, 1H), 6.45 (s, 1H), 6.44 (d, *J* = 2.2 Hz, 2H), 6.40 (t, *J* = 2.2 Hz, 1H), 6.10 (s, 1H), 4.85 (s, 2H), 4.63 (s, 2H), 3.71 (s, 6H), 3.53 (s, 3H), 3.41 (t, *J* = 6.5 Hz, 2H), 3.12 (s, 3H), 2.74 (t, *J* = 6.5 Hz, 2H), 2.17 (s, 3H); LCMS (method 2, ESI): >95%, *R*_t = 1.448 min, *m/z* = 501.1 [M + H]⁺.

2-(3,5-Dimethoxybenzyl)-7-((2-imino-3-methyl-2,3-dihydro-1H-imidazol-1-yl)methyl)-5-(1-methyl-3-(trifluoromethyl)-1H-pyrazol-4-yl)-3,4-dihydroisoquinolin-1(2H)-one (14).—General Procedure

E was followed using **49** (60 mg, 0.12 mmol, 1 equiv), (1-methyl-3-(trifluoromethyl)-1*H*-pyrazol-4-yl)boronic acid (48 mg, 0.25 mmol, 2 equiv), potassium carbonate (43 mg, 0.31 mmol, 2.5 equiv), and PdCl₂(dppf)·CH₂Cl₂ (5.0 mg, 0.006 mmol, 0.05 equiv) to obtain the title compound (48 mg, 0.087 mmol, 70% yield). ¹H NMR (400 MHz, DMSO-*d*₆) δ 8.03 (s, 1H), 7.93 (d, *J* = 1.8 Hz, 1H), 7.31 (d, *J* = 1.5 Hz, 1H), 6.65 (s, 1H), 6.60 (s, 1H), 6.44 (d, *J* = 2.2 Hz, 2H), 6.41 (t, *J* = 2.2 Hz, 1H), 4.92 (s, 2H), 4.62 (s, 2H), 3.95 (s, 3H), 3.71 (s, 6H), 3.39 (t, *J* = 6.5 Hz, 2H), 3.20 (s, 3H), 2.71 (t, *J* = 6.5 Hz, 2H); LCMS (method 2, ESI): >95%, *R*_t = 1.545 min, *m/z* = 555.1 [M + H]⁺.

2-(3,5-Dimethoxybenzyl)-5-(1-ethyl-3-(trifluoromethyl)-1H-pyrazol-4-yl)-7-((2-imino-3-methyl-2,3-dihydro-1H-imidazol-1-yl)methyl)-3,4-dihydroisoquinolin-1(2H)-one (15).—General Procedure E

was followed using **49** (50 mg, 0.10 mmol, 1 equiv), (1-ethyl-3-(trifluoromethyl)-1*H*-pyrazol-4-yl)boronic acid (43 mg, 0.21 mmol, 2 equiv), potassium carbonate (36 mg, 0.26 mmol, 2.5 equiv), and PdCl₂(dppf)·CH₂Cl₂ (4.2 mg, 0.005 mmol, 0.05 equiv) to obtain the title compound (39.7 mg, 0.070 mmol, 68% yield). ¹H NMR (400 MHz, DMSO-*d*₆) δ 8.09 (s, 1H), 7.91 (d, *J* = 1.8 Hz, 1H), 7.34 (d, *J* = 1.4 Hz, 1H), 6.56 (s, 1H), 6.51 (s, 1H), 6.44 (d, *J* = 2.2 Hz, 2H), 6.41 (t, *J* = 2.2 Hz, 1H), 4.86 (s, 2H), 4.62 (s, 2H), 4.24 (q, *J* = 7.3 Hz, 2H), 3.71 (s, 6H), 3.39 (t, *J* = 6.5 Hz, 2H), 3.15 (s, 3H), 2.71 (t, *J* = 6.5 Hz, 2H), 1.43 (t, *J* = 7.3 Hz, 3H); LCMS (method 2, ESI): >95%, *R*_t = 1.611 min, *m/z* = 569.1 [M + H]⁺.

7-((1H-Imidazol-1-yl)methyl)-2-(3,5-dimethoxybenzyl)-5-(1-methyl-3-(trifluoromethyl)-1H-pyrazol-4-yl)-3,4-dihydroisoquinolin-1(2H)-one (16).—

General Procedure F was followed using **52** (50.0 mg, 0.093 mmol, 1 equiv) and 1*H*-imidazole (25.3 mg, 0.37 mmol, 4 equiv), to obtain the title compound (27.3 mg, 52.0 μmol, 56% yield). ¹H NMR (400 MHz, CDCl₃) δ 8.11 (d, *J* = 2.0 Hz, 1H), 7.55 (s, 1H), 7.29 (s, 1H), 7.11–7.05 (m, 2H), 6.92 (s, 1H), 6.45 (d, *J* = 2.3 Hz, 2H), 6.37 (t, *J* = 2.2 Hz, 1H), 5.15 (s, 2H), 4.70 (s, 2H), 3.97 (s, 3H), 3.76 (s, 6H), 3.40 (t, *J* = 6.5 Hz, 2H), 2.72 (t, *J* = 6.5 Hz, 2H); LCMS (method 2, ESI): >95%. *R*_t = 1.537 min, *m/z* = 526.0 [M + H]⁺.

7-((1H-Pyrazol-1-yl)methyl)-2-(3,5-dimethoxybenzyl)-5-(1-methyl-3-(trifluoromethyl)-1H-pyrazol-4-yl)-3,4-dihydroisoquinolin-1(2H)-one (17).—

General Procedure F was followed using **52** (50 mg, 0.093 mmol, 1 equiv), and 1*H*-pyrazole (25.3 mg, 0.37 mmol, 4 equiv) to obtain the title compound (29.2 mg, 0.056 mmol, 60% yield). ¹H NMR (400 MHz, CDCl₃) δ 8.07 (d, *J* = 2.0 Hz, 1H), 7.53 (d, *J* = 1.9 Hz, 1H), 7.43 (d, *J* = 2.3 Hz, 1H), 7.30 (s, 1H), 7.16 (d, *J* = 2.0 Hz, 1H), 6.45 (d, *J* = 2.2 Hz, 2H), 6.36 (t, *J* = 2.3 Hz, 1H), 6.31–6.25 (m, 1H), 5.36 (s, 2H), 4.70 (s, 2H), 3.97 (s, 3H), 3.76 (s, 6H), 3.38 (t, *J* = 6.5 Hz, 2H), 2.70 (t, *J* = 6.5 Hz, 2H); LCMS (method 2, ESI): >95%, *R*_t = 1.789 min, *m/z* = 526.0 [M + H]⁺.

7-((1H-Pyrrol-1-yl)methyl)-2-(3,5-dimethoxybenzyl)-5-(1-methyl-3-(trifluoromethyl)-1H-pyrazol-4-yl)-3,4-dihydroisoquinolin-1(2H)-one (18).

—Sodium hydride (8.9 mg, 0.37 mmol, 4 equiv) was added to a solution of 1*H*-pyrrole (24.9 mg, 0.37 mmol, 4 equiv) in DMF (3 mL) at 0 °C in an ice bath. After the reaction mixture was stirred for 10 min, a solution of **52** (50.0 mg, 0.093 mmol, 1 equiv) in DMF (2 mL) was added. Then the mixture was stirred at 25 °C for 12 h. Saturated aqueous NaHCO₃ was added and the mixture was extracted with CH₂Cl₂. The combined organic phases were dried over anhydrous Na₂SO₄ and concentrated under reduced pressure. The residue was purified by preparative reversed-phase HPLC (Phenomenex Gemini C18, MeCN/H₂O = 15–70% gradient, 0.1% TFA) followed by neutralization with saturated aqueous NaHCO₃ to obtain the title compound (22.4 mg, 0.043 mmol, 46% yield). ¹H NMR (400 MHz, CDCl₃) δ 8.07 (d, *J* = 1.9 Hz, 1H), 7.29 (d, *J* = 1.1 Hz, 1H), 7.06 (d, *J* = 2.0 Hz, 1H), 6.69 (t, *J* = 2.1 Hz, 2H), 6.46 (d, *J* = 2.3 Hz, 2H), 6.37 (t, *J* = 2.3 Hz, 1H), 6.17 (t, *J* = 2.1 Hz, 2H), 5.10 (s, 2H), 4.70 (s, 2H), 3.96 (s, 3H), 3.76 (s, 6H), 3.43–3.36 (m, 2H), 2.70 (t, *J* = 6.5 Hz, 2H); LCMS (method 2, ESI): >95%, *R*_t = 1.963 min, *m/z* = 525.1 [M + H]⁺.

7-((4*H*-1,2,4-Triazol-4-yl)methyl)-2-(3,5-dimethoxybenzyl)-5-(1-methyl-3-(trifluoromethyl)-1*H*-pyrazol-4-yl)-3,4-dihydroisoquinolin-1(2*H*)-one (19).—

General Procedure F was followed using **52** (50 mg, 0.093 mmol, 1 equiv), and 1*H*-1,2,4-triazole (25.6 mg, 0.37 mmol, 4 equiv) to obtain the title compound (15.6 mg, 0.030 mmol, 32% yield). ¹H NMR (400 MHz, CDCl₃) δ 8.19 (s, 2H), 8.14 (d, *J* = 2.0 Hz, 1H), 7.32 (s, 1H), 7.11 (d, *J* = 2.0 Hz, 1H), 6.45 (d, *J* = 2.3 Hz, 2H), 6.37 (t, *J* = 2.3 Hz, 1H), 5.23 (s, 2H), 4.71 (s, 2H), 3.98 (s, 3H), 3.76 (s, 6H), 3.41 (t, *J* = 6.6 Hz, 2H), 2.74 (t, *J* = 6.6 Hz, 2H); LCMS (method 2, ESI): >95%, *R*_t = 1.570 min, *m/z* = 527.1 [M + H]⁺.

2-(3,5-Dimethoxybenzyl)-7-((2-methyl-1*H*-imidazol-1-yl)methyl)-5-(1-methyl-3-(trifluoromethyl)-1*H*-pyrazol-4-yl)-3,4-dihydroisoquinolin-1(2*H*)-one (20).—

General Procedure F was followed using **52** (50 mg, 0.093 mmol, 1 equiv), and 2-methyl-1*H*-imidazole (30.5 mg, 0.37 mmol, 4 equiv) to obtain the title compound (26.1 mg, 0.048 mmol, 52% yield). ¹H NMR (400 MHz, CDCl₃) δ 8.06 (d, *J* = 2.0 Hz, 1H), 7.28 (s, 1H), 6.95–6.89 (m, 2H), 6.85 (s, 1H), 6.46 (d, *J* = 2.3 Hz, 2H), 6.37 (t, *J* = 2.3 Hz, 1H), 5.09 (s, 2H), 4.70 (s, 2H), 3.97 (s, 3H), 3.76 (s, 6H), 3.40 (t, *J* = 6.5 Hz, 2H), 2.71 (t, *J* = 6.5 Hz, 2H), 2.34 (s, 3H); LCMS (method 2, ESI): >95%, *R*_t = 1.551 min, *m/z* = 540.1 [M + H]⁺.

2-(3,5-Dimethoxybenzyl)-7-((2-ethyl-1*H*-imidazol-1-yl)methyl)-5-(1-methyl-3-(trifluoromethyl)-1*H*-pyrazol-4-yl)-3,4-dihydroisoquinolin-1(2*H*)-one (21).—

General Procedure F was followed using **52** (50 mg, 0.093 mmol, 1 equiv), and 2-ethyl-1*H*-imidazole (35.7 mg, 0.37 mmol, 4 equiv) to obtain the title compound (28.2 mg, 0.051 mmol, 55% yield). ¹H NMR (400 MHz, CDCl₃) δ 8.06 (d, *J* = 2.0 Hz, 1H), 7.28 (s, 1H), 7.00–6.96 (m, 1H), 6.90 (d, *J* = 2.0 Hz, 1H), 6.87–6.83 (m, 1H), 6.45 (d, *J* = 2.3 Hz, 2H), 6.37 (t, *J* = 2.3 Hz, 1H), 5.10 (s, 2H), 4.70 (s, 2H), 3.97 (s, 3H), 3.76 (s, 6H), 3.39 (t, *J* = 6.5 Hz, 2H), 2.71 (t, *J* = 6.5 Hz, 2H), 2.63 (q, *J* = 7.5 Hz, 2H), 1.27 (d, *J* = 7.5 Hz, 3H); LCMS (method 2, ESI): >95%, *R*_t = 1.570 min, *m/z* = 554.1 [M + H]⁺.

2-(3,5-Dimethoxybenzyl)-7-((2-isopropyl-1*H*-imidazol-1-yl)methyl)-5-(1-methyl-3-(trifluoromethyl)-1*H*-pyrazol-4-yl)-3,4-dihydroisoquinolin-1(2*H*)-one (22).—General Procedure F was followed using **52** (50 mg, 0.093 mmol, 1 equiv),

and 2-isopropyl-1*H*-imidazole (40.9 mg, 0.37 mmol, 4 equiv) to obtain the title compound (26.4 mg, 0.047 mmol, 50% yield). ¹H NMR (400 MHz, CDCl₃) δ 8.09 (d, *J* = 2.0 Hz, 1H), 7.29 (s, 1H), 7.01 (d, *J* = 1.3 Hz, 1H), 6.90 (d, *J* = 2.0 Hz, 1H), 6.82 (d, *J* = 1.3 Hz, 1H), 6.48 (d, *J* = 2.2 Hz, 2H), 6.39 (t, *J* = 2.3 Hz, 1H), 5.16 (s, 2H), 4.73 (s, 2H), 3.99 (s, 3H), 3.79 (s, 6H), 3.42 (t, *J* = 6.5 Hz, 2H), 2.98 (p, *J* = 6.8 Hz, 1H), 2.73 (t, *J* = 6.5 Hz, 2H), 1.29 (s, 3H), 1.27 (s, 3H); LCMS (method 2, ESI): >95%, *R*_t = 1.602 min, *m/z* = 568.0 [M + H]⁺.

7-((2-Cyclopropyl-1*H*-imidazol-1-yl)methyl)-2-(3,5-dimethoxybenzyl)-5-(1-methyl-3-(trifluoromethyl)-1*H*-pyrazol-4-yl)-3,4-dihydroisoquinolin-1(2*H*)-one (23).—General Procedure F was followed using **52** (50 mg,

0.093 mmol, 1 equiv), and 2-cyclopropyl-1*H*-imidazole (40.1 mg, 0.37 mmol, 4 equiv) to obtain the title compound (30.0 mg, 0.053 mmol, 57% yield). ¹H NMR (400 MHz, CDCl₃) δ 8.11 (d, *J* = 2.0 Hz, 1H), 7.28 (d, *J* = 1.1 Hz, 1H), 6.97 (d, *J* = 2.0 Hz, 1H), 6.89 (d, *J* = 1.3 Hz, 1H), 6.83 (d, *J* = 1.4 Hz, 1H), 6.46 (d, *J* = 2.3 Hz, 2H), 6.37 (t, *J* = 2.3 Hz, 1H), 5.23 (s, 2H), 4.71 (s, 2H), 3.97 (s, 3H), 3.76 (s, 6H), 3.40 (t, *J* = 6.5 Hz, 2H), 2.71 (t, *J* = 6.5 Hz, 2H), 1.71 (tt, *J* = 8.2, 5.0 Hz, 1H), 0.98–0.94 (m, 2H), 0.90–0.86 (m, 2H); LCMS (method 2, ESI): >95%, *R*_t = 1.596 min, *m/z* = 566.1 [M + H]⁺.

7-((2-(Difluoromethyl)-1*H*-imidazol-1-yl)methyl)-2-(3,5-dimethoxybenzyl)-5-(1-methyl-3-(trifluoromethyl)-1*H*-pyrazol-4-yl)-3,4-dihydroisoquinolin-1(2*H*)-one (24).—General Procedure F was followed using **52** (50 mg, 0.093 mmol, 1 equiv),

2-(difluoromethyl)-1*H*-imidazole (43.9 mg, 0.37 mmol, 4 equiv), potassium carbonate (25.7 mg, 0.19 mmol, 2 equiv), and sodium iodide (6.9 mg, 0.046 mmol, 0.5 equiv) to obtain the title compound (26.2 mg, 0.046 mmol, 49% yield). ¹H NMR (400 MHz, CDCl₃) δ 8.12 (s, 1H), 7.30 (s, 1H), 7.08 (d, *J* = 17.1 Hz, 2H), 6.96 (s, 1H), 6.76 (t, *J* = 52.7 Hz, 1H), 6.48–6.42 (m, 2H), 6.37 (s, 1H), 5.35 (s, 2H), 4.70 (s, 2H), 3.97 (s, 3H), 3.76 (s, 6H), 3.40 (t, *J* = 6.5 Hz, 2H), 2.72 (t, *J* = 6.5 Hz, 2H); LCMS (method 2, ESI): >95%, *R*_t = 1.666 min, *m/z* = 576.0 [M + H]⁺.

7-((2-Methyl-1*H*-imidazol-1-yl)methyl)-5-(1-methyl-3-(trifluoromethyl)-1*H*-pyrazol-4-yl)-2-(pyridin-2-ylmethyl)-3,4-dihydroisoquinolin-1(2*H*)-one (25).—

General Procedure G was followed using **57** (20 mg, 0.051 mmol, 1 equiv), and 2-(bromomethyl)pyridine (7.9 mg, 0.0463 mmol, 1.2 equiv) to obtain the title compound (10.1 mg, 0.021 mmol, 41% yield). ¹H NMR (400 MHz, CD₃OD) δ 8.71 (d, *J* = 5.2 Hz, 1H), 8.28 (td, *J* = 8.0, 1.6 Hz, 1H), 7.97 (d, *J* = 2.0 Hz, 1H), 7.83 (s, 1H), 7.81 (s, 1H), 7.74 (t, *J* = 6.4 Hz, 1H), 7.56 (d, *J* = 2.0 Hz, 1H), 7.51 (d, *J* = 2.0 Hz, 1H), 7.42 (d, *J* = 1.6 Hz, 1H), 5.50 (s, 2H), 5.03 (s, 2H), 4.03 (s, 3H), 3.72 (t, *J* = 6.8 Hz, 2H), 2.97 (t, *J* = 6.4 Hz, 2H), 2.64 (s, 3H); LCMS (method 2, ESI): >95%, *R*_t = 1.109 min, *m/z* = 481.0 [M + H]⁺.

7-((2-Methyl-1*H*-imidazol-1-yl)methyl)-5-(1-methyl-3-(trifluoromethyl)-1*H*-pyrazol-4-yl)-2-((6-methylpyridin-3-yl)methyl)-3,4-dihydroisoquinolin-1(2*H*)-one (26).—General Procedure G was followed using **57** (20 mg,

0.051 mmol, 1 equiv), and 2-(chloromethyl)-6-methylpyridine (8.0 mg, 0.0565 mmol, 1.1 equiv) to obtain the title compound (14 mg, 0.028 mmol, 55% yield). ¹H NMR (400 MHz, CDCl₃) δ 8.06 (d, *J* = 1.6 Hz, 1H), 7.56–7.52 (m, 1H), 7.30

(s, 1H), 7.17 (d, $J = 7.6$ Hz, 1H), 7.06 (d, $J = 7.6$ Hz, 1H), 6.95–6.92 (m, 2H), 6.86 (s, 1H), 5.09 (s, 2H), 4.86 (s, 2H), 3.98 (s, 3H), 3.56 (t, $J = 6.8$ Hz, 2H), 2.77 (t, $J = 6.8$ Hz, 2H), 2.53 (s, 3H), 2.35 (s, 3H); LCMS (method 2, ESI): >95%, $R_t = 1.282$ min, $m/z = 495.0$ [M + H]⁺.

7-((2-Methyl-1H-imidazol-1-yl)methyl)-5-(1-methyl-3-(trifluoromethyl)-1H-pyrazol-4-yl)-2-((4-methylpyridin-2-yl)methyl)-3,4-dihydroisoquinolin-1(2H)-one (27).—General Procedure G was followed using **57** (10 mg,

0.0256 mmol, 1 equiv), and 2-(bromomethyl)-4-methylpyridine (5.2 mg, 0.028 mmol, 1.1 equiv) to obtain the title compound (3.7 mg, 0.007 mmol, 29% yield). ¹H NMR (400 MHz, CDCl₃) δ 8.38 (d, $J = 5.2$ Hz, 1H), 8.07 (d, $J = 1.6$ Hz, 1H), 7.33 (s, 1H), 7.20 (s, 1H), 7.08 (s, 1H), 7.02 (d, $J = 4.8$ Hz, 1H), 6.96 (d, $J = 1.6$ Hz, 1H), 6.93 (d, $J = 1.6$ Hz, 1H), 5.14 (s, 2H), 4.84 (s, 2H), 4.00 (s, 3H), 3.59 (t, $J = 6.4$ Hz, 2H), 2.78 (t, $J = 6.4$ Hz, 2H), 2.52 (s, 3H), 2.33 (s, 3H); LCMS (method 2, ESI): >95%, $R_t = 1.091$ min, $m/z = 495.0$ [M + H]⁺.

7-((2-Methyl-1H-imidazol-1-yl)methyl)-5-(1-methyl-3-(trifluoromethyl)-1H-pyrazol-4-yl)-2-((3-methylpyridin-2-yl)methyl)-3,4-dihydroisoquinolin-1(2H)-one (28).—General Procedure G was followed using **57** (20 mg, 0.0514

mmol, 1 equiv), and 2-(chloromethyl)-3-methylpyridine (8.0 mg, 0.0565 mmol, 1.1 equiv) to obtain the title compound (13 mg, 0.026 mmol, 51% yield). ¹H NMR (400 MHz, CD₃OD) δ 8.52 (d, $J = 5.6$ Hz, 1H), 8.20–8.13 (m, 1H), 7.96 (d, $J = 2.4$ Hz, 1H), 7.82 (s, 1H), 7.71–7.66 (m, 1H), 7.55 (d, $J = 2.0$ Hz, 1H), 7.51 (d, $J = 2.0$ Hz, 1H), 7.42 (s, 1H), 5.50 (s, 2H), 5.03 (d, $J = 4.4$ Hz, 2H), 4.02 (s, 3H), 3.70 (t, $J = 6.4$ Hz, 2H), 2.97 (t, $J = 4.4$ Hz, 2H), 2.64 (s, 3H), 2.55 (s, 3H); LCMS (method 2, ESI): >95%, $R_t = 1.302$ min, $m/z = 495.0$ [M + H]⁺.

7-((2-Methyl-1H-imidazol-1-yl)methyl)-5-(1-methyl-3-(trifluoromethyl)-1H-pyrazol-4-yl)-2-((2-methylpyridin-4-yl)methyl)-3,4-dihydroisoquinolin-1(2H)-one (29).—General Procedure G was followed using **57** (20 mg,

0.026 mmol, 1 equiv), and 4-(bromomethyl)-2-methylpyridine (5.2 mg, 0.0283 mmol, 1.1 equiv) to obtain the title compound (13 mg, 0.017 mmol, 65% yield). ¹H NMR (400 MHz, CDCl₃) δ 8.45 (d, $J = 5.2$ Hz, 1H), 8.07 (d, $J = 2.0$ Hz, 1H), 7.30 (s, 1H), 7.09 (s, 1H), 7.04 (d, $J = 4.8$ Hz, 1H), 6.95–6.94 (m, 2H), 6.86 (d, $J = 1.2$ Hz, 1H), 5.10 (s, 2H), 4.73 (s, 2H), 3.98 (s, 3H), 3.42 (t, $J = 6.8$ Hz, 2H), 2.76 (t, $J = 6.8$ Hz, 2H), 2.54 (s, 3H), 2.35 (s, 3H); LCMS (method 2, ESI): >95%, $R_t = 1.136$ min, $m/z = 495.0$ [M + H]⁺.

2-((4-Methoxypyridin-2-yl)methyl)-7-((2-methyl-1H-imidazol-1-yl)methyl)-5-(1-methyl-3-(trifluoromethyl)-1H-pyrazol-4-yl)-3,4-dihydroisoquinolin-1(2H)-one (30).—General Procedure G was followed using **57** (50 mg, 0.13 mmol, 1 equiv),

and 2-(chloromethyl)-4-methoxypyridine (22 mg, 0.14 mmol, 1.1 equiv) to obtain the title compound (15.6 mg, 0.031 mmol, 25% yield). ¹H NMR (400 MHz, CDCl₃) δ 8.35 (d, $J = 5.8$ Hz, 1H), 8.07 (d, $J = 1.9$ Hz, 1H), 7.34 (s, 1H), 7.18 (d, $J = 2.2$ Hz, 1H), 6.97 (s, 2H), 6.92 (d, $J = 2.1$ Hz, 1H), 6.75 (dd, $J = 5.7, 2.2$ Hz, 1H), 5.17 (s, 2H), 4.84 (s, 2H), 4.01 (s, 3H), 3.85 (s, 3H), 3.62 (t, $J = 6.6$ Hz, 2H), 2.81 (t, $J = 6.6$ Hz, 2H), 2.64 (s, 3H); LCMS (method 2, ESI): >95%, $R_t = 1.159$ min, $m/z = 511.0$ [M + H]⁺.

2-((4-Ethylpyridin-2-yl)methyl)-7-((2-methyl-1H-imidazol-1-yl)methyl)-5-(1-methyl-3-(trifluoromethyl)-1H-pyrazol-4-yl)-3,4-dihydroisoquinolin-1(2H)-one

(31).—General Procedure G was followed using **57** (50 mg, 0.13 mmol, 1 equiv), and 2-(chloromethyl)-4-ethylpyridine (22 mg, 0.14 mmol, 1.1 equiv) to obtain the title compound (46.2 mg, 0.091 mmol, 71% yield). ¹H NMR (400 MHz, CDCl₃) δ 8.40 (d, *J* = 5.1 Hz, 1H), 8.07 (s, 1H), 7.31 (s, 1H), 7.21 (s, 1H), 7.05–7.04 (m, 2H), 6.94 (d, *J* = 1.2 Hz, 1H), 6.87 (s, 1H), 5.13 (s, 2H), 4.87 (s, 2H), 3.99 (s, 3H), 3.59 (t, *J* = 6.6 Hz, 2H), 2.77 (t, *J* = 6.5 Hz, 2H), 2.63 (q, *J* = 7.6 Hz, 2H), 2.48 (s, 3H), 1.23 (t, *J* = 7.6 Hz, 3H); LCMS (method 2, ESI): >95%, *R*_t = 1.186 min, *m/z* = 509.1 [M + H]⁺.

5-(1-Ethyl-3-(trifluoromethyl)-1H-pyrazol-4-yl)-2-((4-methoxy-pyridin-2-yl)methyl)-7-((2-methyl-1H-imidazol-1-yl)methyl)-3,4-dihydroisoquinolin-1(2H)-one (32).—General Procedure G was followed using

58 (50 mg, 0.12 mmol, 1 equiv), and 2-(chloromethyl)-4-methoxypyridine (21 mg, 0.14 mmol, 1.1 equiv) to obtain the title compound (45.5 mg, 0.087 mmol, 70% yield). ¹H NMR (400 MHz, CDCl₃) δ 8.35 (d, *J* = 5.6 Hz, 1H), 8.06 (s, 1H), 7.35 (s, 1H), 7.16–7.06 (m, 1H), 6.97 (s, 1H), 6.91 (s, 2H), 6.74 (s, 1H), 5.13 (s, 2H), 4.84 (s, 2H), 4.25 (q, *J* = 7.2 Hz, 2H), 3.84 (s, 3H), 3.86 (brs, 2H), 2.79 (brs, 2H), 2.52 (brs, 3H), 1.56 (t, *J* = 7.3 Hz, 3H); LCMS (method 2, ESI): >95%, *R*_t = 1.201 min, *m/z* = 525.0 [M + H]⁺.

5-(1-Ethyl-3-(trifluoromethyl)-1H-pyrazol-4-yl)-2-((4-ethylpyridin-2-yl)methyl)-7-((2-methyl-1H-imidazol-1-yl)methyl)-3,4-dihydroisoquinolin-1(2H)-one (33).—General Procedure G was followed

using **58** (50 mg, 0.12 mmol, 1 equiv), and 2-(chloromethyl)-4-ethylpyridine (21 mg, 0.14 mmol, 1.1 equiv) to obtain the title compound (46 mg, 0.088 mmol, 71% yield). ¹H NMR (400 MHz, CDCl₃) δ 8.40 (d, *J* = 5.1 Hz, 1H), 8.07 (d, *J* = 1.9 Hz, 1H), 7.34 (s, 1H), 7.21 (s, 1H), 7.07 (s, 1H), 7.04 (dd, *J* = 5.1, 1.5 Hz, 1H), 6.96 (d, *J* = 1.9 Hz, 1H), 6.92 (s, 1H), 5.13 (s, 2H), 4.86 (s, 2H), 4.25 (q, *J* = 7.3 Hz, 2H), 3.59 (t, *J* = 6.6 Hz, 2H), 2.77 (t, *J* = 6.6 Hz, 2H), 2.63 (q, *J* = 7.6 Hz, 2H), 2.51 (s, 3H), 1.56 (t, *J* = 7.3 Hz, 3H), 1.23 (t, *J* = 7.6 Hz, 3H); LCMS (method 2, ESI): >95%, *R*_t = 1.271 min, *m/z* = 523.0 [M + H]⁺.

(S)-5-(1-Ethyl-3-(trifluoromethyl)-1H-pyrazol-4-yl)-2-(1-(4-methoxy-pyridin-2-yl)ethyl)-7-((2-methyl-1H-imidazol-1-yl)methyl)-3,4-dihydroisoquinolin-1(2H)-one (34).—General Procedure F was followed using **73** (60 mg, 0.11

mmol, 1 equiv) and 2-methyl-1*H*-imidazole (18 mg, 0.22 mmol, 2 equiv) to obtain the title compound (21 mg, 0.04 mmol, 35% yield). ¹H NMR (400 MHz, CDCl₃) δ 8.39 (d, *J* = 5.4 Hz, 1H), 8.06 (d, *J* = 1.4 Hz, 1H), 7.31 (s, 1H), 6.97–6.96 (m, 2H), 6.93 (d, *J* = 2.4 Hz, 1H), 6.88 (d, *J* = 1.4 Hz, 1H), 6.74 (dd, *J* = 5.4, 1.4 Hz, 1H), 6.12 (q, *J* = 7.1 Hz, 1H), 5.11 (s, 2H), 4.25 (q, *J* = 7.4 Hz, 2H), 3.85 (s, 3H), 3.53–3.46 (m, 1H), 3.40–3.33 (m, 1H), 2.73–2.60 (m, 2H), 2.38 (s, 3H), 1.64 (t, *J* = 7.1 Hz, 3H), 1.57 (t, *J* = 7.4 Hz, 3H); LCMS (method 1, ESI): >95%, *R*_t = 1.04 min, *m/z* = 538.9 [M + H]⁺.

(R)-5-(1-Ethyl-3-(trifluoromethyl)-1H-pyrazol-4-yl)-2-(1-(4-methoxy-pyridin-2-yl)ethyl)-7-((2-methyl-1H-imidazol-1-yl)methyl)-3,4-dihydroisoquinolin-1(2H)-one (35).—General Procedure F was followed using **74** (50 mg, 0.093 mmol, 1

equiv) and 2-methyl-1*H*-imidazole (31 mg, 0.37 mmol, 4 equiv) to obtain the title compound (36.6 mg, 0.068 mmol, 73% yield). ¹H NMR (400 MHz, DMSO-*d*₆) δ 8.35–8.33 (m,

1H), 8.07 (s, 1H), 7.78 (s, 1H), 7.13 (s, 1H), 7.12 (s, 1H), 6.89–7.87 (m, 2H), 6.76 (s, 1H), 5.87 (q, $J = 7.0$ Hz, 1H), 5.22 (s, 2H), 4.23 (q, $J = 7.2$ Hz, 2H), 3.81 (s, 3H), 3.43–3.35 (m, 1H), 3.29–3.21 (m, 1H), 2.66 (t, $J = 6.3$ Hz, 2H), 2.20 (s, 3H), 1.51 (d, $J = 7.1$ Hz, 3H), 1.42 (t, $J = 7.3$ Hz, 3H); LCMS (method 2, ESI): >95%, $R_t = 1.244$ min, $m/z = 539.1$ [M + H]⁺.

(S)-2-(Cyclopropyl(4-methoxy-pyridin-2-yl)methyl)-5-(1-ethyl-3-(trifluoromethyl)-1H-pyrazol-4-yl)-7-((2-methyl-1H-imidazol-1-yl)methyl)-3,4-dihydroisoquinolin-1(2H)-one (36).—General Procedure F

was followed using **S18** (150 mg, 0.27 mmol, 1 equiv) and 2-methyl-1*H*-imidazole (44 mg, 0.54 mmol, 2 equiv) to obtain the title compound (23 mg, 0.04 mmol, 15% yield). ¹H NMR (400 MHz, CDCl₃) δ 8.37 (d, $J = 5.7$ Hz, 1H), 8.00 (d, $J = 1.2$ Hz, 1H), 7.30 (s, 1H), 6.97 (d, $J = 2.3$ Hz, 1H), 6.93 (s, 2H), 6.85 (s, 1H), 6.71 (dd, $J = 5.7, 2.4$ Hz, 1H), 5.07 (s, 2H), 5.04 (d, $J = 10.2$ Hz, 1H), 4.23 (q, $J = 7.3$ Hz, 2H), 3.83 (s, 3H), 3.75–3.62 (m, 2H), 2.77–2.64 (m, 2H), 2.34 (s, 3H), 1.55 (t, $J = 7.3$ Hz, 3H), 0.81–0.75 (m, 1H), 0.64–0.58 (m, 1H), 0.55–0.48 (m, 2H); LCMS (method 2, ESI): >95%, $R_t = 0.78$ min, $m/z = 565.0$ [M + H]⁺.

(S)-2-(Cyclopropyl(4-methylpyridin-2-yl)methyl)-5-(1-ethyl-3-(trifluoromethyl)-1H-pyrazol-4-yl)-7-((2-methyl-1H-imidazol-1-yl)methyl)-3,4-dihydroisoquinolin-1(2H)-one (37).—General Procedure

F was followed using **S19** (102 mg, 0.19 mmol, 1 equiv) and 2-methyl-1*H*-imidazole (46 mg, 0.56 mmol, 3 equiv) to obtain the title compound (67.0 mg, 0.12 mmol, 65% yield). ¹H NMR (400 MHz, CD₃OD) δ 8.58 (d, $J = 6.0$ Hz, 1H), 8.03 (s, 1H), 7.93 (d, $J = 2.0$ Hz, 1H), 7.87 (s, 1H), 7.74 (d, $J = 5.6$ Hz, 1H), 7.54 (d, $J = 2.0$ Hz, 1H), 7.51 (d, $J = 2.0$ Hz, 1H), 7.42 (d, $J = 1.2$ Hz, 1H), 5.49 (s, 2H), 4.90 (s, 1H), 4.32 (q, $J = 7.2$ Hz, 2H), 3.86–3.80 (m, 1H), 3.75–3.68 (m, 1H), 2.96 (t, $J = 6.4$ Hz, 2H), 2.66 (s, 3H), 2.63 (s, 3H), 1.71–1.62 (m, 1H), 1.55 (t, $J = 7.2$ Hz, 3H), 0.99–0.95 (m, 1H), 0.87–0.82 (m, 1H), 0.70–0.63 (m, 2H); LCMS (method 2, ESI): >95%, $R_t = 1.197$ min, $m/z = 549.0$ [M + H]⁺.

(S)-7-((1H-imidazol-1-yl)methyl)-5-(1-ethyl-3-(trifluoromethyl)-1H-pyrazol-4-yl)-2-(1-(4-methoxy-pyridin-2-yl)ethyl)-3,4-dihydroisoquinolin-1(2H)-one (38).—

General Procedure F was followed using **73** (50 mg, 0.09 mmol, 1 equiv) and 1*H*-imidazole (12 mg, 0.18 mmol, 2 equiv) to obtain the title compound (8 mg, 0.015 mmol, 16% yield). ¹H NMR (400 MHz, CDCl₃) δ 8.36 (d, $J = 5.8$ Hz, 1H), 8.09 (d, $J = 1.7$ Hz, 1H), 7.57 (s, 1H), 7.31 (s, 1H), 7.09 (s, 2H), 6.92 (s, 1H), 6.91 (d, $J = 2.4$ Hz, 1H), 6.72 (dd, $J = 5.7, 2.4$ Hz, 1H), 6.10 (q, $J = 7.0$ Hz, 1H), 5.15 (s, 2H), 4.23 (q, $J = 7.3$ Hz, 2H), 3.82 (s, 3H), 3.51–3.44 (m, 1H), 3.30–3.32 (m, 1H), 2.72–2.58 (m, 2H), 1.62 (d, $J = 7.1$ Hz, 3H), 1.54 (t, $J = 7.3$ Hz, 3H); LCMS (method 2, ESI): >95%, $R_t = 1.04$ min, $m/z = 525.0$ [M + H]⁺.

(R)-7-((1H-imidazol-1-yl)methyl)-5-(1-ethyl-3-(trifluoromethyl)-1H-pyrazol-4-yl)-2-(1-(4-methoxy-pyridin-2-yl)ethyl)-3,4-dihydroisoquinolin-1(2H)-one (39).—

General Procedure F was followed using **74** (50 mg, 0.093 mmol, 1 equiv) and 1*H*-imidazole (25 mg, 0.37 mmol, 4 equiv) to obtain the title compound (35.5 mg, 0.068 mmol, 73% yield). ¹H NMR (400 MHz, DMSO-*d*₆) δ 8.34 (d, $J = 6.6$ Hz, 1H), 8.07 (s, 1H), 7.89 (s, 1H), 7.76 (s, 1H), 7.30 (s, 1H), 7.18 (s, 1H), 6.90–6.87 (m, 3H), 5.87 (q, $J = 7.2$ Hz, 1H), 5.26 (s, 2H), 4.24 (q, $J = 7.3$ Hz, 2H), 3.81 (s, 3H),

3.40–3.35 (m, 1H), 3.27–3.20 (m, 1H), 2.65 (t, $J = 6.5$ Hz, 2H), 1.51 (d, $J = 7.1$ Hz, 3H), 1.42 (t, $J = 7.3$ Hz, 3H); LCMS (method 2, ESI): $R_t = 1.216$ min, $m/z = 525.1$ [M + H]⁺.

(S)-7-((1H-Imidazol-1-yl)methyl)-2-(cyclopropyl(4-methoxypyridin-2-yl)methyl)-5-(1-ethyl-3-(trifluoromethyl)-1H-pyrazol-4-yl)-3,4-dihydroisoquinolin-1(2H)-one (40).—General Procedure

F was followed using **S18** (150 mg, 0.27 mmol, 1 equiv) and 1*H*-imidazole (37 mg, 0.54 mmol, 2 equiv) to obtain the title compound (24 mg, 0.04 mmol, 16% yield). ¹H NMR (400 MHz, CDCl₃) δ 8.37 (d, $J = 5.7$ Hz, 1H), 8.05 (s, 1H), 7.54 (s, 1H), 7.31 (s, 1H), 7.07 (s, 2H), 6.97 (d, $J = 2.3$ Hz, 1H), 6.91 (s, 1H), 6.72 (dd, $J = 2.4$ Hz, 1H), 5.13 (s, 2H), 5.04 (d, $J = 10.2$ Hz, 1H), 4.24 (q, $J = 7.3$ Hz, 2H), 3.84 (s, 3H), 3.76–3.62 (m, 2H), 2.76–2.65 (m, 2H), 1.55 (t, $J = 7.3$ Hz, 3H), 0.81–0.75 (m, 1H), 0.64–0.58 (m, 1H), 0.55–0.48 (m, 2H); LCMS (method 2, ESI): >95%, $R_t = 1.20$ min, $m/z = 551.5$ [M + H]⁺.

(S)-7-((1H-Imidazol-1-yl)methyl)-2-(cyclopropyl(4-methylpyridin-2-yl)methyl)-5-(1-ethyl-3-(trifluoromethyl)-1H-pyrazol-4-yl)-3,4-dihydroisoquinolin-1(2H)-one (41).—General Procedure F was

followed using **S19** (30 mg, 0.055 mmol, 1 equiv) and 1*H*-imidazole (11 mg, 0.17 mmol, 3 equiv) to obtain the title compound (7.8 mg, 0.015 mmol, 27% yield). ¹H NMR (400 MHz, CDCl₃) δ 8.41 (d, $J = 5.2$ Hz, 1H), 8.06 (d, $J = 2.0$ Hz, 1H), 7.53 (s, 1H), 7.31 (s, 1H), 7.24 (s, 1H), 7.08 (d, $J = 2.4$ Hz, 2H), 7.01 (d, $J = 4.4$ Hz, 1H), 6.91 (s, 1H), 5.13 (s, 2H), 5.07 (d, $J = 10.0$ Hz, 1H), 4.25 (q, $J = 7.2$ Hz, 2H), 3.76–3.63 (m, 2H), 2.76–2.65 (m, 2H), 2.33 (s, 3H), 1.66–1.62 (m, 1H), 1.55 (t, $J = 7.2$ Hz, 3H), 0.80–0.75 (m, 1H), 0.63–0.59 (m, 1H), 0.54–0.51 (m, 2H); LCMS (method 2, ESI): >95%, $R_t = 1.306$ min, $m/z = 535.0$ [M + H]⁺.

Methyl 2-(3,5-dimethoxybenzyl)-5-hydroxy-1-oxo-1,2,3,4-tetrahydroisoquinoline-7-carboxylate (43).—General Procedure A was followed using

42 (15.0 g, 59.5 mmol, 1 equiv), 3,5-dimethoxybenzylamine (13.4 mL, 89.2 mmol, 1.5 equiv), and sodium triacetoxyborohydride (25.2 g, 118.9 mmol, 2 equiv) to obtain the title compound (22 g, 59.2 mmol, 99% yield). ¹H NMR (400 MHz, CDCl₃) δ 8.81 (d, $J = 1.6$ Hz, 1H), 8.03 (d, $J = 1.6$ Hz, 1H), 6.45 (d, $J = 2.3$ Hz, 2H), 6.38 (t, $J = 2.3$ Hz, 1H), 4.72 (s, 2H), 3.95 (s, 3H), 3.76 (s, 6H), 3.53 (t, $J = 6.6$ Hz, 2H), 3.06 (t, $J = 6.6$ Hz, 2H); LCMS (method 2, ESI): $R_t = 1.624$ min, $m/z = 372.1$ [M + H]⁺.

Methyl 2-(3,5-dimethoxybenzyl)-1-oxo-5-(((trifluoromethyl)sulfonyl)oxy)-1,2,3,4-tetrahydroisoquinoline-7-carboxylate (44).—General

Procedure B was followed using **43** (15.0 g, 40.4 mmol, 1 equiv), phenyl triflimide (17 g, 48.5 mmol, 1.2 equiv), and *N,N*-diisopropylethylamine (18 mL, 101.0 mmol, 2.5 equiv) to obtain the title compound (16.1 g, 31.9 mmol, 79% yield). ¹H NMR (400 MHz, CDCl₃) δ 8.83 (d, $J = 1.6$ Hz, 1H), 8.04 (d, $J = 1.6$ Hz, 1H), 6.47 (d, $J = 2.3$ Hz, 2H), 6.39 (t, $J = 2.3$ Hz, 1H), 4.73 (s, 2H), 3.96 (s, 3H), 3.77 (s, 6H), 3.54 (t, $J = 6.6$ Hz, 2H), 3.07 (t, $J = 6.6$ Hz, 2H); LCMS (method 2, ESI): $R_t = 2.069$ min, $m/z = 504.0$ [M + H]⁺.

Methyl 2-(3,5-dimethoxybenzyl)-1-oxo-5-(4,4,5,5-tetramethyl-1,3,2-dioxaborolan-2-yl)-1,2,3,4-tetrahydroisoquinoline-7-carboxylate (45).—

Compound **44** (7.55 g, 15.0 mmol, 1 equiv), bis-(pinacolato)diboron (7.61 g, 30.0 mmol, 2 equiv), KOAc (4.41 g, 45.0 mmol, 3 equiv), and PdCl₂(dppf)·CH₂Cl₂ (0.612 g, 0.75 mmol) were dissolved in 1,4-dioxane (40 mL) and placed under an Ar atmosphere. The reaction mixture was stirred at 100 °C overnight. Brine was added to the cooled mixture and extracted with EtOAc. The combined organic layers were dried over MgSO₄ and concentrated under reduced pressure. The residue was purified by flash chromatography (Combi-flash Rf, EtOAc/hexanes = 0–50% gradient) to afford the title compound (7.15 g, 14.9 mmol, 99% yield). ¹H NMR (400 MHz, CDCl₃) δ 8.87 (d, *J* = 2.0 Hz, 1H), 8.57 (d, *J* = 2.0 Hz, 1H), 6.48 (d, *J* = 2.3 Hz, 2H), 6.37 (t, *J* = 2.3 Hz, 1H), 4.73 (s, 2H), 3.93 (s, 3H), 3.76 (s, 6H), 3.47 (t, *J* = 6.6 Hz, 2H), 3.32 (t, *J* = 6.6 Hz, 2H), 1.33 (s, 12H); LCMS (method 2, ESI): *R*_t = 2.200 min, *m/z* = 482.1 [M + H]⁺.

Methyl 5-bromo-2-(3,5-dimethoxybenzyl)-1-oxo-1,2,3,4-tetrahydroisoquinoline-7-carboxylate (46).—

A mixture of **45** (6.68 g, 13.9 mmol, 1 equiv), copper(II) bromide (9.30 g, 41.6 mmol, 3 equiv) and MeOH/H₂O (1:1 v/v, 160 mL) was stirred and refluxed at 80 °C. The mixture was cooled to room temperature and diluted with EtOAc. The layers were separated, and the aqueous layer was extracted with EtOAc. The combined organic layers were dried over MgSO₄ and concentrated under reduced pressure. The residue was purified by flash chromatography (Combi-flash Rf, EtOAc/hexanes = 0–50% gradient) to afford the title compound (5.43 g, 12.5 mmol, 90% yield). ¹H NMR (400 MHz, CDCl₃) δ 8.75 (d, *J* = 1.7 Hz, 1H), 8.33 (d, *J* = 1.7 Hz, 1H), 6.46 (d, *J* = 2.3 Hz, 2H), 6.38 (t, *J* = 2.3 Hz, 1H), 4.72 (s, 2H), 3.94 (s, 3H), 3.77 (s, 6H), 3.51 (t, *J* = 6.7 Hz, 2H), 3.07 (t, *J* = 6.7 Hz, 2H); LCMS (method 2, ESI): *R*_t = 1.971 min, *m/z* = 433.9 [M + H]⁺.

5-Bromo-2-(3,5-dimethoxybenzyl)-7-(hydroxymethyl)-3,4-dihydroisoquinolin-1(2H)-one (47).—

General Procedure C was followed using **46** (5.43 g, 12.5 mmol, 1 equiv) to obtain the title compound (2.07 g, 5.1 mmol, 41% yield). ¹H NMR (400 MHz, CDCl₃) δ 8.08 (d, *J* = 1.6 Hz, 1H), 7.74 (d, *J* = 1.7 Hz, 1H), 6.46 (d, *J* = 2.3 Hz, 2H), 6.38 (t, *J* = 2.3 Hz, 1H), 4.73 (d, *J* = 6.0 Hz, 2H), 4.72 (s, 2H), 3.82 (s, 1H), 3.77 (s, 6H), 3.49 (t, *J* = 6.7 Hz, 2H), 3.02 (t, *J* = 6.7 Hz, 2H); LCMS (method 2, ESI): *R*_t = 1.686 min, *m/z* = 406.0 [M + H]⁺.

5-Bromo-7-(bromomethyl)-2-(3,5-dimethoxybenzyl)-3,4-dihydroisoquinolin-1(2H)-one (48).—

General Procedure C was followed using **47** (2.07 g, 5.10 mmol, 1 equiv) to obtain the title compound (992 mg, 2.11 mmol, 42% yield). ¹H NMR (400 MHz, CDCl₃) δ 8.14 (d, *J* = 1.9 Hz, 1H), 7.72 (d, *J* = 1.9 Hz, 1H), 6.46 (d, *J* = 2.3 Hz, 2H), 6.38 (t, *J* = 2.3 Hz, 1H), 4.71 (s, 2H), 4.46 (s, 2H), 3.77 (s, 6H), 3.49 (t, *J* = 6.7 Hz, 2H), 3.02 (t, *J* = 6.7 Hz, 2H); LCMS (method 2, ESI): *R*_t = 2.010 min, *m/z* = 467.8 [M + H]⁺.

5-Bromo-2-(3,5-dimethoxybenzyl)-7-((2-imino-3-methyl-2,3-dihydro-1H-imidazol-1-yl)methyl)-3,4-dihydroisoquinolin-1(2H)-one (49).—

1-Methyl-1*H*-imidazol-2-amine hydrochloride (847 mg, 6.34 mmol, 3 equiv) was added to a solution of **48** (992 mg, 2.11 mmol,

1 equiv), and *N,N*-diisopropylethylamine (1.5 mL, 8.46 mmol, 4 equiv) in acetonitrile (18 mL) at 23 °C. The reaction mixture was stirred for 12 h at 60 °C, then cooled to ambient temperature and concentrated under reduced pressure. Saturated aqueous NaHCO₃ was added and the mixture was extracted with CH₂Cl₂. The combined organic layers were dried over MgSO₄ and concentrated under reduced pressure to provide the title compound (1.03 g, 2.11 mmol, quant.), which was used in the next step without further purification. ¹H NMR (400 MHz, CDCl₃) δ 7.90 (d, *J* = 1.6 Hz, 1H), 7.77 (d, *J* = 1.7 Hz, 1H), 6.74 (d, *J* = 2.5 Hz, 1H), 6.63 (d, *J* = 2.5 Hz, 1H), 6.44 (d, *J* = 2.2 Hz, 2H), 6.41 (t, *J* = 2.2 Hz, 1H), 4.91 (s, 2H), 4.62 (s, 2H), 3.71 (s, 6H), 3.50 (t, *J* = 6.7 Hz, 2H), 3.22 (s, 3H), 2.97 (t, *J* = 6.6 Hz, 2H); LCMS (method 2, ESI): *R*_t = 1.518 min, *m/z* = 484.9 [M + H]⁺.

Methyl 2-(3,5-dimethoxybenzyl)-5-(1-methyl-3-(trifluoromethyl)-1H-pyrazol-4-yl)-1-oxo-1,2,3,4-tetrahydroisoquinoline-7-carboxylate (50).—General Procedure E was followed using **44** (7.0 g, 13.9 mmol, 1 equiv), (1-methyl-3-(trifluoromethyl)-1*H*-pyrazol-4-yl)boronic acid (4.1 g, 20.9 mmol, 1.5 equiv), potassium carbonate (4.8 g, 34.8 mmol, 2.5 equiv), and PdCl₂(dppf) (814.0 mg, 1.2 mmol, 0.08 equiv) to obtain the title compound (5.95 g, 11.8 mmol, 85% yield). ¹H NMR (400 MHz, CDCl₃) δ 8.77 (d, *J* = 1.9 Hz, 1H), 7.95 (d, *J* = 1.9 Hz, 1H), 7.33–7.27 (m, 1H), 6.40 (d, *J* = 2.3 Hz, 2H), 6.30 (t, *J* = 2.3 Hz, 1H), 4.66 (s, 2H), 3.94 (s, 3H), 3.86 (s, 3H), 3.70 (s, 6H), 3.35 (t, *J* = 6.5 Hz, 2H), 2.71 (t, *J* = 6.5 Hz, 2H); LCMS (method 2, ESI): *R*_t = 1.878 min, *m/z* = 504.0 [M + H]⁺.

2-(3,5-Dimethoxybenzyl)-7-(hydroxymethyl)-5-(1-methyl-3-(trifluoromethyl)-1H-pyrazol-4-yl)-3,4-dihydroisoquinolin-1(2H)-one (51).—General Procedure C was followed using **50** (4.0 g, 7.9 mmol, 1 equiv) to obtain the title compound (3.6 g, 7.5 mmol, 95% yield). ¹H NMR (400 MHz, CDCl₃) δ 8.12 (d, *J* = 1.9 Hz, 1H), 7.37 (d, *J* = 1.8 Hz, 1H), 7.33 (d, *J* = 1.0 Hz, 1H), 6.43 (d, *J* = 2.3 Hz, 2H), 6.34 (t, *J* = 2.3 Hz, 1H), 4.67 (d, *J* = 1.3 Hz, 4H), 3.95 (s, 3H), 3.72 (s, 6H), 3.39–3.32 (m, 2H), 2.69 (t, *J* = 6.6 Hz, 2H); LCMS (method 2, ESI): *R*_t = 1.645 min, *m/z* = 476.0 [M + H]⁺.

7-(Bromomethyl)-2-(3,5-dimethoxybenzyl)-5-(1-methyl-3-(trifluoromethyl)-1H-pyrazol-4-yl)-3,4-dihydroisoquinolin-1(2H)-one (52).—General Procedure D was followed using **51** (1.0 g, 2.1 mmol, 1 equiv) to obtain the title compound (1.07 g, 1.9 mmol, 90% yield). The residue was purified by flash chromatography (Combi-flash Rf, MeOH/CH₂Cl₂ = 0–10% gradient). ¹H NMR (400 MHz, CDCl₃) δ 8.22 (s, *J* = 2.0 Hz, 1H), 7.39 (d, *J* = 2.0 Hz, 1H), 7.38–7.35 (m, 1H), 6.46 (d, *J* = 2.3 Hz, 2H), 6.37 (t, *J* = 2.3 Hz, 1H), 4.71 (s, 2H), 4.52 (s, 2H), 4.00 (s, 3H), 3.76 (d, *J* = 2.2 Hz, 6H), 3.40 (t, *J* = 6.6 Hz, 2H), 2.72 (t, *J* = 6.5 Hz, 2H); LCMS (method 2, ESI): *R*_t = 1.965 min, *m/z* = 537.9 [M + H]⁺.

Methyl 2-(2,4-dimethoxybenzyl)-5-(1-methyl-3-(trifluoromethyl)-1H-pyrazol-4-yl)-1-oxo-1,2,3,4-tetrahydroisoquinoline-7-carboxylate (54).—General Procedure E was followed using **53** (12.3 g, 24.3 mmol, 1 equiv), (1-methyl-3-(trifluoromethyl)-1*H*-pyrazol-4-yl)boronic acid (7.1 g, 36.4 mmol, 1.5 equiv), potassium carbonate (8.4 g, 60.8 mmol, 2.5 equiv), and PdCl₂(dppf) (890 mg, 1.2 mmol, 0.05 equiv) to obtain the title compound (11.0 g, 21.8 mmol, 90% yield). ¹H NMR (400 MHz, CDCl₃) δ 8.81 (d, *J* = 1.9 Hz, 1H), 7.99 (d, *J* = 1.8 Hz, 1H), 7.36 (d, *J* = 1.1 Hz, 1H), 7.31–7.27 (m, 1H), 6.45 (dd, *J* =

6.2, 2.5 Hz, 2H), 4.73 (s, 2H), 4.00 (s, 3H), 3.92 (s, 3H), 3.80 (s, 3H), 3.79 (s, 3H), 3.46 (t, $J = 6.6$ Hz, 2H), 2.75 (t, $J = 6.5$ Hz, 2H); LCMS (method 2, ESI): $R_t = 1.072$ min, $m/z = 504.4$ $[M + H]^+$.

Methyl 5-(1-methyl-3-(trifluoromethyl)-1H-pyrazol-4-yl)-1-oxo-1,2,3,4-tetrahydroisoquinoline-7-carboxylate (55).—Anisole (24 mL, 218 mmol, 5 equiv) was added to a solution of **54** (22.0 g, 43.7 mmol, 1 equiv) in CH_2Cl_2 (50 mL) and TFA (100 mL). The reaction was stirred at room temperature overnight and then concentrated under reduced pressure. The residue was dissolved in EtOAc and washed with saturated aqueous NaHCO_3 . The organic layer was dried over MgSO_4 and concentrated under reduced pressure. The residue was purified by flash chromatography (Combi-flash Rf, EtOAc/hexanes = 0–100% gradient followed by MeOH/ CH_2Cl_2 = 0–10% gradient) to provide the title compound (13.5 g, 38.2 mmol, 87% yield). ^1H NMR (400 MHz, CDCl_3) δ 8.77 (d, $J = 1.6$ Hz, 1H), 8.05 (d, $J = 1.6$ Hz, 1H), 7.40 (s, 1H), 6.25 (s, 1H), 4.03 (s, 3H), 3.92 (s, 3H), 3.51 (td, $J = 6.5, 2.8$ Hz, 2H), 2.84 (t, $J = 6.5$ Hz, 1H); LCMS (method 2, ESI): $R_t = 1.363$ min, $m/z = 354.1$ $[M + H]^+$.

7-(Bromomethyl)-5-(1-methyl-3-(trifluoromethyl)-1H-pyrazol-4-yl)-3,4-dihydroisoquinolin-1(2H)-one (56).—General Procedure C was followed using **55** (457 mg, 1.3 mmol, 1 equiv) to obtain 7-(hydroxymethyl)-5-(1-methyl-3-(trifluoromethyl)-1H-pyrazol-4-yl)-3,4-dihydroisoquinolin-1(2H)-one (420 mg, 1.3 mmol, quant.), which was used without further purification. LCMS (method 2, ESI): $R_t = 1.145$ min, $m/z = 326.1$ $[M + H]^+$. Then General Procedure D was followed using 7-(hydroxymethyl)-5-(1-methyl-3-(trifluoromethyl)-1H-pyrazol-4-yl)-3,4-dihydroisoquinolin-1(2H)-one (420 mg, 1.3 mmol, 1 equiv) to obtain the title compound (440 mg, 1.3 mmol, quant.), which was used in the next step without further purification. ^1H NMR (400 MHz, CDCl_3) δ 8.15 (d, $J = 1.7$ Hz, 1H), 7.42 (d, $J = 1.9$ Hz, 1H), 7.40 (s, 1H), 4.51 (s, 2H), 4.02 (s, 3H), 3.48 (td, $J = 6.5, 2.7$ Hz, 2H), 2.79 (t, $J = 6.5$ Hz, 2H); LCMS (ESI): $m/z = 387.9$ $[M + H]^+$.

7-((2-Methyl-1H-imidazol-1-yl)methyl)-5-(1-methyl-3-(trifluoromethyl)-1H-pyrazol-4-yl)-3,4-dihydroisoquinolin-1(2H)-one (57).—General Procedure F was followed using **56** (1.0 g, 2.6 mmol, 1 equiv) and 2-methyl-1H-imidazole (846 mg, 10.3 mmol, 4 equiv), to obtain the title compound (700 mg, 1.8 mmol, 70% yield). ^1H NMR (400 MHz, CDCl_3) δ 8.01 (d, $J = 2.0$ Hz, 1H), 7.32 (s, 1H), 6.95 (d, $J = 1.4$ Hz, 1H), 6.94 (d, $J = 2.0$ Hz, 1H), 6.85 (d, $J = 1.4$ Hz, 1H), 5.99 (s, 1H), 5.09 (s, 2H), 4.00 (s, 3H), 3.48 (td, $J = 6.5, 2.8$ Hz, 2H), 2.79 (t, $J = 6.5$ Hz, 2H), 2.35 (s, 3H); LCMS (method 2, ESI): $R_t = 0.973$ min, $m/z = 390.0$ $[M + H]^+$.

5-(1-Ethyl-3-(trifluoromethyl)-1H-pyrazol-4-yl)-7-((2-methyl-1H-imidazol-1-yl)methyl)-3,4-dihydroisoquinolin-1(2H)-one (58).—General Procedure F was followed using **S3** (909 mg, 2.3 mmol, 1 equiv) and 2-methyl-1H-imidazole (557 mg, 6.8 mmol, 3 equiv), to obtain the title compound (522 mg, 1.3 mmol, 57% yield). ^1H NMR (400 MHz, CDCl_3) δ 8.01 (d, $J = 2.1$ Hz, 1H), 7.34 (d, $J = 1.1$ Hz, 1H), 6.96 (d, $J = 2.0$ Hz, 1H), 6.94 (d, $J = 1.4$ Hz, 1H), 6.85 (d, $J = 1.4$ Hz, 1H),

5.97 (s, 1H), 5.09 (s, 2H), 4.26 (q, $J = 7.3$ Hz, 2H), 3.48 (td, $J = 6.5, 2.8$ Hz, 2H), 2.78 (t, $J = 6.5$ Hz, 2H), 2.34 (s, 3H), 1.58 (t, $J = 7.3$ Hz, 3H); LCMS (ESI): $m/z = 404.0$ [M + H]⁺.

(S,E)-N-((4-Methoxypyridin-2-yl)methylene)-2-methylpropane-2-sulfinamide (59).—Cesium carbonate (1.0 g, 3.1 mmol, 1.5 equiv) was added to a solution of (*S*)-2-methylpropane-2-sulfinamide (0.28 g, 2.1 mmol, 1 equiv) and 4-methoxypicolinaldehyde (0.25 g, 2.1 mmol, 1 equiv) in 10 mL of CH₂Cl₂. The reaction was stirred at rt for 16 h. The reaction was filtered through celite and concentrated to dryness. The residue was purified by flash chromatography (Combi-flash Rf, EtOAc/hexanes = 5–75% gradient) to afford the title compound (0.38 g, 1.60 mmol, 77% yield). ¹H NMR (400 MHz, CDCl₃) δ 8.68 (s, 1H), 8.58 (d, $J = 5.8$ Hz, 1H), 7.55 (d, $J = 2.6$ Hz, 1H), 6.94 (dd, $J = 5.8, 2.6$ Hz, 1H), 3.94 (s, 3H), 1.31 (s, 9H); LCMS (method 2, ESI): $R_t = 0.85$ min, $m/z = 241.2$ [M + H]⁺.

(S)-N-((S)-1-(4-Methoxypyridin-2-yl)ethyl)-2-methylpropane-2-sulfinamide (60).—A 3.4 M solution of methyl magnesium bromide in 2-methyltetrahydrofuran (35 mL, 118.2 mmol, 2.5 equiv) was added dropwise to a –78 °C solution of **59** (11.36 g, 47.3 mmol, 1 equiv) in 350 mL of THF. After 30 min, the reaction was quenched by addition of 30 mL of saturated aqueous NH₄Cl solution. This was stirred for 30 min and then filtered. The filtrate was extracted with EtOAc, the combined organic layers were dried with MgSO₄, filtered, and concentrated under reduced pressure. The major diastereomer was isolated by flash chromatography (Combi-flash Rf, EtOAc/hexanes = 0–100% gradient) to afford the title compound (10.12 g, 39.5 mmol, 84% yield). ¹H NMR (400 MHz, CDCl₃) δ 8.36 (d, $J = 5.7$ Hz, 1H), 6.81 (d, $J = 2.4$ Hz, 1H), 6.70 (dd, $J = 5.8, 2.5$ Hz, 1H), 4.74 (d, $J = 5.2$ Hz, 1H), 4.52 (p, $J = 6.4$ Hz, 1H), 3.84 (s, 3H), 1.49 (d, $J = 6.7$ Hz, 3H), 1.25 (s, 9H); LCMS (method 2, ESI): $R_t = 0.176$ min, $m/z = 257.1$ [M + H]⁺.

(S)-1-(4-Methoxypyridin-2-yl)ethan-1-amine hydrochloride (61).—A 4.0 M solution of HCl in dioxane (39 mL, 157.7 mmol, 4 equiv) was added to a solution of **60** (10.1 g, 39.4 mmol, 1 equiv) in 400 mL of THF. The reaction was stirred at room temperature for 45 min and followed by TLC. The reaction mixture was concentrated under reduced pressure to provide the title compound (5.62 g, 36.9 mmol, 94% yield), which was used without further purification. ¹H NMR (400 MHz, CDCl₃) δ 8.70 (d, $J = 6.9$ Hz, 1H), 7.72 (d, $J = 2.6$ Hz, 1H), 7.56 (dd, $J = 6.9, 2.6$ Hz, 1H), 4.85 (q, $J = 7.0$ Hz, 1H), 4.20 (s, 3H), 1.79 (d, $J = 7.0$ Hz, 3H); LCMS (method 2, ESI): $m/z = 153.2$ [M + H]⁺.

(R,E)-N-((4-Methoxypyridin-2-yl)methylene)-2-methylpropane-2-sulfinamide (62).—Cesium carbonate (17.82 g, 54.7 mmol, 1.5 equiv) was added to a solution of (*R*)-2-methylpropane-2-sulfinamide (4.86 g, 40.1 mmol, 1.1 equiv) and 4-methoxypicolinaldehyde (5.00 g, 36.5 mmol, 1 equiv) in 200 mL of CH₂Cl₂. The reaction was stirred at rt for 16 h. Water was added to the mixture and extracted with CH₂Cl₂. The combined organic layers were dried with over MgSO₄, filtered, and concentrated under reduced pressure. The residue was purified by flash chromatography (Combi-flash Rf, EtOAc/hexanes = 0–40% gradient) to afford the title compound (5.67 g, 23.6 mmol, 65% yield). ¹H NMR (400 MHz, CDCl₃) δ 8.66 (s, 1H), 8.56 (d, $J = 5.7$ Hz, 1H), 7.52 (d, $J = 2.5$ Hz, 1H), 6.92 (dd, $J = 5.7, 2.5$ Hz,

1H), 3.92 (s, 3H), 1.28 (s, 9H); LCMS (method 2, ESI): $R_t = 0.345$ min, $m/z = 241.1$ [M + H]⁺.

(R)-N-((R)-1-(4-Methoxypyridin-2-yl)ethyl)-2-methylpropane-2-sulfinamide (63).

—A 3.4 M solution of methyl magnesium bromide in 2-methyltetrahydrofuran (6.4 mL, 21.8 mmol, 1.5 equiv) was added dropwise to a -78 °C solution of **62** (3.50 g, 14.6 mmol, 1 equiv) in 100 mL of THF. After 30 min, the reaction was quenched by addition of 30 mL of saturated aqueous NH₄Cl solution. This was stirred for 30 min and then filtered. The filtrate was extracted with EtOAc, the combined organic layers were dried with MgSO₄, filtered, and concentrated under reduced pressure. The major diastereomer was isolated by flash chromatography (Combi-flash Rf, EtOAc/hexanes = 0–100% gradient) to afford the title compound (3.4278 g, 13.4 mmol, 92% yield). ¹H NMR (400 MHz, CDCl₃) δ 8.35 (d, $J = 5.8$ Hz, 1H), 6.81 (d, $J = 2.3$ Hz, 1H), 6.70 (dd, $J = 5.7, 2.4$ Hz, 1H), 4.78 (d, $J = 4.9$ Hz, 1H), 4.51 (p, 6.4 Hz, 1H), 3.84 (s, 3H), 1.50 (d, $J = 6.7$ Hz, 3H), 1.25 (s, 9H); LCMS (method 2, ESI): $R_t = 0.355$ min, $m/z = 257.1$ [M + H]⁺.

(R)-1-(4-Methoxypyridin-2-yl)ethan-1-amine hydrochloride (64).—A 4.0 M solution of HCl in dioxane (33.9 mL, 135 mmol, 10 equiv) was added to a solution of **63** (3.48 g, 13.6 mmol, 1 equiv) in 100 mL of THF. The reaction was stirred at room temperature for 45 min and followed by TLC. The reaction mixture was concentrated under reduced pressure to provide the title compound (2.67 g, 14.2 mmol, quant.), which was used without further purification. ¹H NMR (400 MHz, DMSO-*d*₆) δ 8.84 (brs, 3H), 8.59 (brs, 1H), 7.60 (brs, 1H), 7.26 (brs, 1H), 4.63 (brs, 1H), 3.98 (brs, 3H), 1.56 (brs, 3H); LCMS (method 2, ESI): $R_t = 0.259$ min, $m/z = 153.2$ [M + H]⁺.

Methyl (S)-5-hydroxy-2-(1-(4-methoxypyridin-2-yl)ethyl)-1-oxo-1,2,3,4-tetrahydroisoquinoline-7-carboxylate (65).—General Procedure A was followed using **42** (5.3 g, 21.0 mmol, 1 equiv), **61** (7.1 g, 31.5 mmol, 1.5 equiv), 2,4,6-trimethylpyridine (8.5 mL, 63 mmol, 3 equiv), and sodium cyanoborohydride (4.0 g, 63 mmol, 3 equiv) to obtain the crude title compound (7.5 g, 21.0 mmol, quant.). ¹H NMR (400 MHz, CDCl₃) δ 8.43 (dd, $J = 5.9, 2.6$ Hz, 1H), 8.26–8.24 (m, 1H), 7.61 (d, $J = 1.5$ Hz, 1H), 7.02–7.00 (m, 1H), 6.83–6.80 (m, 1H), 6.04–6.00 (m, 1H), 3.88–3.86 (m, 6H), 3.65–3.56 (m, 1H), 3.47–3.43 (m, 1H), 3.02–2.93 (m, 1H), 2.90–2.81 (m, 1H), 1.69 (d, $J = 7.0$ Hz, 3H); LCMS (method 2, ESI): $m/z = 357.1$ [M + H]⁺.

Methyl (R)-5-hydroxy-2-(1-(4-methoxypyridin-2-yl)ethyl)-1-oxo-1,2,3,4-tetrahydroisoquinoline-7-carboxylate (66).—General Procedure A was followed using **42** (1.0 g, 3.96 mmol, 1 equiv), **64** (1.12 g, 5.95 mmol, 1.5 equiv), *N,N*-diisopropylethylamine (2.1 mL, 11.9 mmol, 3 equiv) and sodium triacetoxyborohydride (2.52 g, 11.9 mmol, 3 equiv) to obtain the title compound (1.18 g, 3.31 mmol, 84% yield). ¹H NMR (400 MHz, CDCl₃) δ 8.43 (dd, $J = 5.9, 2.6$ Hz, 1H), 8.26–8.24 (m, 1H), 7.61 (d, $J = 1.5$ Hz, 1H), 7.02–7.00 (m, 1H), 6.83–6.80 (m, 1H), 6.04–6.00 (m, 1H), 3.88–3.86 (m, 6H), 3.65–3.56 (m, 1H), 3.47–3.43 (m, 1H), 3.02–2.93 (m, 1H), 2.90–2.81 (m, 1H), 1.69 (d, $J = 7.0$ Hz, 3H); LCMS (method 2, ESI): $R_t = 1.190$ min, $m/z = 357.1$ [M + H]⁺.

Methyl (S)-2-(1-(4-methoxypyridin-2-yl)ethyl)-1-oxo-5-(((trifluoromethyl)sulfonyl)oxy)-1,2,3,4-tetrahydroisoquinoline-7-carboxylate (67).—General Procedure B was followed using **65** (7.5 g, 21.0 mmol, 1 equiv), phenyl triflimide (11.2 g, 31.5 mmol, 1.5 equiv), and triethylamine (8.8 mL, 63 mmol, 3 equiv) to obtain the title compound (10.1 g, 20.7 mmol, 98% yield). ¹H NMR (400 MHz, CDCl₃) δ 8.83 (d, *J* = 1.9 Hz, 1H), 8.41 (d, *J* = 5.8 Hz, 1H), 8.05 (d, *J* = 1.9 Hz, 1H), 6.93 (d, *J* = 2.7 Hz, 1H), 6.77 (dd, *J* = 5.8, 2.7 Hz, 1H), 6.11 (q, *J* = 7.2 Hz, 1H), 3.98 (s, 3H), 3.86 (s, 3H), 3.67–3.54 (m, 2H), 3.11–2.94 (m, 2H), 1.67 (d, *J* = 7.2 Hz, 3H); LCMS (method 2, ESI): *R*_t = 1.34 min, *m/z* = 488.8 [M + H]⁺.

Methyl (R)-2-(1-(4-methoxypyridin-2-yl)ethyl)-1-oxo-5-(((trifluoromethyl)sulfonyl)oxy)-1,2,3,4-tetrahydroisoquinoline-7-carboxylate (68).—General Procedure B was followed using **66** (1.18 g, 3.31 mmol, 1 equiv), phenyl triflimide (1.42 g, 3.97 mmol, 1.2 equiv), and *N,N*-diisopropylethylamine (1.4 mL, 8.82 mmol, 2.5 equiv) to obtain the title compound (1.50 g, 3.08 mmol, 93% yield). ¹H NMR (400 MHz, CDCl₃) δ 8.80 (s, 1H), 8.39 (d, *J* = 5.8 Hz, 1H), 8.02 (s, 1H), 6.92 (s, 1H), 6.76 (dd, *J* = 5.7 Hz, 2.1 Hz, 1H), 6.06 (q, *J* = 6.9 Hz, 1H), 3.96 (s, 3H), 3.84 (s, 3H), 3.68–3.54 (m, 2H), 3.11–2.93 (m, 2H), 1.67 (d, *J* = 7.1 Hz, 3H); LCMS (method 2, ESI): *R*_t = 1.497 min, *m/z* = 489.0 [M + H]⁺.

Methyl (S)-5-(1-ethyl-3-(trifluoromethyl)-1H-pyrazol-4-yl)-2-(1-(4-methoxypyridin-2-yl)ethyl)-1-oxo-1,2,3,4-tetrahydroisoquinoline-7-carboxylate (69).—General Procedure E was followed using **67** (6 g, 12.3 mmol, 1 equiv), (1-ethyl-3-(trifluoromethyl)-1H-pyrazol-4-yl)boronic acid (3.1 g, 14.8 mmol, 1.2 equiv), potassium carbonate (4.2 g, 30.7 mmol, 2.5 equiv), and tetrakis(triphenylphosphine)-palladium(0) (710 mg, 0.61 mmol, 0.05 equiv) to obtain the title compound (4.4 g, 8.8 mmol, 72% yield). ¹H NMR (400 MHz, CDCl₃) δ 8.80 (d, *J* = 1.9 Hz, 1H), 8.37 (d, *J* = 5.8 Hz, 1H), 8.02 (d, *J* = 1.9 Hz, 1H), 7.37 (s, 1H), 6.93 (d, *J* = 2.7 Hz, 1H), 6.73 (dd, *J* = 5.8, 2.7 Hz, 1H), 6.10 (q, *J* = 7.2 Hz, 1H), 4.25 (q, *J* = 7.4 Hz, 2H), 3.92 (s, 3H), 3.83 (s, 3H), 3.53–3.47 (m, 1H), 3.40–3.34 (m, 1H), 2.78–2.64 (m, 2H), 1.67 (d, *J* = 7.2 Hz, 3H), 1.56 (t, *J* = 7.4 Hz, 3H); LCMS (method 2, ESI): *R*_t = 1.33 min, *m/z* = 502.9 [M + H]⁺.

Methyl (R)-5-(1-ethyl-3-(trifluoromethyl)-1H-pyrazol-4-yl)-2-(1-(4-methoxypyridin-2-yl)ethyl)-1-oxo-1,2,3,4-tetrahydroisoquinoline-7-carboxylate (70).—General Procedure E was followed using **68** (500 mg, 1.02 mmol, 1 equiv), (1-ethyl-3-(trifluoromethyl)-1H-pyrazol-4-yl)boronic acid (277 mg, 1.33 mmol, 1.3 equiv), sodium carbonate (271 mg, 2.56 mmol, 2.5 equiv), and tetrakis-(triphenylphosphine)palladium(0) (59.1 mg, 0.51 mmol, 0.05 equiv) to obtain the title compound (491 mg, 0.98 mmol, 96% yield). ¹H NMR (400 MHz, CDCl₃) δ 8.79 (d, *J* = 1.6 Hz, 1H), 8.37 (d, *J* = 5.8 Hz, 1H), 8.01 (d, *J* = 1.7 Hz, 1H), 7.37 (s, 1H), 6.95 (d, *J* = 2.2 Hz, 1H), 6.74 (dd, *J* = 5.8, 2.4 Hz, 1H), 6.07 (q, *J* = 6.8 Hz, 1H), 4.26 (q, *J* = 7.3 Hz, 2H), 3.92 (s, 3H), 3.84 (s, 3H), 3.56–3.49 (m, 1H), 3.43–3.37 (m, 1H), 2.81–2.66 (m, 2H), 1.64 (d, *J* = 7.1 Hz, 3H), 1.56 (t, *J* = 7.3 Hz, 3H); LCMS (method 2, ESI): *R*_t = 1.444 min, *m/z* = 503.1 [M + H]⁺.

(S)-5-(1-Ethyl-3-(trifluoromethyl)-1H-pyrazol-4-yl)-7-(hydroxymethyl)-2-(1-(4-methoxy-pyridin-2-yl)ethyl)-3,4-dihydroisoquinolin-1(2H)-one (71).—General Procedure C was followed using **69** (4.4 g, 8.8 mmol, 1 equiv) and a lithium borohydride solution (2 M THF, 44.0 mL, 88.0 mmol, 10 equiv) to obtain the title compound (3.0 g, 6.3 mmol, 72% yield). ¹H NMR (400 MHz, CDCl₃) δ 8.35 (d, *J* = 5.8 Hz, 1H), 8.14 (d, *J* = 1.7 Hz, 1H), 7.39 (d, *J* = 1.5 Hz, 1H), 7.34 (s, 1H), 6.91 (d, *J* = 2.7 Hz, 1H), 6.71 (dd, *J* = 5.8, 2.7 Hz, 1H), 6.11 (q, *J* = 7.2 Hz, 1H), 4.73 (s, 2H), 4.25 (q, *J* = 7.4 Hz, 2H), 3.82 (s, 3H), 3.47–3.42 (m, 1H), 3.34–3.27 (m, 1H), 2.70–2.60 (m, 2H), 1.61 (d, *J* = 7.2 Hz, 3H), 1.54 (t, *J* = 7.4 Hz, 3H); LCMS (method 2, ESI): *R*_t = 1.16 min, *m/z* = 475.0 [M + H]⁺.

(R)-5-(1-Ethyl-3-(trifluoromethyl)-1H-pyrazol-4-yl)-7-(hydroxymethyl)-2-(1-(4-methoxy-pyridin-2-yl)ethyl)-3,4-dihydroisoquinolin-1(2H)-one (72).—General Procedure C was followed using **70** (491 mg, 0.98 mmol, 1 equiv) and a lithium triethylborohydride solution (1 M THF, 2.9 mL, 2.93 mmol, 3 equiv) to obtain the title compound (394 mg, 0.83 mmol, 85% yield). ¹H NMR (400 MHz, CDCl₃) δ 8.42–8.39 (m, 1H), 8.09 (d, *J* = 6.4 Hz, 1H), 7.40 (s, 1H), 7.36 (s, 1H), 7.07–7.00 (m, 1H), 6.85–6.78 (m, 1H), 5.99–5.86 (m, 1H), 4.74–4.72 (m, 2H), 4.25 (q, *J* = 7.3 Hz, 2H), 3.91–3.86 (m, 3H), 3.65–3.41 (m, 2H), 2.86–2.66 (m, 2H), 1.77–1.66 (m, 3H), 1.56 (t, *J* = 7.3 Hz, 3H); LCMS (method 2, ESI): *R*_t = 1.319 min, *m/z* = 475.0 [M + H]⁺.

(S)-7-(Bromomethyl)-5-(1-ethyl-3-(trifluoromethyl)-1H-pyrazol-4-yl)-2-(1-(4-methoxy-pyridin-2-yl)ethyl)-3,4-dihydroisoquinolin-1(2H)-one (73).—A solution of **71** (1.35 g, 2.9 mmol, 1 equiv) in CH₂Cl₂ (30 mL) was cooled in an ice bath. *N,N*-Diisopropylethylamine (1 mL, 5.8 mmol, 2 equiv) and methanesulfonyl chloride (0.33 mL, 4.3 mmol, 1.5 equiv) were added, and the reaction was stirred for 1 h. The reaction was diluted with saturated aqueous NaHCO₃, and the layers were separated. The organic layer was dried over MgSO₄ and concentrated under reduced pressure. This material was dissolved in 20 mL of THF. Lithium bromide (0.62 g, 7.10 mmol, 2.5 equiv) was added, and the reaction mixture was refluxed for 1 h. The reaction was concentrated under reduced pressure, and the crude product was diluted with EtOAc and washed with water. The organic layer was dried over MgSO₄ and concentrated under reduced pressure. The residue was purified by flash chromatography (Combi-flash Rf, EtOAc/hexanes = 0–100% gradient) to obtain the title compound (0.8 g, 1.5 mmol, 53% yield). ¹H NMR (400 MHz, CDCl₃) δ 8.36 (d, *J* = 5.8 Hz, 1H), 8.19 (d, *J* = 1.7 Hz, 1H), 7.39 (d, *J* = 1.5 Hz, 1H), 7.36 (s, 1H), 6.91 (d, *J* = 2.7 Hz, 1H), 6.72 (dd, *J* = 5.8, 2.7 Hz, 1H), 6.11 (q, *J* = 7.2 Hz, 1H), 4.51 (s, 2H), 4.25 (q, *J* = 7.4 Hz, 2H), 3.82 (s, 3H), 3.50–3.44 (m, 1H), 3.33–3.30 (m, 1H), 2.71–2.58 (m, 2H), 1.61 (d, *J* = 7.2 Hz, 3H), 1.54 (t, *J* = 7.4 Hz, 3H); LCMS (method 2, ESI): *R*_t = 1.42 min, *m/z* = 536.8 [M + H]⁺.

(R)-7-(Bromomethyl)-5-(1-ethyl-3-(trifluoromethyl)-1H-pyrazol-4-yl)-2-(1-(4-methoxy-pyridin-2-yl)ethyl)-3,4-dihydroisoquinolin-1(2H)-one (74).—General Procedure D was followed using **72** (390 mg, 0.82 mmol, 1 equiv) to obtain the title compound (431 mg, 0.80 mmol, 98% yield), which was used in the next step without further purification. ¹H NMR (400 MHz, CDCl₃) δ 8.36 (d, *J* = 5.8 Hz, 1H), 8.18 (d, *J* = 1.9 Hz, 1H), 7.38 (d, *J* = 1.9 Hz, 1H), 7.36 (s, 1H), 6.91 (d, *J* = 2.4 Hz, 1H), 6.72 (dd,

$J = 5.8, 2.4$ Hz, 1H), 6.10 (q, $J = 7.1$ Hz, 1H), 4.51 (s, 2H), 4.24 (q, $J = 7.3$ Hz, 2H), 3.82 (s, 3H), 3.56–3.40 (m, 1H), 3.36–3.28 (m, 1H), 2.73–2.58 (m, 2H), 1.61 (d, $J = 7.1$ Hz, 3H), 1.55 (t, $J = 7.3$ Hz, 3H); LCMS (method 2, ESI): $R_t = 1.568$ min, $m/z = 537.0$ [M + H]⁺.

Protein Expression and Purification.

Human WDR5 (aa: 22–334) was cloned into a modified pET27 vector (pBG104) with a 6×His-SUMO tag present at the N terminus. The plasmid was then transformed into *E. coli* BL21-Gold (DE3) cells. LB starter (100 mL) was used to inoculate a 10 L fermentation culture (BioFlo 415, New Brunswick Scientific), grown at 37 °C. Fermentation growth media contained KH₂PO₄ (4 g/L), K₂HPO₄ (6 g/L), Na₂SO₄ (2 g/L), K₂SO₄ (1 g/L), NaCl (0.5 g/L), Yeast Extract (5 g/L), glycerol (2 mL/L), Antifoam (0.2 mL/L), 5% LB medium, glucose (25 g/L), MgCl₂ (2 mM), CaCl₂ (0.1 mM), NH₄Cl (2.5 g/L), and Kanamycin (50 μg/mL). When the cell density reached OD₆₀₀ = 2.0, the temperature was lowered to 25 °C, and WDR5 expression induced by treatment with 1 mM isopropyl-β-D-thioga-lactoside (IPTG) overnight. Cell pellets were collected, dissolved in lysis buffer containing 1× PBS plus 300 mM NaCl, 20 mM imidazole, 5 mM BME, and 10% glycerol, and lysed by homogenization (APV-2000, APV). The lysate was cleared by centrifugation, filtered, and then applied to the Ni-column (140 mL, ProBond, Invitrogen). Bound protein was eluted using an imidazole gradient (0–500 mM). The His-SUMO-tag was cleaved by SUMO protease during dialysis and subsequently eliminated through a second Ni-column. WDR5 protein was then purified by size exclusion chromatography (HiLoad 26/60, Superdex 75, GE Healthcare) using crystallization buffer consisting of 20 mM HEPES, pH 7.0, 250 mM NaCl, and 5 mM DTT. The purity of protein was checked using SDS-PAGE. Purified WDR5 was then concentrated to 10 mg/mL and was stored at –80 °C.

Protein Crystallization, Data Collection, and Structure Refinement.

WDR5 apo- and co-crystals were obtained at 18 °C using the sitting drop vapor diffusion method. The crystallization condition was 0.1 M Bis-Tris or HEPES or HCl-Tris pH 6.0–8.0, 0.2 M ammonium acetate, 20–30% PEG3350. Compound **20** was crystallized under these conditions supplemented with 0.05% benzamidine hydrochloride. Crystals were flash-frozen directly in liquid nitrogen. Diffraction data were collected on the Life Sciences Collaborative Access Team (LS-CAT) 21-ID-D and G beamlines at the Advanced Photon Source (APS) at Argonne National Laboratory. Diffraction data were indexed, integrated, and scaled using HKL2000.⁴⁶ Molecular replacement was applied using Phaser as implemented in CCP4⁴⁷ using a published structure (PDB code 3EG6). Refinement of the structural models was performed using PHENIX⁴⁸ along with rounds of manual model building in COOT.⁴⁹ All structure images were prepared with PyMOL. A summary of the final refinement statistics for structures including compounds **20** and **37** can be found in Table S1.

TR-FRET Competition Assay.

The 10-mer-Thr-FAM (AR-TEVHLRKS-(Ahx-Ahx)(Lys-(5-FAM)))⁴⁴ peptide was purchased from GeneScript and used without additional purification. TR-FRET emissions were recorded on a BioTek Cytation3 instrument.

For the 10-mer-Thr-FAM peptide TR-FRET assay, LanthaScreen Elite Tb-anti His antibody (Tb-Ab) was purchased from Thermo-Fisher and used at 1 nM. The 10-mer-Thr-FAM peptide was used at 150 nM, while WDR5-His-SUMO tag protein was used at 2 nM. The working assay buffer composition was modified to pH 7.2 (1× phosphate buffered saline, 300 mM NaCl, 0.5 mM TCEP, 0.1% CHAPS). Stock compounds were dispensed to a white, flat-bottom OptiPlate plate (PerkinElmer) using an Echo Liquid Handler. An 11-point, semi-log dilution scheme with a top concentration of 1 μ M (0.010 nM low concentration) was used with a final volume of 20 μ L. Both the top concentration and the dilution scheme were adjusted to fit the anticipated potency of the compounds. The range of K_i values was calculated using the above probe concentration and assay conditions. The calculated upper and lower K_i limits were $\sim 6.7 \pm 0.010$ and 0.020 ± 0.010 nM, respectively. Positive control wells (0% displacement) consisted of His-SUMO-WDR5 and 10-mer-Thr-FAM probe/Tb antibody mix occupying column 24, while negative control wells (100% displacement) consisted of the 10-mer-Thr-FAM probe/terbium antibody mix alone occupy column 1. The assay performed with an average Z' value of 0.7 and was found to be tolerant to up to 5% DMSO, but routinely screened at 1% DMSO.

For IC₅₀ determinations, plates were covered, shielded from light, and incubated for 1 h at room temperature with rocking. For the TR-FRET assay, measurement plates were excited at a wavelength of 340 nm and emission wavelengths of 495 and 520 nm were used. The ratio of the 520/495 wavelengths was used to assess the degree of the FRET signal and resulting peptide displacement. TR-FRET plate positive control wells include column 24 containing 10-mer-Thr-FAM peptide, His-SUMO-WDR5, and Tb-anti-His antibody to measure the maximum signal from the FRET response. The 520/495 emission ratio (TR-FRET) was used to calculate an IC₅₀ (inhibitor concentration at which 50% of the bound peptide is displaced) by fitting the inhibition data using XLFit software (Guilford, U.K.) to single-site binding model. This was converted into a binding inhibition/displacement constant (K_i) using the formula⁵⁰

$$\text{compound } K_i = \frac{[I]_{50}}{\frac{[L]_{50}}{K_d^{\text{pep}}} + \frac{[P]_0}{K_d^{\text{pep}}} + 1}$$

where $[I]_{50}$ is the concentration of the free inhibitor at 50% inhibition, $[L]_{50}$ is the concentration of the free labeled ligand at 50% inhibition, $[P]_0$ is the concentration of the free protein at 0% inhibition, and K_d^{pep} represents the dissociation constant of the 10-mer-Thr-FAM probe. The reported K_i values represent four independent replicate determinations \pm standard deviation.

Cellular Proliferation Assays.

Cell proliferation was assayed using the Promega CellTiter-Glo Luminescent Kit in white, opaque, flat-bottomed 384-well plates. Two hundred cells were seeded per well for all cell lines in IMDM (K562, MV4:11) or RPMI (MOLM-13) supplemented with 10% fetal bovine serum. The cells were treated with 0.3% DMSO vehicle-only or 22 twofold dilutions of WDR5 inhibitors with a top concentration of 30 μ M. The final DMSO concentration was

0.3% in all compound treatment experiments and at least two biological replicates were performed. The total volume of cells with inhibitor was 32 μL per well. Sterile media (30 μL) was added to all of the empty wells around the edge of the plate to prevent evaporation. Plates were incubated at 37 °C, 5% CO₂ for 5 days. At the end of incubation, the plates were allowed to reach room temperature before adding 16 μL of CellTiter-Glo reagent per well. Plates were incubated at room temperature, covered from light, for 15 min before the luminescence was measured using the CellTiter-Glo protocol on a Cytation3 plate reader (BioTek, Winooski, VT). The raw luminescence values were normalized to the DMSO vehicle-only wells and PRISM software or XLfit (IDBS, Guildford, United Kingdom) was used to generate GI₅₀ values. The reported GI₅₀ values represent four independent replicate determinations \pm standard deviation.

PAMPA Assay.

The passive permeability of **1** and **20** was assessed using a PAMPA assay performed at Curia Global, Inc. (Albany, NY). The artificial membrane was added to the acceptor well and overlaid with phosphate-buffered saline at pH 7.4. The compound (100 μM) was added to the donor plate, which was placed in the acceptor plate and incubated for 5 h at 20 °C. Verapamil was used as a positive control. Compound concentrations were determined by UV-vis absorbance, and the effective permeability (P_e , cm/s) was calculated. Two replicates were obtained, and average P_e values are reported.

Kinetic Solubility Assay.

The solubilities of **34**, **36**, **37**, **38**, **40**, and **41** were assessed using a kinetic solubility assay performed at Curia Global, Inc. (Albany, NY). The tested compound (100 μM) was incubated for 1 h in 0.1 M phosphate-buffered saline (pH 7.4) and 0.1% DMSO at ambient room temperature. The dissolved concentration was determined by UV-vis absorbance. Verapamil and tamoxifen were used as controls. Two replicates were obtained, and average soluble concentrations (μM) are reported.

Microsomal Intrinsic Clearance Assay.

The metabolic stabilities of **30**, **34**, and **38** were assessed using a microsomal intrinsic clearance assay performed at Curia Global, Inc. (Albany, NY). The tested compound (1 μM) was incubated with 1 mg/mL of pooled rat liver microsomes, in phosphate buffer at 37 °C. Samples were taken at 0, 5, 10, 15, 30, and 45 min and analyzed by LCMS. Testosterone was used as the positive control. Two replicates were obtained, and average CL_{int} and half-life values are reported.

In Vivo Pharmacokinetic Studies in Rodent.

All *in vivo* PK assessments were performed by Pharmaron, Inc. (Beijing, P. R. China). The studies were performed according to guidelines approved by the Institutional Animal Care and Use Committee (IACUC) of Pharmaron following the guidance of the Association for Assessment and Accreditation of Laboratory Animal Care (AAALAC). Compound **1** was administered to male CD-1 mice at 3 mg/kg iv ($n = 3$) and 3 mg/kg po ($n = 3$) and formulated as follows: iv, 0.6 mg/mL solution in DMSO, PEG400, and saline (v/v/v,

5/50/45); po, 0.3 mg/mL solution in DMSO and 20% captisol in DI water (v/v, 10/90). Compounds **34**, **36**, **37**, **38**, **40**, and **41** were administered to male CD-1 mice at 3 mg/kg iv ($n = 3$) and 10 mg/kg po ($n = 3$). Compounds **34**, **36**, **37**, **38**, and **40** were formulated as follows: iv, 0.6 mg/mL solution in DMSO, PEG400, and saline (v/v/v, 5/35/60); po, 1 mg/mL solution in DMSO and 20% captisol in DI water (v/v, 10/90). Compound **41** was formulated as 0.6 and 1 mg/mL solutions in ethanol, tocopherol poly(ethylene glycol) succinate (TPGS), PEG400 and water (v/v/v/v, 5/5/30/60) for iv and po dosing, respectively. Animals given **1** (3 mg/kg iv) experienced signs of severe acute toxicity, such as reduced locomotive activity, lowered body temperature, and lethality. The animals that were administered **34**, **36**, **37**, **38**, **40**, and **41** behaved normally during the study and showed no adverse effects. Blood samples were collected from all mice at 5, 15, 30 min and 1, 2, 4, 8, and 24 h post-dose. Plasma samples were separated from blood by centrifugation and analyzed by LC-MS/MS.

Supplementary Material

Refer to Web version on PubMed Central for supplementary material.

ACKNOWLEDGMENTS

The authors thank the Vanderbilt High-Throughput Screening Core facility for compound management services and Vanderbilt University Biomolecular NMR Facility for use of Bruker NMR spectrometers, which receives support from an NIH SIG Grant (1S-10RR025677-01) and Vanderbilt University matching funds. The authors also thank contributing and supporting members of Leidos Biomedical Research at Frederick National Labs for Cancer Research, Curia Global, Inc. and Pharmaron, Inc. Use of the Advanced Photon Source, an Office of Science User Facility operated for the U.S. Department of Energy Office of Science by the Argonne National Laboratory, was supported by U.S. Department of Energy [Contract No. DE-AC02-06CH11357]. Use of the Life Sciences Collaborative Access Team Sector 21 was supported by the Michigan Economic Development Corporation and Michigan Technology Tri-Corridor Grant [grant number 085P1000817].

Funding

This work was generously supported in part with Federal funds from the National Cancer Institute, National Institutes of Health, under Chemical Biology Consortium Contract No. HHSN261200800001E (to S.W.F.), The Vanderbilt Ingram Cancer Center Support grant (NIH: CA68485), CA236733 (to S.W.F. and W.P.T.), CA200709 (to W.P.T.), and startup funds to S.W.F. provided by Vanderbilt University. The content of this publication does not necessarily reflect the views or policies of the Department of Health and Human Services, nor does mention of trade names, commercial products, or organizations imply endorsement by the U.S. Government.

ABBREVIATIONS

ALL	acute lymphoid leukemia
AML	acute myeloid leukemia
ATAC	Ada2-containing
AUC_{inf}	area under the plasma concentration–time curve from time 0 to infinity
CRBN	pomalidomide
GI₅₀	half-maximal growth inhibition

HAT	histone acetyltransferase
HMT	histone methyltransferase
H3K4	histone H3 lysine 4
histone H3K4me2	me3, H3 lysine 4 di- and tri-methylation
H4K16	histone H4 lysine 16
MLL	mixed-lineage leukemia
NSL	WDR5-containing nonspecific lethal
PROTACs	proteolysis-targeting chimeras
RBBP5	retinoblastoma binding protein 5
RLM	rat liver microsomes
RPGs	ribosomal protein genes
TR-FRET	time-resolved fluorescence energy transfer
WBM	WDR5 binding motif
WDR5	WD repeat domain 5 protein
WIN	WDR5 interaction motif

REFERENCES

- (1). Smith TF; Gaitatzes C; Saxena K; Neer EJ The WD Repeat: A Common Architecture for Diverse Functions. *Trends Biochem. Sci.* 1999, 24, 181–185. [PubMed: 10322433]
- (2). Stirnimann CU; Petsalaki E; Russell RB; Müller, C. W. WD40 Proteins Propel Cellular Networks. *Trends Biochem. Sci.* 2010, 35, 565–574. [PubMed: 20451393]
- (3). Xu C; Min J Structure and Function of WD40 Domain Proteins. *Protein Cell* 2011, 2, 202–214. [PubMed: 21468892]
- (4). Guarnaccia AD; Tansey WP Moonlighting with WDR5: A Cellular Multitasker. *J. Clin. Med.* 2018, 7, 21. [PubMed: 29385767]
- (5). Couture JF; Collazo E; Trievel RC Molecular Recognition of Histone H3 by the WD40 Protein WDR5. *Nat. Struct. Mol. Biol.* 2006, 13, 698–703. [PubMed: 16829960]
- (6). Li D; Roberts R WD-Repeat Proteins: Structure Characteristics, Biological Function, and Their Involvement in Human Diseases. *Cell. Mol. Life Sci.* 2001, 58, 2085–2097. [PubMed: 11814058]
- (7). Patel A; Vought VE; Dharmarajan V; Cosgrove MS A Conserved Arginine-Containing Motif Crucial for the Assembly and Enzymatic Activity of the Mixed Lineage Leukemia Protein-1 Core Complex. *J. Biol. Chem.* 2008, 283, 32162–32175. [PubMed: 18829457]
- (8). Odho Z; Southall SM; Wilson JR Characterization of a Novel WDR5-Binding Site That Recruits RbBP5 through a Conserved Motif to Enhance Methylation of Histone H3 Lysine 4 by Mixed Lineage Leukemia Protein-1. *J. Biol. Chem.* 2010, 285, 32967–32976. [PubMed: 20716525]
- (9). Han Z; Guo L; Wang H; Shen Y; Deng XW; Chai J Structural Basis for the Specific Recognition of Methylated Histone H3 Lysine 4 by the WD-40 Protein WDR5. *Mol. Cell* 2006, 22, 137–144. [PubMed: 16600877]

- (10). Chen X; Xu J; Wang X; Long G; You Q; Guo X Targeting WD Repeat-Containing Protein 5 (WDR5): A Medicinal Chemistry Perspective. *J. Med. Chem.* 2021, 64, 10537–10556. [PubMed: 34283608]
- (11). Li Y; Han J; Zhang Y; Cao F; Liu Z; Li S; Wu J; Hu C; Wang Y; Shuai J; Chen J; Cao L; Li D; Shi P; Tian C; Zhang J; Dou Y; Li G; Chen Y; Lei M Structural Basis for Activity Regulation of MLL Family Methyltransferases. *Nature* 2016, 530, 447–452. [PubMed: 26886794]
- (12). Jain BP; Pandey S WD40 Repeat Proteins: Signalling Scaffold with Diverse Functions. *Protein J.* 2018, 37, 391–406. [PubMed: 30069656]
- (13). Wu M; Shu HB MLL1/WDR5 Complex in Leukemogenesis and Epigenetic Regulation. *Chin. J. Cancer* 2011, 30, 240–246. [PubMed: 21439245]
- (14). Patel A; Dharmarajan V; Cosgrove MS Structure of WDR5 Bound to Mixed Lineage Leukemia Protein-1 Peptide. *J. Biol. Chem.* 2008, 283, 32158–32161. [PubMed: 18829459]
- (15). Hess JL MLL: A Histone Methyltransferase Disrupted in Leukemia. *Trends Mol. Med.* 2004, 10, 500–507. [PubMed: 15464450]
- (16). Dharmarajan V; Lee J-H; Patel A; Skalnik DG; Cosgrove MS Structural Basis for WDR5 Interaction (Win) Motif Recognition in Human SET1 Family Histone Methyltransferases. *J. Biol. Chem.* 2012, 287, 27275–27289. [PubMed: 22665483]
- (17). Alicea-Velázquez NL; Shinsky SA; Loh DM; Lee JH; Skalnik DG; Cosgrove MS Targeted Disruption of the Interaction between WD-40 Repeat Protein 5 (WDR5) and Mixed Lineage Leukemia (MLL)/SET1 Family Proteins Specifically Inhibits MLL1 and SETD1A Methyltransferase Complexes. *J. Biol. Chem.* 2016, 291, 22357–22372. [PubMed: 27563068]
- (18). Thomas LR; Adams CM; Fesik SW; Eischen CM; Tansey WP Targeting MYC through WDR5. *Mol. Cell. Oncol.* 2020, 7, No. 1709388. [PubMed: 32158922]
- (19). Thomas LR; Wang Q; Grieb BC; Phan J; Foshage AM; Sun Q; Olejniczak ET; Clark T; Dey S; Lorey S; Alicie B; Howard GC; Cawthon B; Ess KC; Eischen CM; Zhao Z; Fesik SW; Tansey WP Interaction with WDR5 Promotes Target Gene Recognition and Tumorigenesis by MYC. *Mol. Cell* 2015, 58, 440–452. [PubMed: 25818646]
- (20). Thomas LR; Adams CM; Wang J; Weissmiller AM; Creighton J; Lorey SL; Liu Q; Fesik SW; Eischen CM; Tansey WP Interaction of the Oncoprotein Transcription Factor MYC with Its Chromatin Cofactor WDR5 Is Essential for Tumor Maintenance. *Proc. Natl. Acad. Sci. U.S.A.* 2019, 116, 25260–25268. [PubMed: 31767764]
- (21). Chen X; Xie W; Gu P; Cai Q; Wang B; Xie Y; Dong W; He W; Zhong G; Lin T; Huang J Upregulated WDR5 Promotes Proliferation, Self-Renewal and Chemoresistance in Bladder Cancer via Mediating H3K4 Trimethylation. *Sci. Rep.* 2015, 5, No. 8293. [PubMed: 25656485]
- (22). Dai X; Guo W; Zhan C; Liu X; Bai Z; Yang Y WDR5 Expression Is Prognostic of Breast Cancer Outcome. *PLoS One* 2015, 10, No. e0124964. [PubMed: 26355959]
- (23). Tan X; Chen S; Wu J; Lin J; Pan C; Ying X; Pan Z; Qiu L; Liu R; Geng R; Huang W PI3K/AKT-Mediated Upregulation of WDR5 Promotes Colorectal Cancer Metastasis by Directly Targeting ZNF407. *Cell Death Dis.* 2017, 8, No. e2686. [PubMed: 28300833]
- (24). Sun W; Guo F; Liu M Up-Regulated WDR5 Promotes Gastric Cancer Formation by Induced Cyclin D1 Expression. *J. Cell. Biochem.* 2018, 119, 3304–3316. [PubMed: 29125890]
- (25). Carugo A; Genovese G; Seth S; Nezi L; Rose JL; Bossi D; Cicalese A; Shah PK; Viale A; Pettazoni PF; Akdemir KC; Bristow CA; Robinson FS; Tepper J; Sanchez N; Gupta S; Estecio MR; Giuliani V; Dellino GI; Riva L; Yao W; Di Francesco ME; Green T; D'Alesio C; Corti D; Kang Y; Jones P; Wang H; Fleming JB; Maitra A; Pelicci PG; Chin L; DePinho RA; Lanfrancone L; Heffernan TP; Draetta GF In Vivo Functional Platform Targeting Patient-Derived Xenografts Identifies WDR5-Myc Association as a Critical Determinant of Pancreatic Cancer. *Cell Rep.* 2016, 16, 133–147. [PubMed: 27320920]
- (26). Malek R; Gajula RP; Williams RD; Nghiem B; Simons BW; Nugent K; Wang H; Taparra K; Lemtiri-Chlieh G; Yoon AR; True L; An SS; DeWeese TL; Ross AE; Schaeffer EM; Pienta KJ; Hurley PJ; Morrissey C; Tran PT TWIST1-WDR5- *Hottip* Regulates *Hoxa9* Chromatin to Facilitate Prostate Cancer Metastasis. *Cancer Res.* 2017, 77, 3181–3193. [PubMed: 28484075]

- (27). Tran PT; Gajula R; Williams R; Malek R; Nugent K; Walker A; Chettiar S; Wang H; Tapparra K; Cades J; Herman J A Twist1-MLL-WDR5-HOTTIP Complex Regulates HOXA9 Chromatin to Facilitate Metastasis of Prostate Cancer. *Int. J. Radiat. Oncol.* 2014, 90, S177.
- (28). Sun Y; Bell JL; Carter D; Gherardi S; Poulos RC; Milazzo G; Wong JWH; Al-Awar R; Tee AE; Liu PY; Liu B; Atmadibrata B; Wong M; Trahair T; Zhao Q; Shohet JM; Haupt Y; Schulte JH; Brown PJ; Arrowsmith CH; Vedadi M; MacKenzie KL; Huttelmaier S; Perini G; Marshall GM; Braithwaite A; Liu T WDR5 Supports an N-Myc Transcriptional Complex That Drives a Protumorigenic Gene Expression Signature in Neuroblastoma. *Cancer Res.* 2015, 75, 5143–5154. [PubMed: 26471359]
- (29). Wu Y; Diao P; Li Z; Zhang W; Wang D; Wang Y; Cheng J Overexpression of WD Repeat Domain 5 Associates with Aggressive Clinicopathological Features and Unfavorable Prognosis in Head Neck Squamous Cell Carcinoma. *J. Oral Pathol. Med.* 2018, 47, 502–510. [PubMed: 29569374]
- (30). Cui Z; Li H; Liang F; Mu C; Mu Y; Zhang X; Liu J Effect of High WDR5 Expression on the Hepatocellular Carcinoma Prognosis. *Oncol. Lett.* 2018, 15, 7864–7870. [PubMed: 29731905]
- (31). Ge Z; Song EJ; Kawasaki YI; Li J; Dovat S; Song C WDR5 High Expression and Its Effect on Tumorigenesis in Leukemia. *Oncotarget* 2016, 7, 37740–37754. [PubMed: 27192115]
- (32). Ge Z; Song E; Li J; Dovat S; Song C Clinical Significance of WDR5 High Expression and Its Effect on Tumorigenesis in Adult Leukemia. *Blood* 2015, 126, 3657.
- (33). Lu K; Tao H; Si X; Chen Q The Histone H3 Lysine 4 Presenter WDR5 as an Oncogenic Protein and Novel Epigenetic Target in Cancer. *Front. Oncol.* 2018, 8, 502. [PubMed: 30488017]
- (34). Aho ER; Wang J; Gogliotti RD; Howard GC; Phan J; Acharya P; Macdonald JD; Cheng K; Lorey SL; Lu B; Wenzel S; Foshage AM; Alvarado J; Wang F; Shaw JG; Zhao B; Weissmiller AM; Thomas LR; Vakoc CR; Hall MD; Hiebert SW; Liu Q; Stauffer SR; Fesik SW; Tansey WP Displacement of WDR5 from Chromatin by a WIN Site Inhibitor with Picomolar Affinity. *Cell Rep.* 2019, 26, 2916–2928. [PubMed: 30865883]
- (35). Tian J; Teuscher KB; Aho ER; Alvarado JR; Mills JJ; Meyers KM; Gogliotti RD; Han C; Macdonald JD; Sai J; Shaw JG; Sensintaffar JL; Zhao B; Rietz TA; Thomas LR; Payne WG; Moore WJ; Stott GM; Kondo J; Inoue M; Coffey RJ; Tansey WP; Stauffer SR; Lee T; Fesik SW Discovery and Structure-Based Optimization of Potent and Selective WD Repeat Domain 5 (WDR5) Inhibitors Containing a Dihydroisoquinolinone Bicyclic Core. *J. Med. Chem.* 2020, 63, 656–675. [PubMed: 31858797]
- (36). Karatas H; Li Y; Liu L; Ji J; Lee S; Chen Y; Yang J; Huang L; Bernard D; Xu J; Townsend EC; Cao F; Ran X; Li X; Wen B; Sun D; Stuckey JA; Lei M; Dou Y; Wang S Discovery of a Highly Potent, Cell-Permeable Macrocyclic Peptidomimetic (MM-589) Targeting the WD Repeat Domain 5 Protein (WDR5)–Mixed Lineage Leukemia (MLL) Protein–Protein Interaction. *J. Med. Chem.* 2017, 60, 4818–4839. [PubMed: 28603984]
- (37). Grebien F; Vedadi M; Getlik M; Giambro R; Grover A; Avellino R; Skucha A; Vittori S; Kuznetsova E; Smil D; Barsyte-Lovejoy D; Li F; Poda G; Schapira M; Wu H; Dong A; Senisterra G; Stukalov A; Huber KVM; Schönegger A; Marcellus R; Bilban M; Bock C; Brown PJ; Zuber J; Bennett KL; Al-awar R; Delwel R; Nerlov C; Arrowsmith CH; Superti-Furga G Pharmacological Targeting of the Wdr5-MLL Interaction in C/EBP α N-Terminal Leukemia. *Nat. Chem. Biol.* 2015, 11, 571–578. [PubMed: 26167872]
- (38). Getlik M; Smil D; Zepeda-Velázquez C; Bolshan Y; Poda G; Wu H; Dong A; Kuznetsova E; Marcellus R; Senisterra G; Dombrowski L; Hajian T; Kiyota T; Schapira M; Arrowsmith CH; Brown PJ; Vedadi M; Al-awar R Structure-Based Optimization of a Small Molecule Antagonist of the Interaction Between WD Repeat-Containing Protein 5 (WDR5) and Mixed-Lineage Leukemia 1 (MLL1). *J. Med. Chem.* 2016, 59, 2478–2496. [PubMed: 26958703]
- (39). Chen W; Chen X; Li D; Wang X; Long G; Jiang Z; You Q; Guo X Discovery of a Potent MLL1 and WDR5 Protein-Protein Interaction Inhibitor with in Vivo Antitumor Activity. *Eur. J. Med. Chem.* 2021, 223, No. 113667. [PubMed: 34225181]
- (40). Chen W; Chen X; Li D; Zhou J; Jiang Z; You Q; Guo X Discovery of DDO-2213 as a Potent and Orally Bioavailable Inhibitor of the WDR5-Mixed Lineage Leukemia 1 Protein-Protein Interaction for the Treatment of MLL Fusion Leukemia. *J. Med. Chem.* 2021, 64, 8221–8245. [PubMed: 34105966]

- (41). Wang F; Jeon KO; Salovich JM; Macdonald JD; Alvarado J; Gogliotti RD; Phan J; Olejniczak ET; Sun Q; Wang S; Camper D; Yuh JP; Shaw JG; Sai J; Rossanese OW; Tansey WP; Stauffer SR; Fesik SW Discovery of Potent 2-Aryl-6,7-Dihydro-5 H -Pyrrolo[1,2- a]imidazoles as WDR5-WIN-Site Inhibitors Using Fragment-Based Methods and Structure-Based Design. *J. Med. Chem.* 2018, 61, 5623–5642. [PubMed: 29889518]
- (42). Dölle A; Adhikari B; Krämer A; Weckesser J; Berner N; Berger LM; Diebold M; Szewczyk MM; Barsyte-Lovejoy D; Arrowsmith CH; Gebel J; Löhr F; Dötsch V; Eilers M; Heinzlmeir S; Kuster B; Sotriffer C; Wolf E; Knapp S Design, Synthesis, and Evaluation of WD-Repeat-Containing Protein 5 (WDR5) Degraders. *J. Med. Chem.* 2021, 64, 10682–10710. [PubMed: 33980013]
- (43). Yu X; Li D; Kottur J; Shen Y; Kim HS; Park KS; Tsai YH; Gong W; Wang J; Suzuki K; Parker J; Herring L; Kaniskan HÜ; Cai L; Jain R; Liu J; Aggarwal AK; Wang GG; Jin J A Selective WDR5 Degradator Inhibits Acute Myeloid Leukemia in Patient-Derived Mouse Models. *Sci. Transl. Med.* 2021, 13, No. eabj1578. [PubMed: 34586829]
- (44). Karatas H; Townsend EC; Bernard D; Dou Y; Wang S Analysis of the Binding of Mixed Lineage Leukemia 1 (MLL1) and Histone 3 Peptides to WD Repeat Domain 5 (WDR5) for the Design of Inhibitors of the MLL1–WDR5 Interaction. *J. Med. Chem.* 2010, 53, 5179–5185. [PubMed: 20575550]
- (45). Bia H; Bailey S; Bhuralkar DR; Bi FC; Guo F; He M; Humphries PS; Ling AL; Lou J; Nukul S; Zhou R Fused Phenyl Amido Heterocyclic Compounds. U.S. Patent US7,842,713, November 30, 2010.
- (46). Otwinowski Z; Minor W Processing of X-Ray Diffraction Data Collected in Oscillation Mode. *Methods Enzymol.* 1997, 276, 307–326. [PubMed: 27754618]
- (47). Winn MD; Ballard CC; Cowtan KD; Dodson EJ; Emsley P; Evans PR; Keegan RM; Krissinel EB; Leslie AGW; McCoy A; McNicholas SJ; Murshudov GN; Pannu NS; Potterton EA; Powell HR; Read RJ; Vagin A; Wilson KS Overview of the *CCP4* Suite and Current Developments. *Acta Crystallogr., Sect. D: Biol. Crystallogr.* 2011, 67, 235–242. [PubMed: 21460441]
- (48). Adams PD; Grosse-Kunstleve RW; Hung L-W; Ioerger TR; McCoy AJ; Moriarty NW; Read RJ; Sacchettini JC; Sauter NK; Terwilliger TC PHENIX: Building New Software for Automated Crystallographic Structure Determination. *Acta Crystallogr., Sect. D: Biol. Crystallogr.* 2002, 58, 1948–1954. [PubMed: 12393927]
- (49). Emsley P; Cowtan K *Coot*. Model-Building Tools for Molecular Graphics. *Acta Crystallogr., Sect. D: Biol. Crystallogr.* 2004, 60, 2126–2132. [PubMed: 15572765]
- (50). Nikolovska-Coleska Z; Wang R; Fang X; Pan H; Tomita Y; Li P; Roller PP; Krajewski K; Saito NG; Stuckey JA; Wang S Development and Optimization of a Binding Assay for the XIAP BIR3 Domain Using Fluorescence Polarization. *Anal. Biochem.* 2004, 332, 261–273. [PubMed: 15325294]

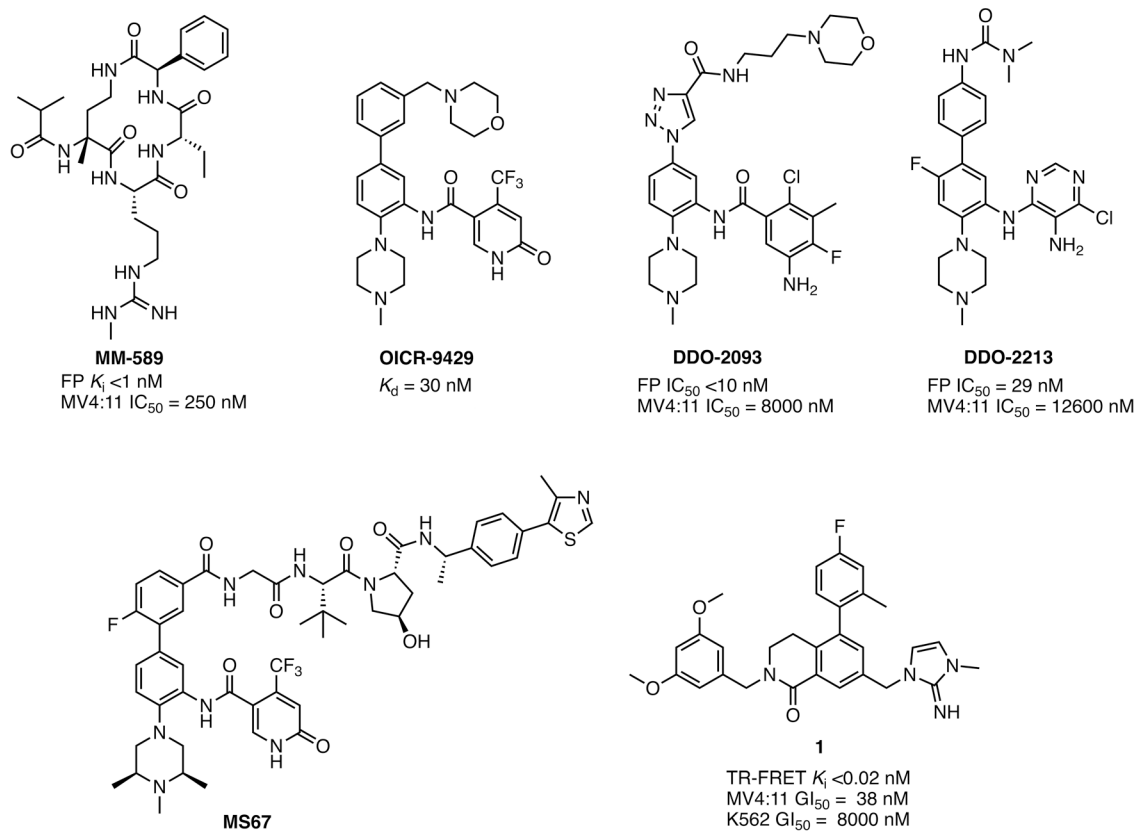


Figure 1. Chemical structures and *in vitro* profiles of representative WDR5 WIN-site inhibitors and WDR5 PROTAC. Compound **1** is also known as **16** in our previous report.³⁵

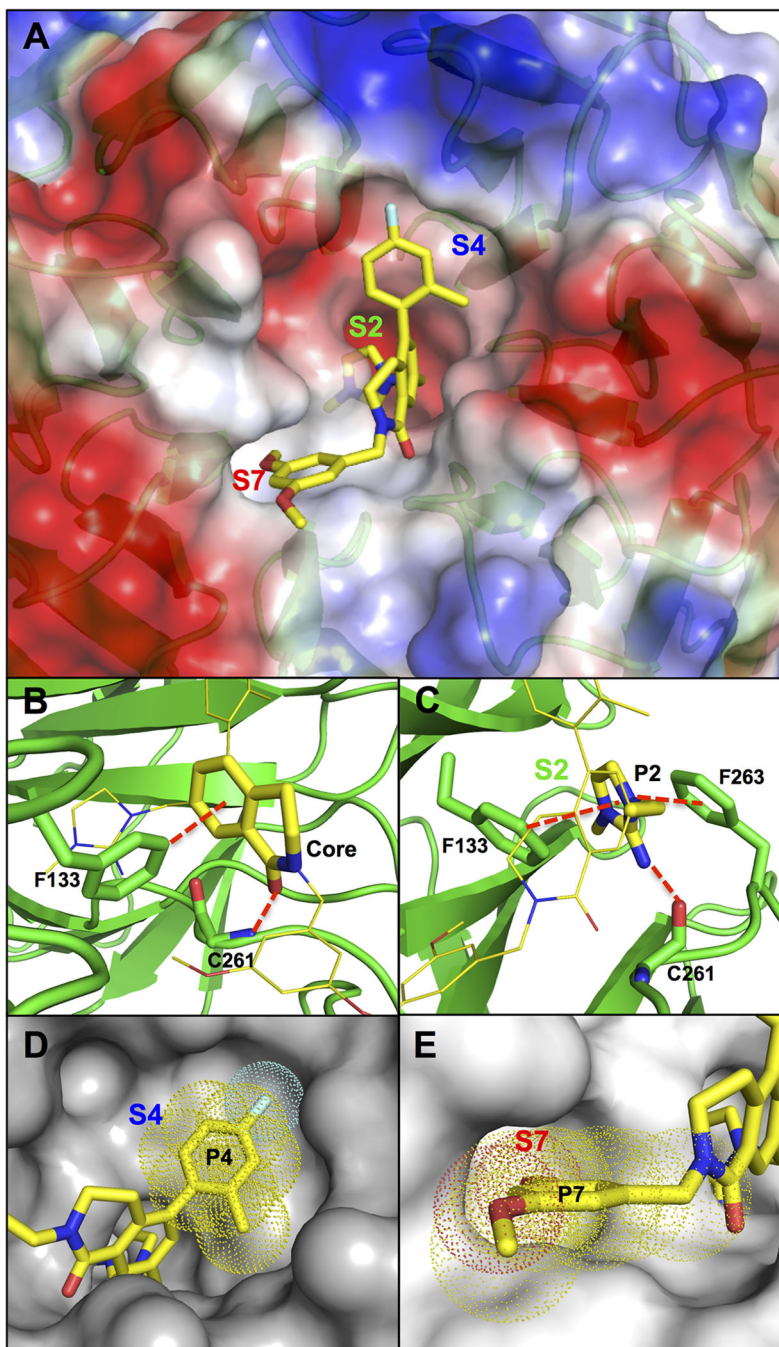


Figure 2. X-ray co-crystal structure of **1** bound to the WDR5 WIN site (PDB ID: 6UCS).³⁵ (A) Compound **1** (yellow carbon-capped sticks) bound to WDR5 represented as semitransparent electrostatic potential surface with labeled S₂, S₄, and S₇ binding regions. (B) Key H-bond and π - π stacking binding interactions (red dashed lines) of the core unit and denoted WDR5 residues (green sticks). (C) Key H-bond and π - π stacking binding interactions (red dashed lines) of the P₂ unit in the S₂ subsite and denoted WDR5 residues (green sticks). (D) Binding interactions of the P₄ unit represented as space-filling dots in the S₄ subsite (gray

surface). (E) Binding interactions of the P₇ unit represented as space-filling dots in the S₇ subsite (gray surface).

Author Manuscript

Author Manuscript

Author Manuscript

Author Manuscript

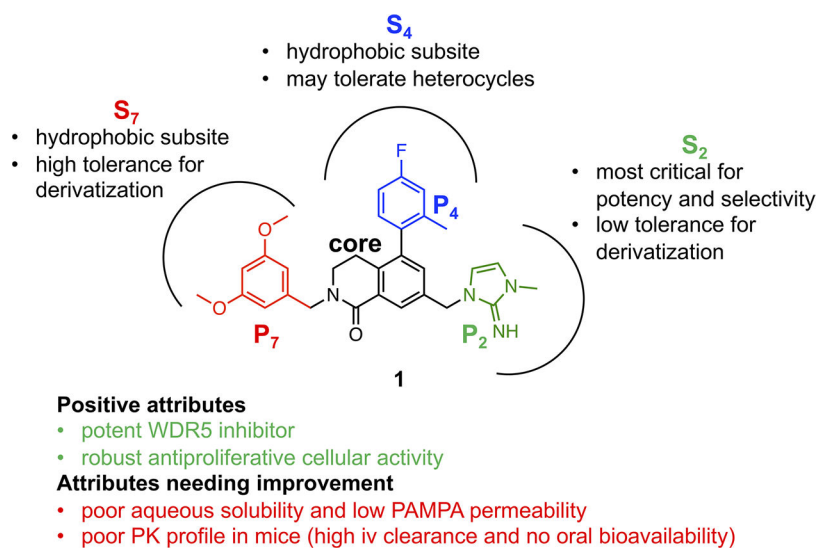


Figure 3.
Profile overview of **1** and considerations for the pharmacophore-based optimization strategy.

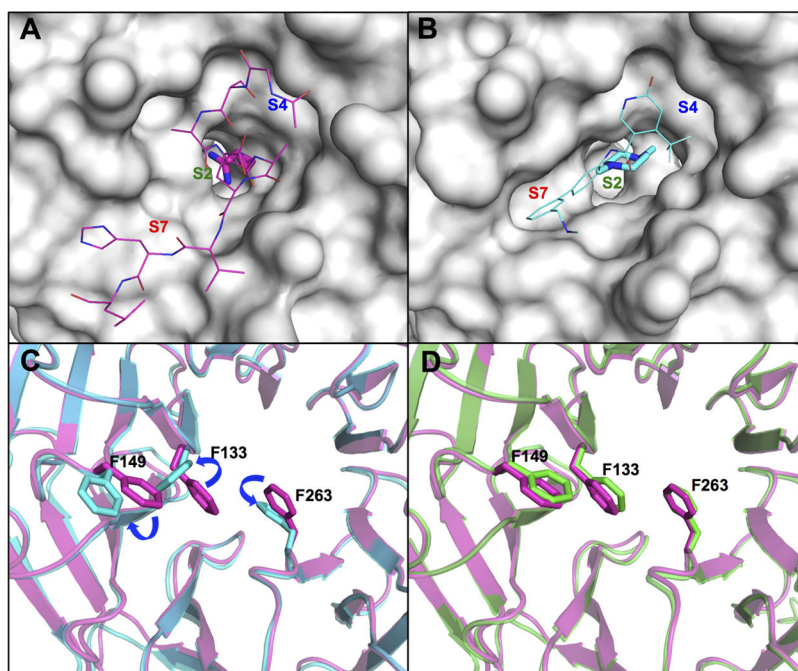


Figure 4. (A) Surface representation of the WDR5 WIN site (PDB ID: 3EG6)¹⁴ when bound to MLL1 peptide (magenta carbon-capped lines and sticks (P₂ residue)) with labeled S₂, S₄, and S₇ binding regions. (B) Surface representation of the WDR5 WIN site (PDB ID: 4QL1)³⁸ when bound to OICR-9429 (cyan carbon-capped lines and sticks (S₂ binding moiety)) with labeled S₂, S₄, and S₇ binding regions. (C) Overlay of MLL1 peptide (magenta) and OICR-9429 (cyan) bound WDR5 protein structures in cartoon representation. The side chains of WDR5 residues F133, F149, and F263 of both structures are represented as sticks to demonstrate conformational changes. (D) Overlay of MLL1 peptide (magenta) and compound **1** (green) bound WDR5 protein structures in cartoon representation. The side chains of WDR5 residues F133, F149, and F263 for both structures are represented as sticks to demonstrate retention of binding poses.

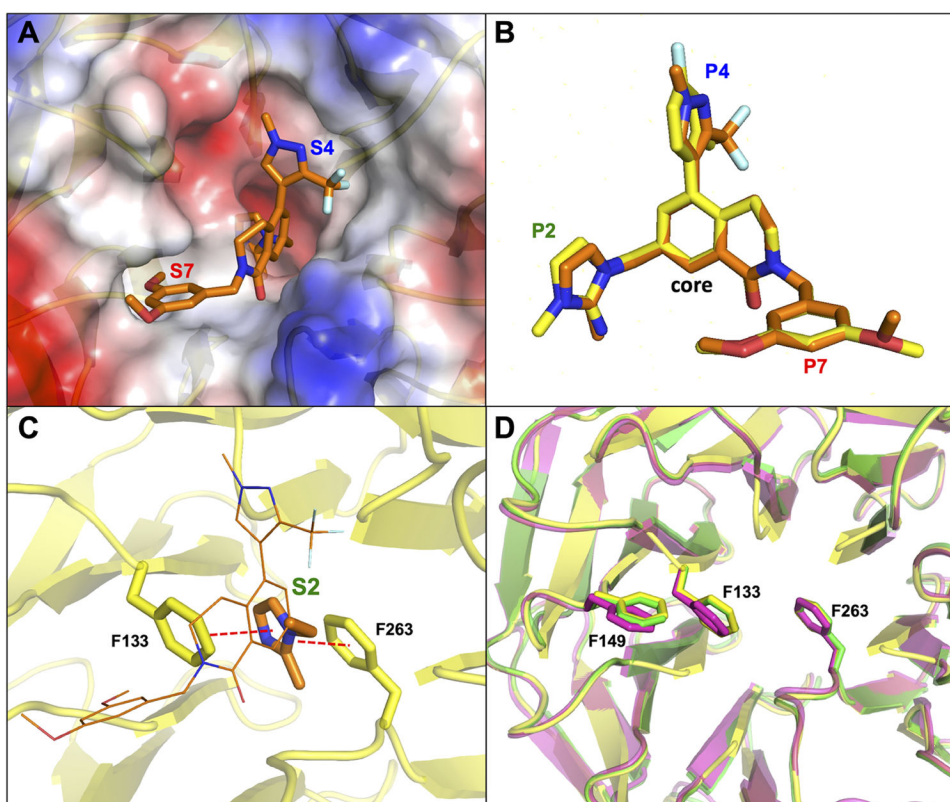


Figure 5. X-ray co-crystal structure of **20** bound to WDR5 (PDB ID: 7U9Y). (A) Compound **20** (orange carbon-capped sticks) bound to WDR5 represented as a semitransparent electrostatic potential surface with labeled S₂, S₄, and S₇ binding regions. (B) Overlay of **20** (orange sticks) and **1** (yellow sticks; PDB ID: 6UCS).³⁵ (C) Key π - π stacking binding interactions (red dashed lines) of the 2-methyl imidazole P₂ unit of **20** in the S₂ subsite with denoted WDR5 residues. (D) Overlay of MLL1 peptide (magenta sticks, PDB ID: 3EG6),¹⁴ **1** (green sticks, PDB ID: 6UCS),³⁵ and **20** (yellow sticks) bound WDR5 protein structures in cartoon representation. The side chains of WDR5 residues F133, F149, and F263 for the structures are represented as sticks to demonstrate retention of binding poses.

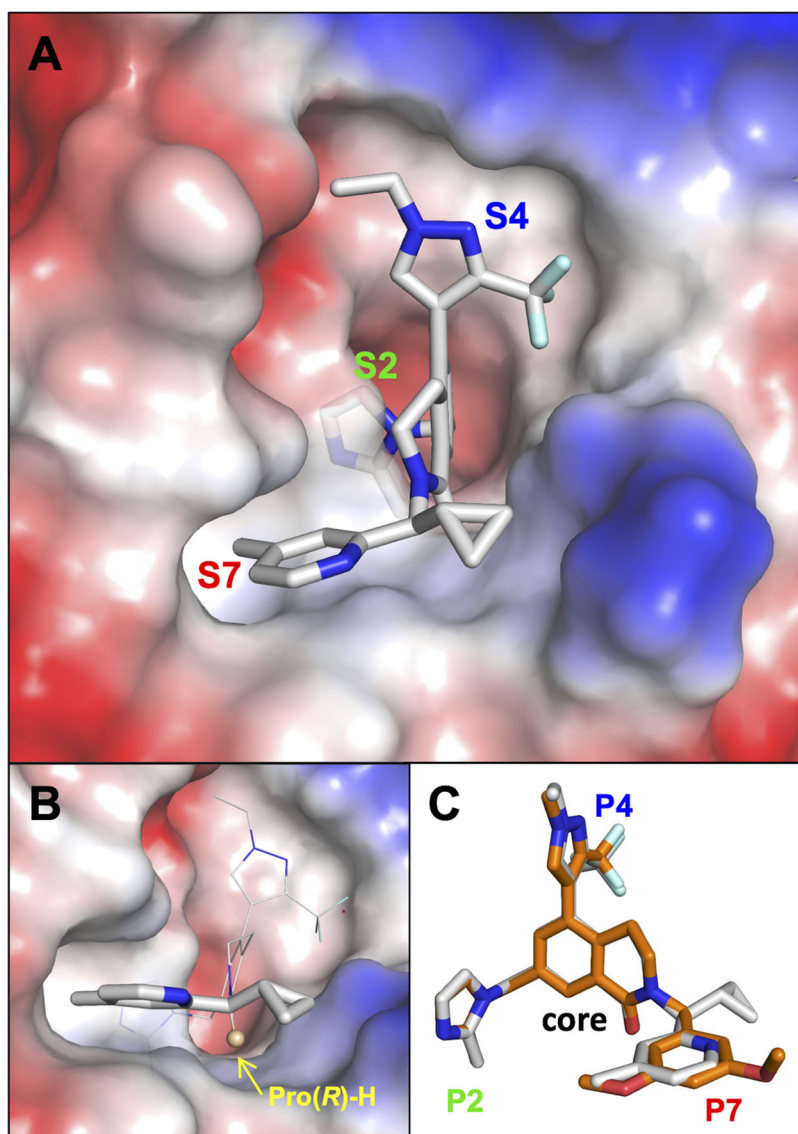
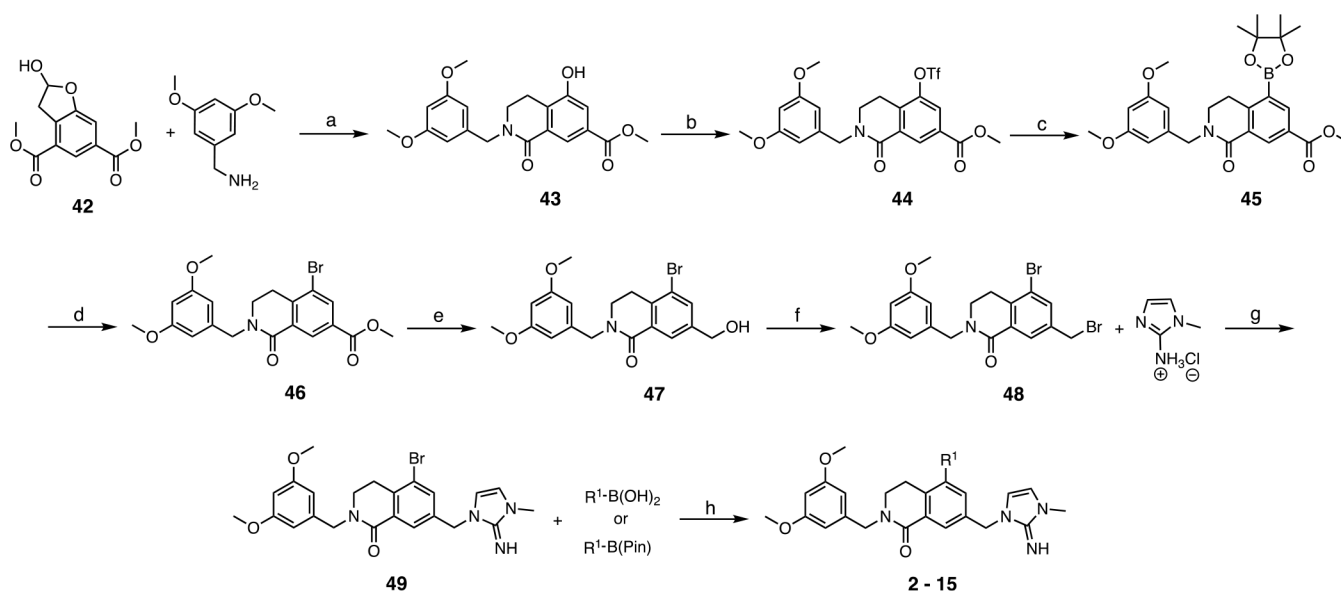
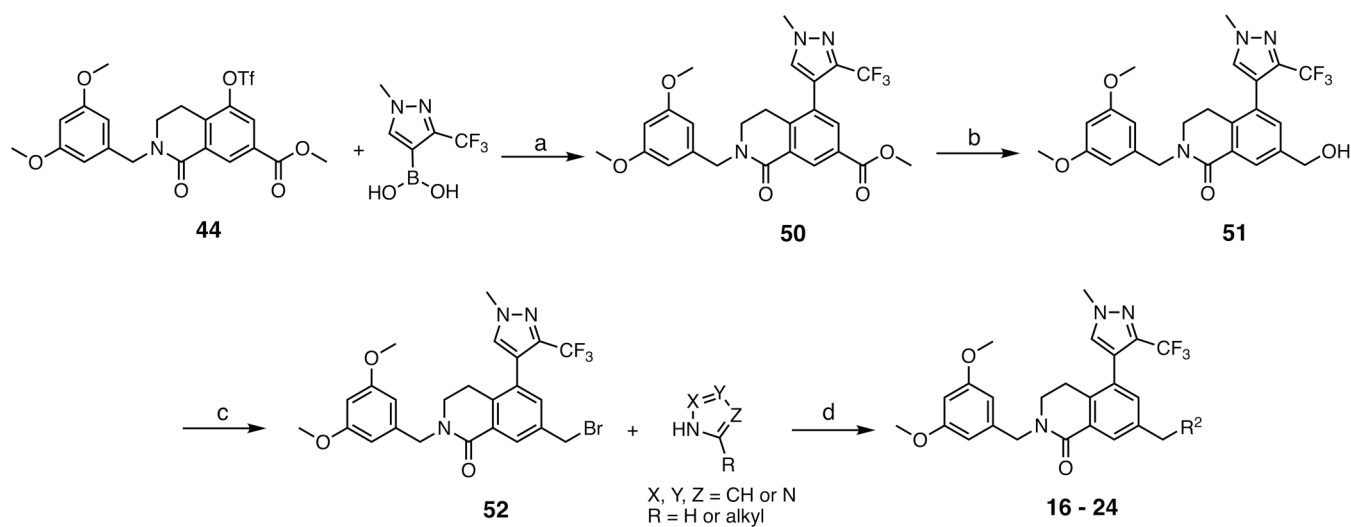


Figure 6. X-ray co-crystal structure of **37** bound to WDR5 (PDB ID: 7UAS). (A) Compound **37** (white carbon-capped sticks) bound to WDR5 represented as semitransparent electrostatic potential surface with labeled S₂, S₄, and S₇ binding regions. (B) Binding interactions of the (*S*)-1-cyclopropyl-1-(4-methylpyridine-2-yl)methyl P₇ unit in the S₇ subsite, pro(*R*)-H represented as a light orange ball. (C) Overlay of **20** (orange sticks) and **37** (white sticks).

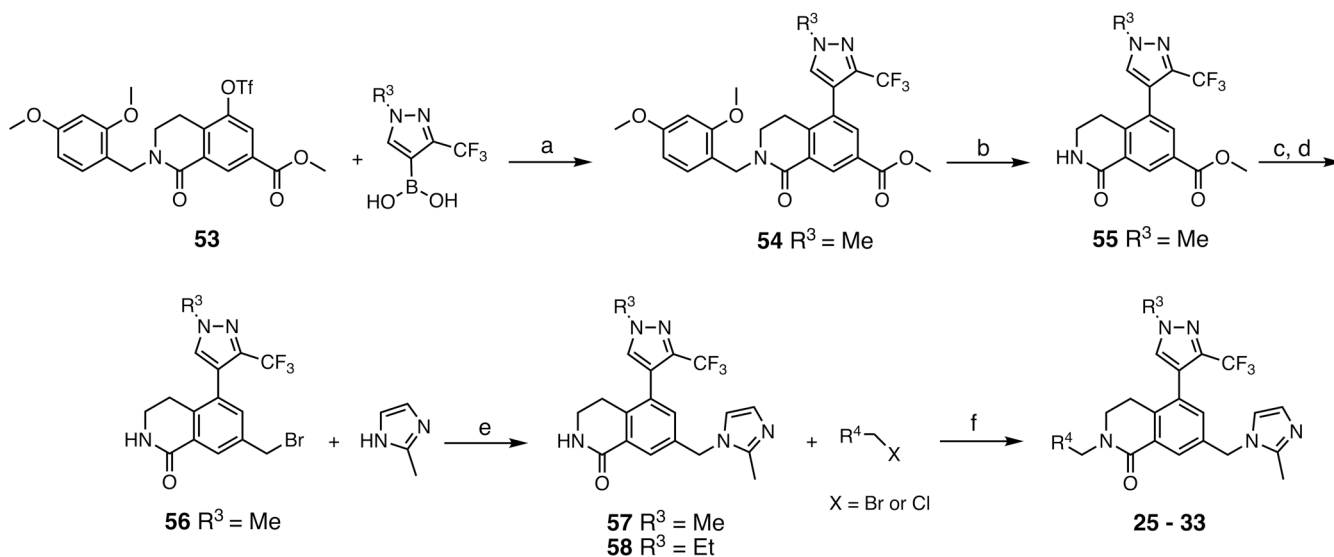
**Scheme 1.****Synthesis of Imidazole-Imine Series Compounds 2–15^a**

^aR¹ is defined in Table 1. Conditions: (a) 3,5-dimethoxybenzylamine, NaBH(OAc)₃, CH₂Cl₂, rt, overnight, then 1,4-dioxane, 110 °C, 99%; (b) phenyl triflimide, *i*-Pr₂NEt, THF/CH₂Cl₂, rt, overnight, 79%; (c) B₂Pin₂, KOAc, PdCl₂(dppf)·CH₂Cl₂, 1,4-dioxane, 100 °C overnight, 99%; (d) CuBr₂, MeOH/H₂O, 80 °C, 90%; (e) LiBHEt₃ (1 M THF), THF, 0 °C, 1 h, 41%; (f) PBr₃, CH₂Cl₂, 0 °C, 42%; (g) 1-methyl-1*H*-imidazol-2-amine hydrochloride, *i*-Pr₂NEt, MeCN, 60 °C, overnight, quant.; (h) R¹-B(OH)₂ or R¹-B(Pin), PdCl₂(dppf)·CH₂Cl₂, K₂CO₃, 1,4-dioxane/H₂O, 80 °C, overnight, 20–70%.

**Scheme 2.**

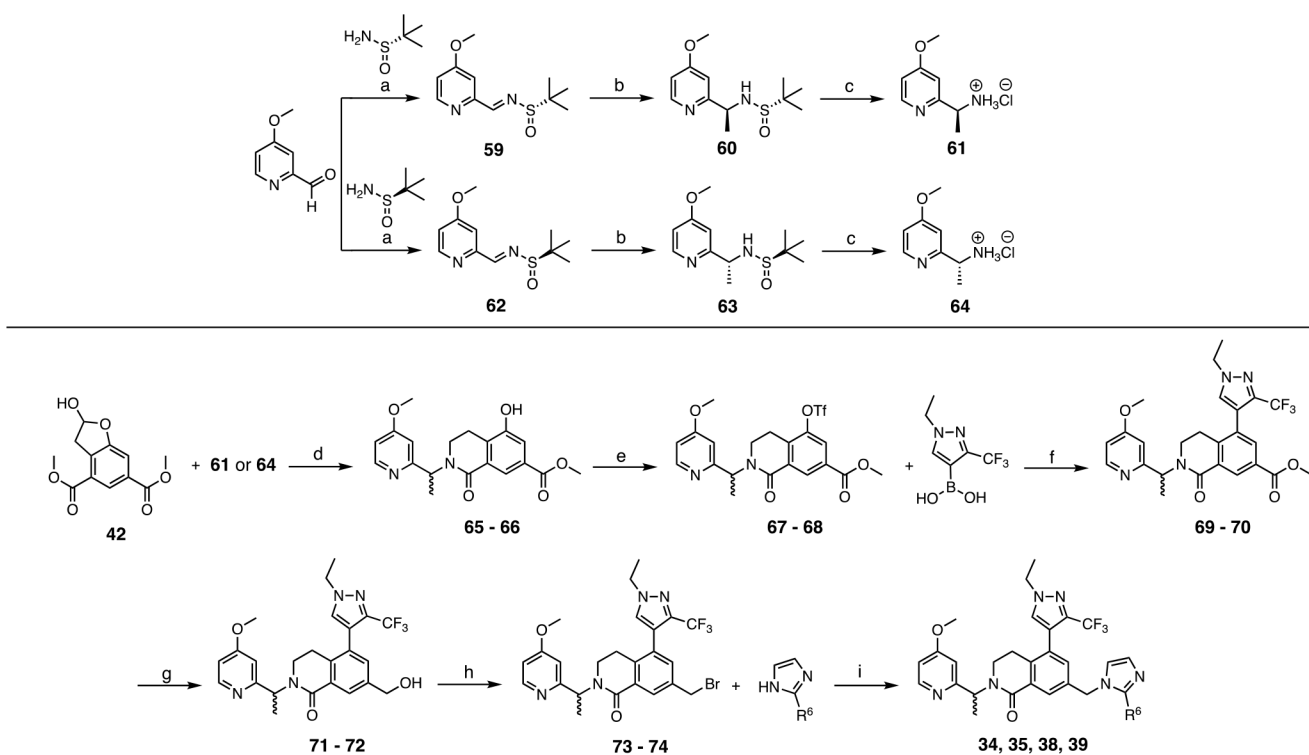
Synthesis of Nonbasic Warhead Series Compounds 16–24^a

^aR² is defined in Table 2. Conditions: (a) (1-methyl-3-(trifluoromethyl)-1*H*-pyrazol-4-yl)boronic acid, PdCl₂(dppf)·CH₂Cl₂, K₂CO₃, 1,4-dioxane/H₂O, 90 °C, overnight, 85%; (b) LiBHEt₃ (1 M THF), THF, 0 °C, 1 h, 95%; (c) PBr₃, CH₂Cl₂, 0 °C, 90%; (d) R²-azole, MeCN, 50 °C, overnight, 45–60%.

**Scheme 3.**Synthesis of Pyridyl Series Compounds 25–33^a

^a R^3 and R^4 are defined in Table 3. Synthesis of **58** was reported in Scheme S1. Conditions:

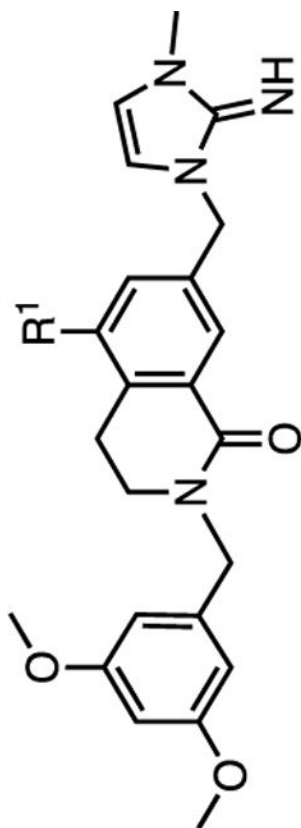
- (a) R^3 -boronic acid, $\text{PdCl}_2(\text{dppf})\cdot\text{CH}_2\text{Cl}_2$, K_2CO_3 , 1,4-dioxane/ H_2O , 90 °C, overnight, 90%;
 (b) TFA, anisole, CH_2Cl_2 , rt, overnight, 87%; (c) LiBHET_3 (1 M THF), THF, 0 °C, 1 h, quant.; (d) PBr_3 , CH_2Cl_2 , 0 °C, quant.; (e) 2-methyl-1*H*-imidazole, MeCN, 50 °C, overnight, 70%; (f) R^4 -pyridylmethyl halide, NaH, DMF, 0 °C, 2 h, 25–71%.

**Scheme 4.**

Synthesis of Compounds 34, 35, 38, and 39^a

^aR⁶ is defined in Table 4. Conditions: (a) (*S*)- or (*R*)-2-methylpropane-2-sulfinamide, Cs₂CO₃, CH₂Cl₂, rt, overnight, 65%; (b) MeMgBr (3.4 M 2-MeTHF), THF, -78 °C, 84–92%; (c) HCl (4 M 1,4-dioxane), THF, 94%—quant.; (d) chiral amine, *i*-Pr₂NEt, NaBH(OAc)₃, CH₂Cl₂, rt, overnight, then 1,4-dioxane, 110 °C, 84%; (e) phenyl triflimide, *i*-Pr₂NEt, THF/CH₂Cl₂, rt, overnight, 93%; (f) (1-ethyl-3-(trifluoromethyl)-1*H*-pyrazol-4-yl)boronic acid, Pd(PPh₃)₄, Na₂CO₃, 1,4-dioxane/H₂O, 80 °C, 96%; (g) LiBH₄ (2 M THF) or LiBHEt₃ (1 M THF), THF, 0 °C, 1 h, 72–85%; (h) CH₃SO₂Cl, *i*-Pr₂NEt, CH₂Cl₂, 0 °C, then LiBr, THF, reflux, 53% or PBr₃, CH₂Cl₂, 0 °C, 98%; (i) R⁶-imidazole, MeCN, 50 °C, overnight, 73%.

Table 1.

SAR Profile of P₄ Imidazole-Imine Series**1-15**

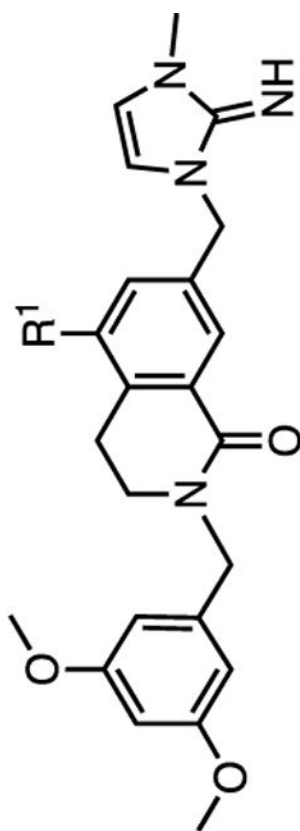
compnd	R ¹ =	cLogP	K _i (nM) TR-FRET ^d		Cell Proliferation Assays GI ₅₀ (nM) ^d			Selectivity ^b K562/MV4:11
			WDR5	MV4:11	MOLM-13	K562	K562/MV4:11	
1 ^c		4.8	<0.02	38 ± 9.0	78 ± 13	8000 ± 4100	210	

Author Manuscript

Author Manuscript

Author Manuscript

Author Manuscript

**1-15**

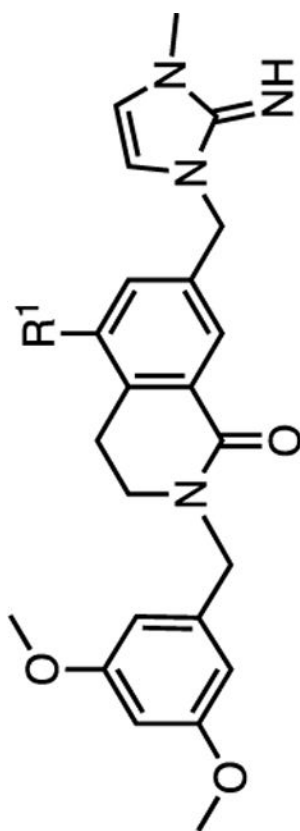
compnd	R ¹ =	cLogP	K _i (nM) TR-FRET ^d				Cell Proliferation Assays GI ₅₀ (nM) ^a				Selectivity ^b K562/MV4:11
			WDR5	MV4:11	MOLM-13	K562	MV4:11	MOLM-13	K562	K562/MV4:11	
2		4.0	0.033 ± 0.005	210 ± 19	420 ± 30	18000 ± 2800				86	
3		3.7	0.035 ± 0.005	88 ± 20	220 ± 23	>30000				>340	

Author Manuscript

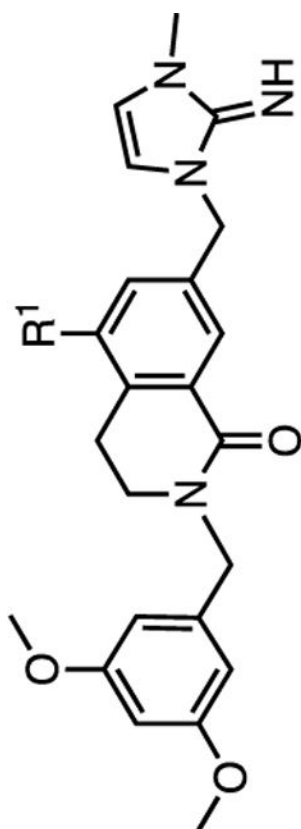
Author Manuscript

Author Manuscript

Author Manuscript

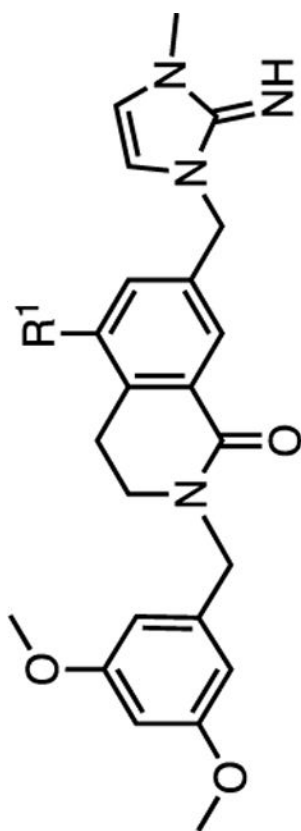
**1-15**

compnd	R ¹ =	cLogP	K_i (nM) TR-FRET ^d			Cell Proliferation Assays GI ₅₀ (nM) ^d			Selectivity ^b K562/MV4:11
			WDR5	MV4:11	MOLM-13	MV4:11	MOLM-13	K562	
4		3.2	0.036 ± 0.005	1200 ± 310	3900 ± 410	>30000	>30000	>25	
5		2.7	0.055 ± 0.005	560 ± 84	1600 ± 200	>30000	>30000	>54	
6		3.7	0.022 ± 0.001	640 ± 120	2400 ± 240	>30000	>30000	>47	



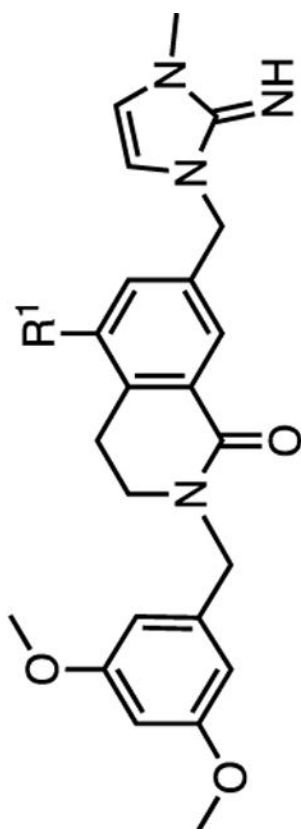
1-15

compound	R ¹ =	cLogP	K _i (nM) TR-FRET ^d			Cell Proliferation Assays GI ₅₀ (nM) ^d			Selectivity ^b K562/MV4:11
			WDR5	MV4:11	MOLM-13	MV4:11	MOLM-13	K562	
7		3.9	<0.02	120 ± 59	290 ± 170	>29000	>240		
8		3.2	0.029 ± 0.002	230 ± 52	640 ± 120	>30000	>130		
9		3.7	<0.02	200 ± 52	560 ± 76	>30000	>150		



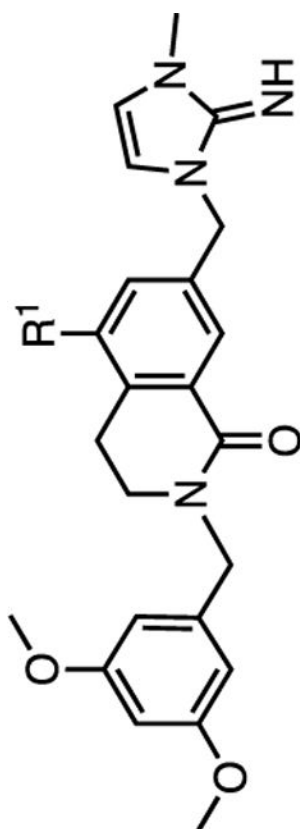
1-15

compnd	R ¹ =	cLogP	K _i (nM) TR-FRET ^d				Cell Proliferation Assays GI ₅₀ (nM) ^a				Selectivity ^b K562/MV4:11
			WDR5	MV4:11	MOLM-13	K562	MV4:11	MOLM-13	K562	K562/MV4:11	
10		2.4	0.046 ± 0.002	850 ± 240	2100 ± 410	>30000	>30000	>30000	>35		
11		2.6	0.023 ± 0.001	210 ± 49	570 ± 85	>30000	>30000	>140			



1-15

compnd	R ¹ =	cLogP	K _i (nM) TR-FRET ^d				Cell Proliferation Assays GI ₅₀ (nM) ^d				Selectivity ^b K562/MV4:11
			WDR5	MV4:11	MOLM-13	K562	MV4:11	MOLM-13	K562	K562/MV4:11	
12		2.5	0.21 ± 0.008	19000 ± 3000	>30000	>30000	>30000	>2			
13		3.1	0.025 ± 0.003	85 ± 17	270 ± 31	>30000	>350				



1 – 15

compnd	R ¹ =	K _i (nM) TR-FRET ^a		Cell Proliferation Assays GI ₅₀ (nM) ^a			Selectivity ^b	
		cLogP	WDR5	MV4:11	MOLM-13	K562	K562/MV4:11	K562/MV4:11
14		3.5	<0.02	39 ± 9.0	110 ± 7.8	>30000	>770	>770
15		4.0	<0.02	36 ± 11	110 ± 9.8	>30000	>830	>830

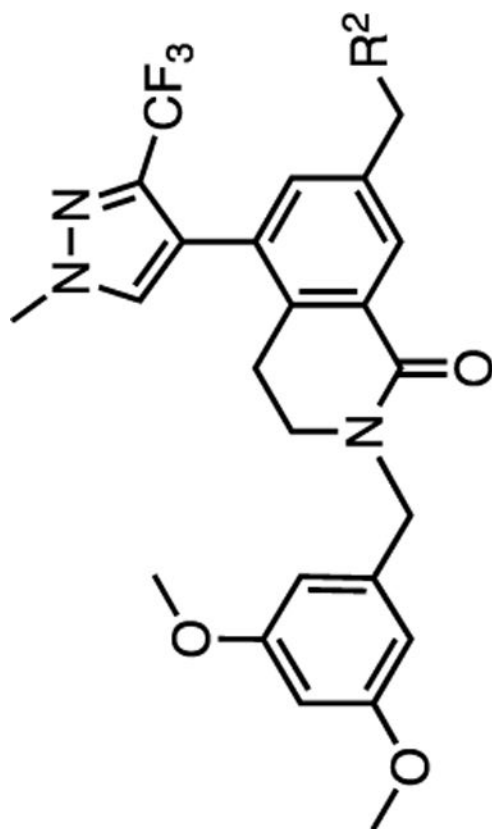
^aTR-FRET K_i and cell proliferation GI₅₀ values represent four independent replicate determinations ± standard deviation.

^bSelectivity is defined as GI₅₀,K562/GI₅₀,MV4:11 and is used to generally distinguish between on- and off-target inhibition mechanisms.

^cThe data for **1** were reported in our previous report.^{3,5}

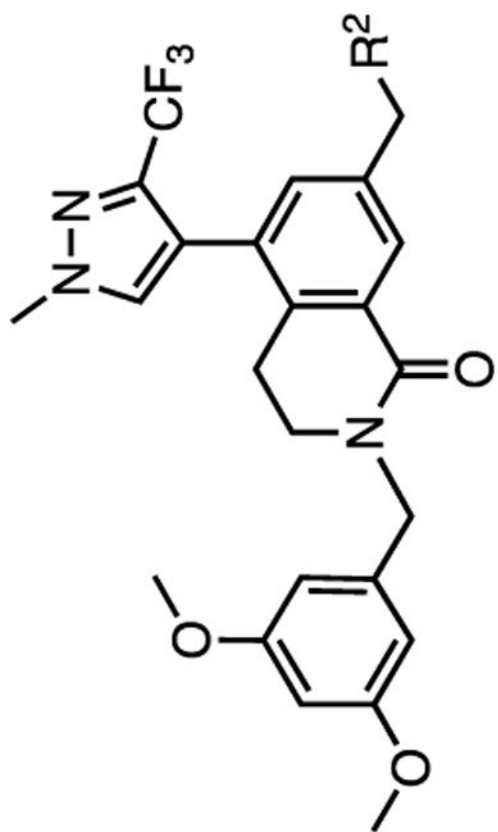
SAR Profile of Nonbasic Warhead Series

Table 2.

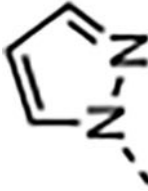
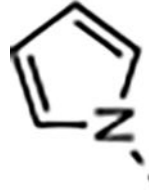


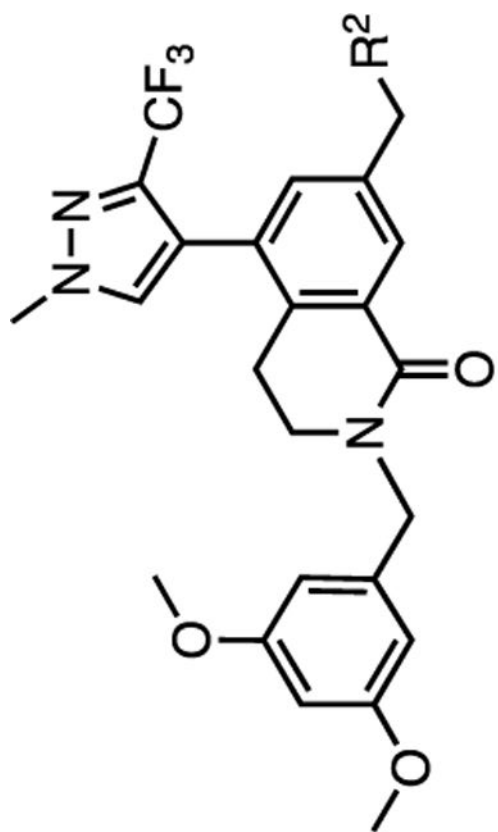
16 – 24

compnd	R ² =	cLogP	K _i (nM) TR-FRET ^a		Cell Proliferation Assays GI ₅₀ (nM) ^a			Selectivity ^b K562/MV4:11
			WDR5	MOLM-13	MV4:11	K562	K562/MV4:11	
16		2.9	<0.02	180 ± 51	59 ± 5.6	9100 ± 2100	150	



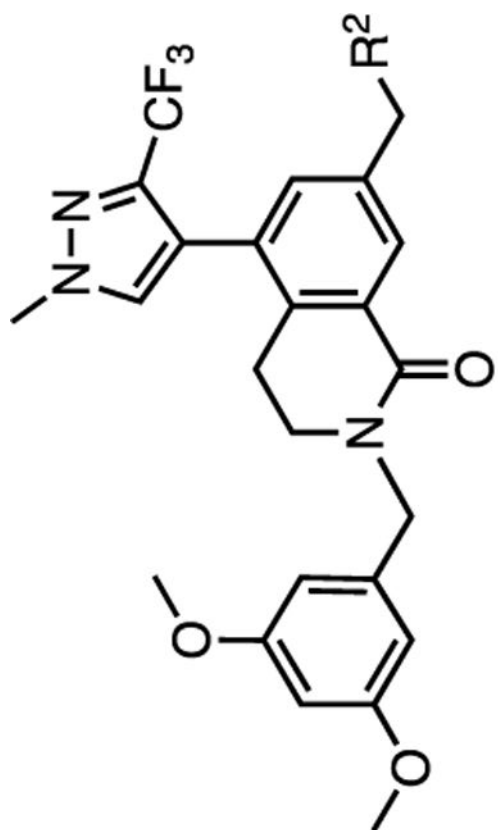
16-24

compnd	R ² =	K _i (nM) TR-FRET ^d		Cell Proliferation Assays GI ₅₀ (nM) ^d			Selectivity ^b K562/MV4:11
		cLogP	WDR5	MV4:11	MOLM-13	K562	
17		3.9	>6.7	22000 ± 6000	20000 ± 5400	>30000	>1
18		4.4	>6.7	15000 ± 4000	15000 ± 3600	>30000	>2



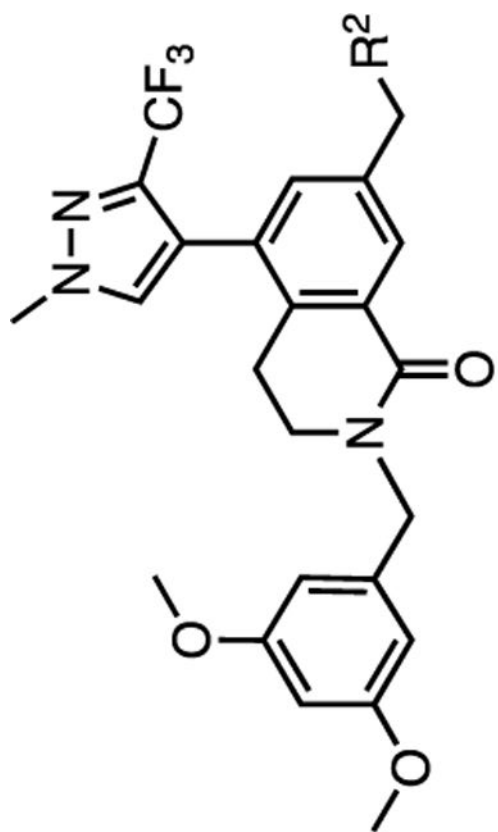
16-24

compnd	R ² =	K _i (nM) TR-FRET ^d		Cell Proliferation Assays GI ₅₀ (nM) ^d			Selectivity ^b	
		cLogP	WDR5	MV4:11	MOLM-13	K562	K562/MV4:11	K562/MV4:11
19		1.6	6.5 ± 1.7	16000 ± 1300	>30000	>30000	>2	>2
20		3.1	<0.02	32 ± 13	110 ± 33	3700 ± 2500	120	120



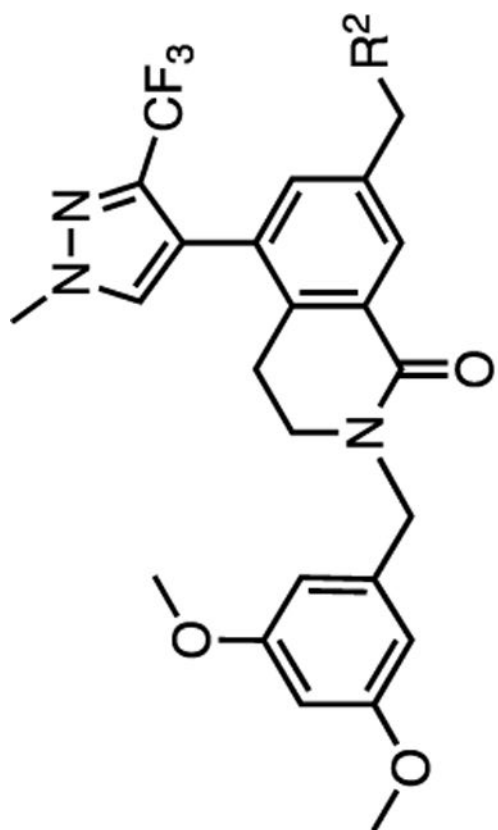
16-24

compnd	R ² =	K _i (nM) TR-FRET ^d		Cell Proliferation Assays GI ₅₀ (nM) ^d			Selectivity ^b	
		cLogP	WDR5	MV4:11	MOLM-13	K562	K562/MV4:11	K562/MV4:11
21		3.7	0.022 ± 0.001	94 ± 10	240 ± 53	7500 ± 1300		80



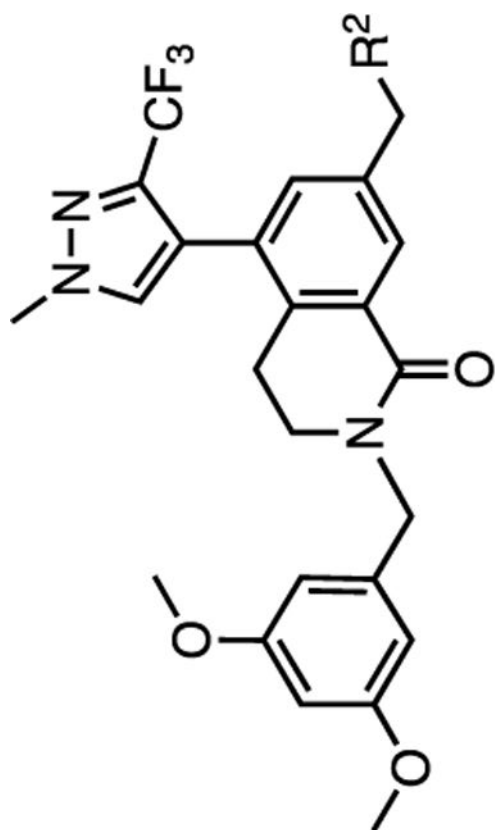
16-24

compnd	R ² =	K _i (nM) TR-FRET ^d		Cell Proliferation Assays GI ₅₀ (nM) ^d			Selectivity ^b	
		cLogP	WDR5	MV4:11	MOLM-13	K562	K562/MV4:11	
22		4.1	3.4 ± 0.17	4700 ± 500	7700 ± 2000	16000 ± 3100		3



16-24

compnd	R ² =	K _i (nM) TR-FRET ^d		Cell Proliferation Assays GI ₅₀ (nM) ^d			Selectivity ^b	
		cLogP	WDR5	MV4:11	MOLM-13	K562	K562/MV4:11	K562/MV4:11
23		3.6	0.028 ± 0.002	240 ± 64	710 ± 140	8500 ± 2000		35



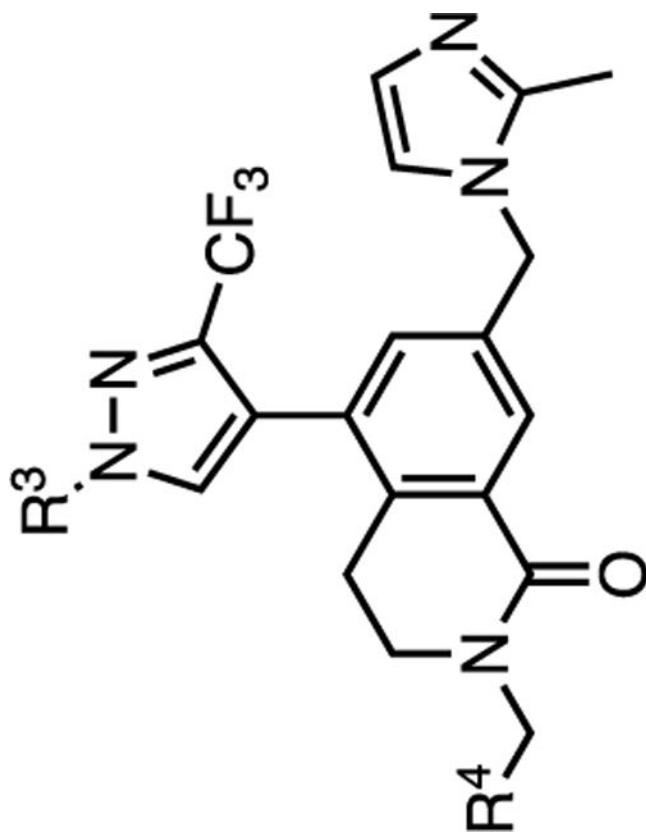
16-24

compnd	R ² =	cLogP	K _i (nM) TR-FRET ^a			Cell Proliferation Assays GI ₅₀ (nM) ^d			Selectivity ^b K562/MV4:11
			WDR5	MV4:11	MOLM-13	K562	K562		
24		3.1	>6.7	12000 ± 2800	20000 ± 4900	>30000	>30000	>3	

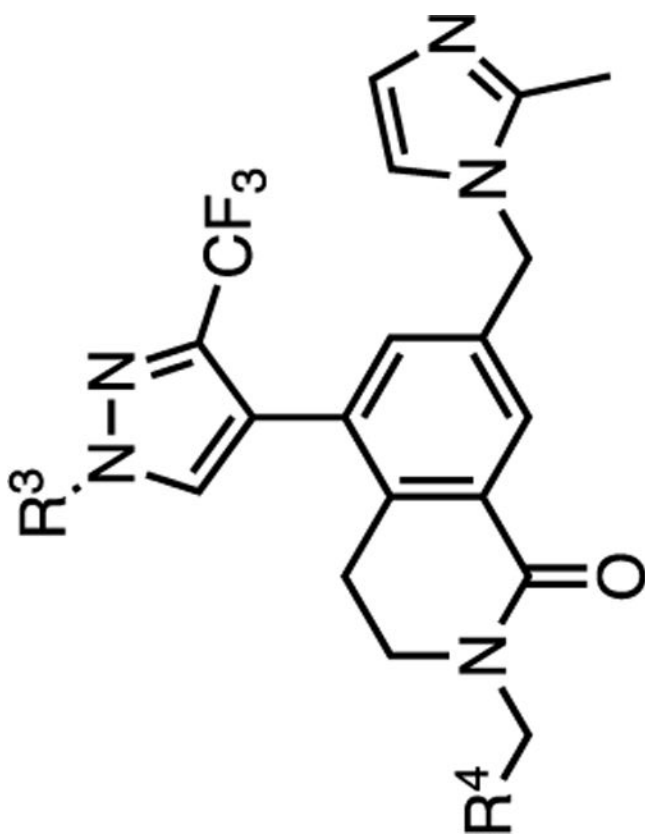
^aTR-FRET K_i and cell proliferation GI₅₀ values represent four independent replicate determinations ± standard deviation.

^bSelectivity is defined as GI_{50,K562}/GI_{50,MV4:11} and is used to generally distinguish between on- and off-target inhibition mechanisms.

Table 3.

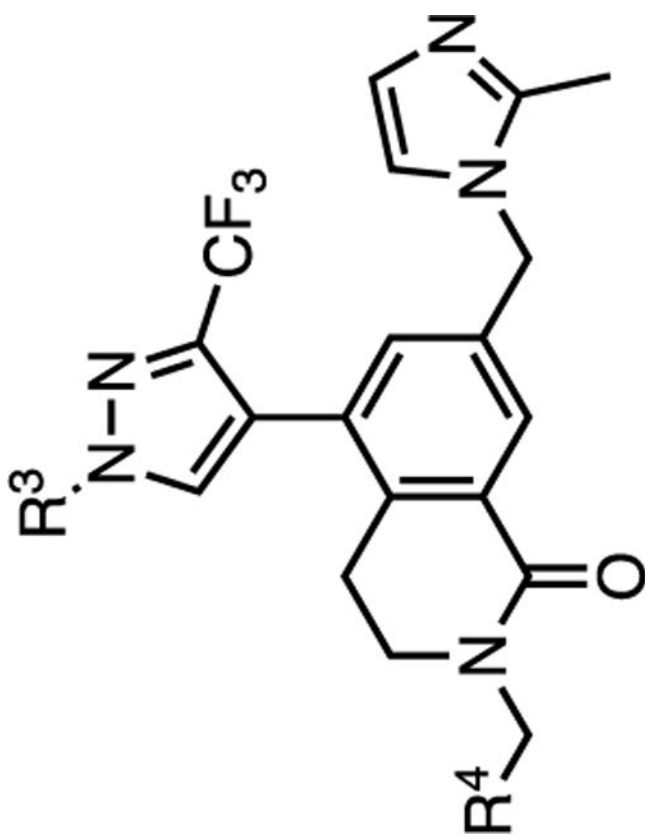
SAR Profile of the P₇ Pyridylmethyl Series WDR5 Inhibitors**25 – 33**

compnd	R ³ =	R ⁴ =	cLogP	K _i (nM) TR-FRET ^d			Cell Proliferation Assays GI ₅₀ (nM) ^a			Selectivity ^b K562/MV4:11
				WDR5	MV4:11	MOLM-13	K562	K562/MV4:11		

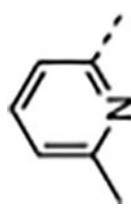


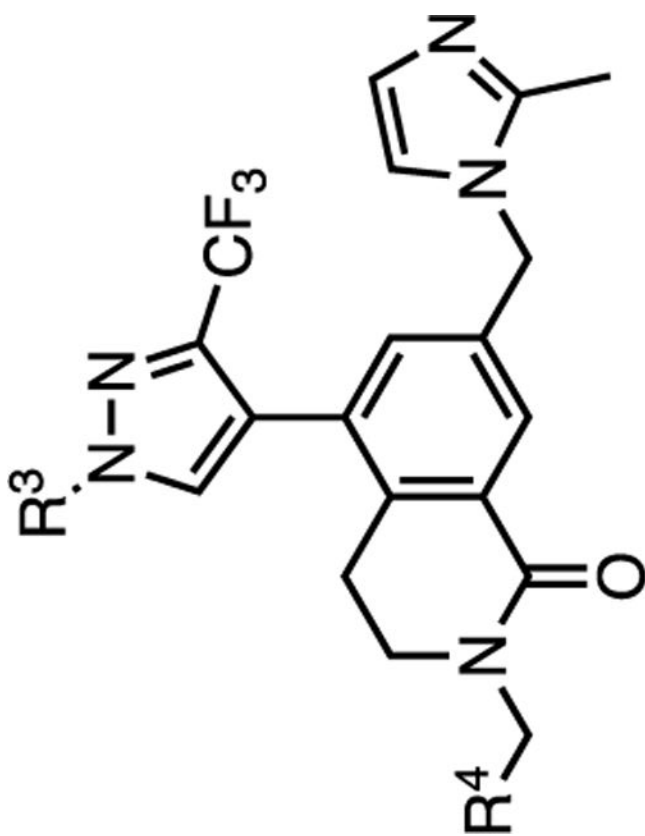
25 – 33

compnd	R ³ =	R ⁴ =	cLogP	K _i (nM) TR-FRET ^a			Cell Proliferation Assays GI ₅₀ (nM) ^a			Selectivity ^b K562/MV4:11
				WDR5	MV4:11	MOLM-13	K562	K562/MV4:11		
25	Me		1.8	0.23 ± 0.03	1500 ± 160	3100 ± 200	>30000	>20	>20	



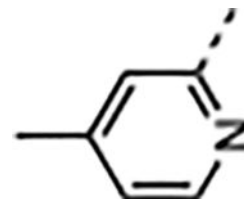
25 – 33

compnd	R ³ =	R ⁴ =	cLogP	K _i (nM) TR-FRET ^a			Cell Proliferation Assays GI ₅₀ (nM) ^a			Selectivity ^b K562/MV4:11
				WDR5	MV4:11	MOLM-13	MOLM-13	K562	K562/MV4:11	
26	Me		2.3	0.039 ± 0.005	170 ± 53	330 ± 120	13000 ± 2500		76	

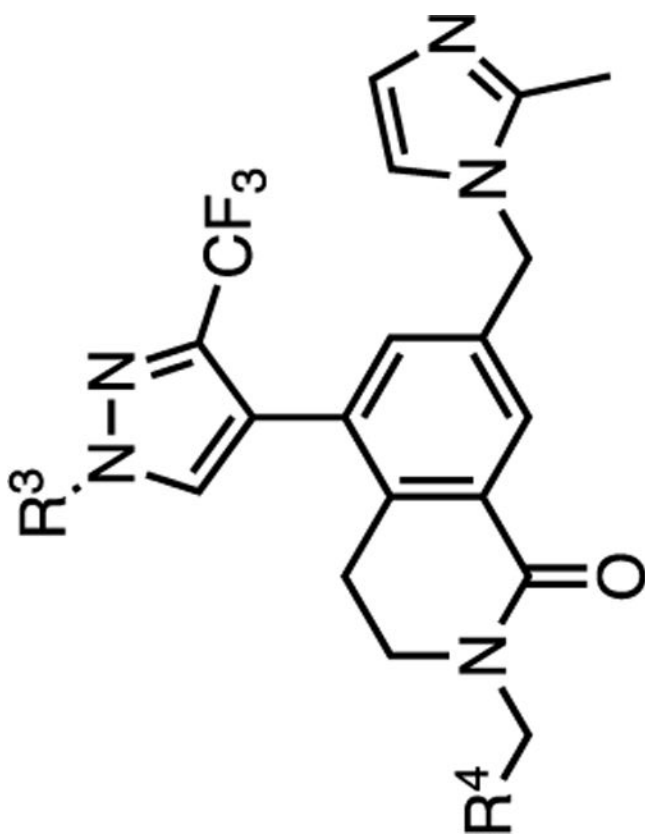


27

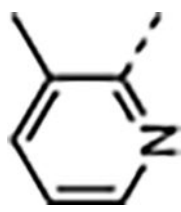
compnd	R ³ =	R ⁴ =	cLogP	K _i (nM) TR-FRET ^a				Cell Proliferation Assays GI ₅₀ (nM) ^a			Selectivity ^b K562/MV4:11
				WDR5	MV4:11	MOLM-13	K562	MV4:11	MOLM-13	K562	

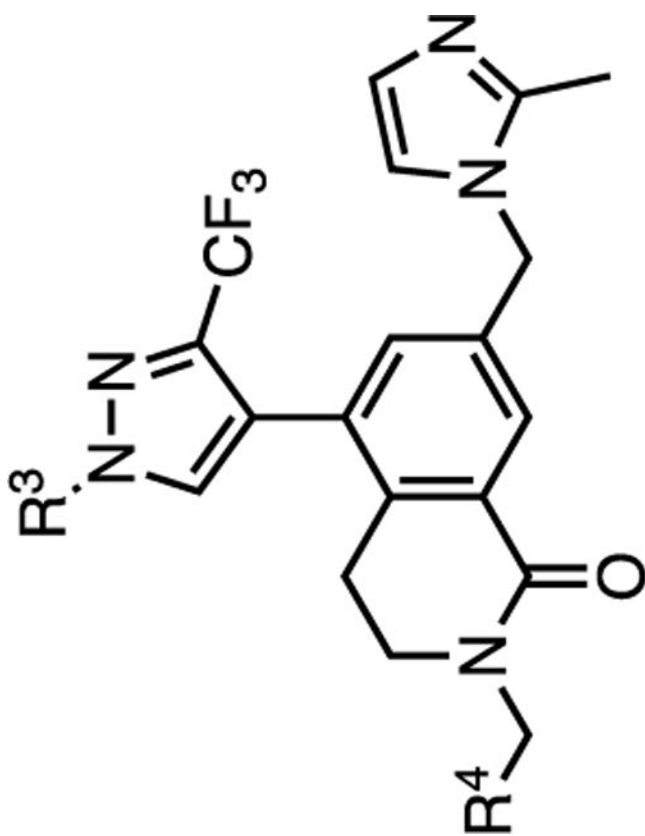


27	Me		2.3	0.020 ± 0.004	23 ± 9.1	33 ± 12	3600 ± 310	160
----	----	--	-----	---------------	----------	---------	------------	-----



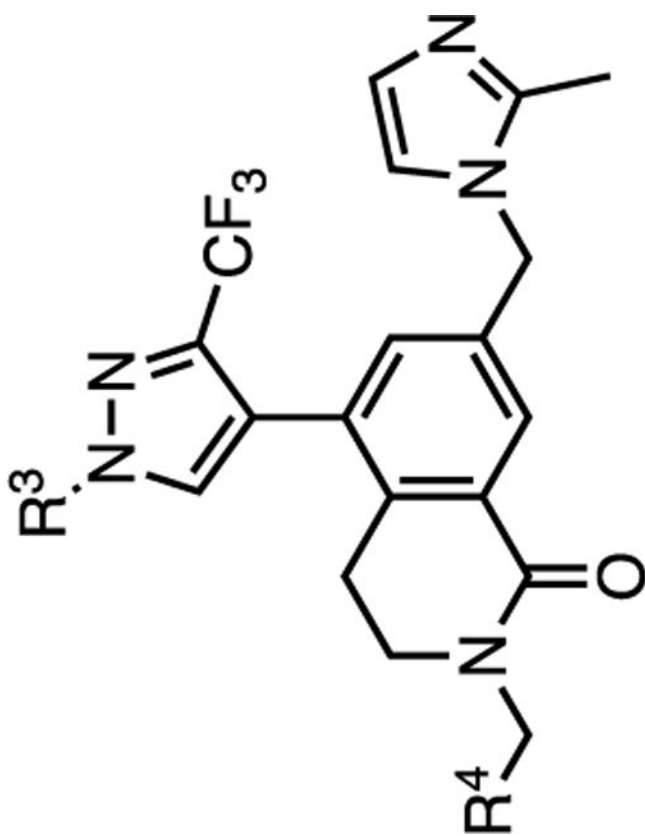
27

compnd	R ³ =	R ⁴ =	cLogP	K _i (nM) TR-FRET ^a			Cell Proliferation Assays GI ₅₀ (nM) ^a			Selectivity ^b K562/MV4:11
				WDR5	MV4:11	MOLM-13	K562	K562/MV4:11		
28	Me		2.3	0.59 ± 0.19	3000 ± 840	4700 ± 790	22000 ± 6500		7	



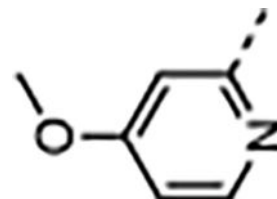
25 – 33

compnd	R ³ =	R ⁴ =	cLogP	K _i (nM) TR-FRET ^a			Cell Proliferation Assays GI ₅₀ (nM) ^a			Selectivity ^b K562/MV4:11
				WDR5	MV4:11	MOLM-13	K562	MOLM-13	K562	
29	Me		2.3	0.064 ± 0.009	270 ± 94	550 ± 200	13000 ± 7100	48		

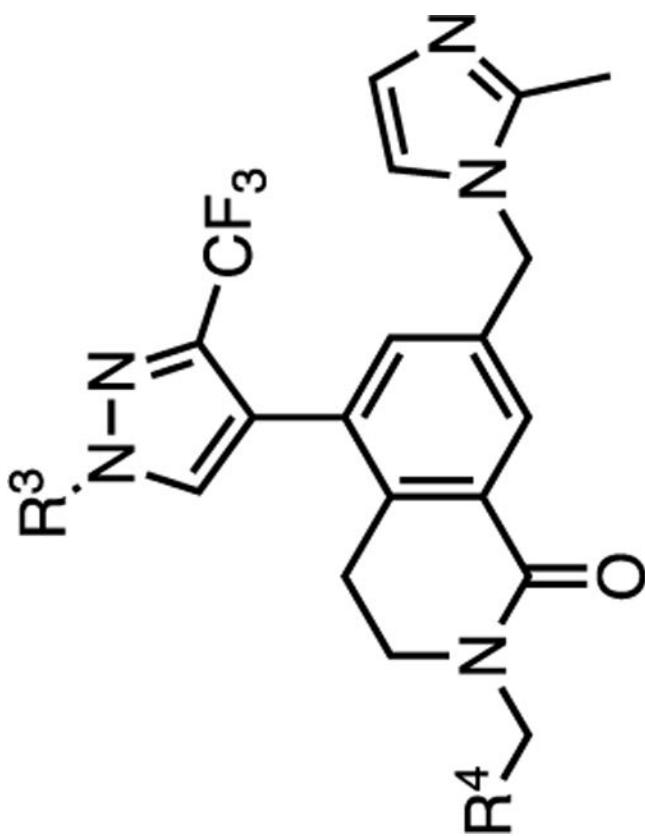


25 – 33

compnd	R ³ =	R ⁴ =	cLogP	Cell Proliferation Assays GI ₅₀ (nM) ^a				Selectivity ^b
				WDR5	MV4:11	MOLM-13	K562	

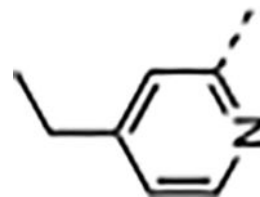


30	Me		1.7	<0.02	24 ± 8.6	39 ± 14	9500 ± 4800	400
----	----	--	-----	-------	----------	---------	-------------	-----

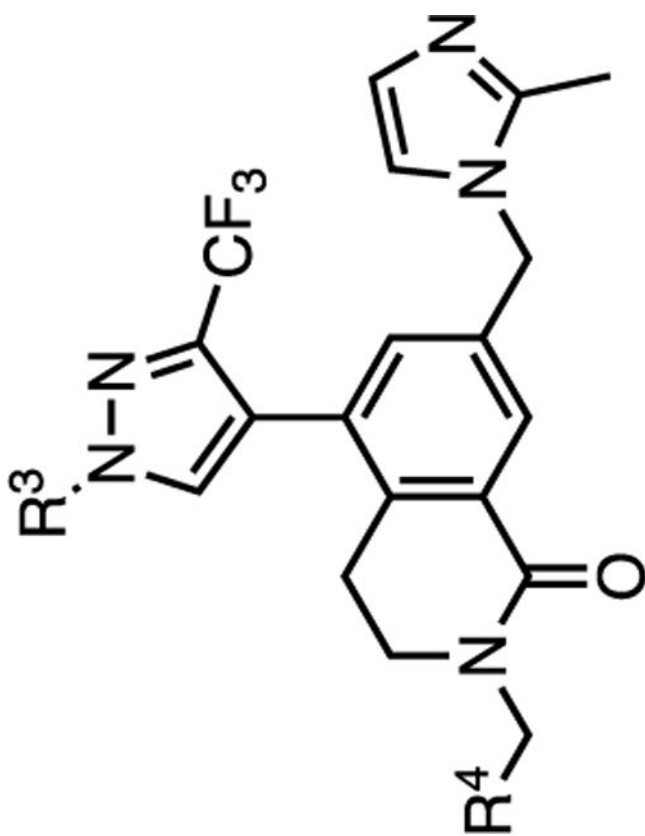


25 – 33

compnd	R ³ =	R ⁴ =	cLogP	K _i (nM) TR-FRET ^a			Cell Proliferation Assays GI ₅₀ (nM) ^a			Selectivity ^b K562/MV4:11
				WDR5	MV4:11	MOLM-13	K562	MOLM-13	K562	

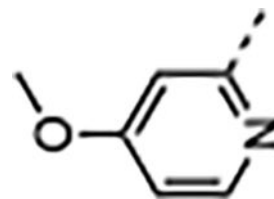


31	Me		2.8	<0.02	16 ± 7.3	25 ± 9.6	4100 ± 1300		260
----	----	--	-----	-------	----------	----------	-------------	--	-----

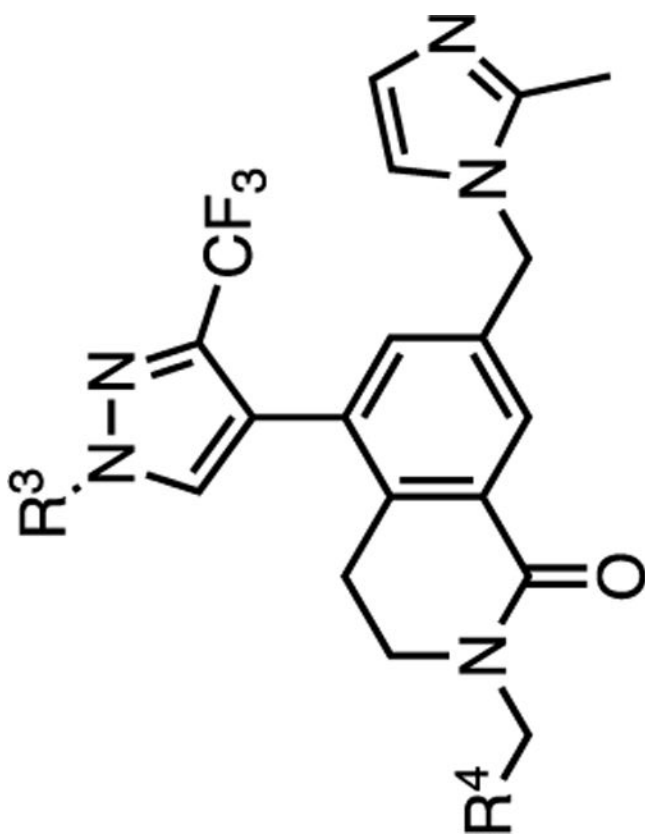


25 – 33

compnd	R ³ =	R ⁴ =	cLogP	K _i (nM) TR-FRET ^a			Cell Proliferation Assays GI ₅₀ (nM) ^a			Selectivity ^b K562/MV4:11
				WDR5	MV4:11	MOLM-13	K562	K562/MV4:11		



32	Et		2.3	<0.02	34 ± 18	59 ± 30	13000 ± 10000	380
----	----	--	-----	-------	---------	---------	---------------	-----



25 – 33

compnd	R ³ =	R ⁴ =	cLogP	K _i (nM) TR-FRET ^a				Cell Proliferation Assays GI ₅₀ (nM) ^a			Selectivity ^b K562/MV4:11
				WDR5	MV4:11	MOLM-13	K562	MV4:11	MOLM-13	K562	
33	Et		3.4	<0.02	24 ± 8.2	43 ± 15	5600 ± 1100	230			

Author Manuscript

Author Manuscript

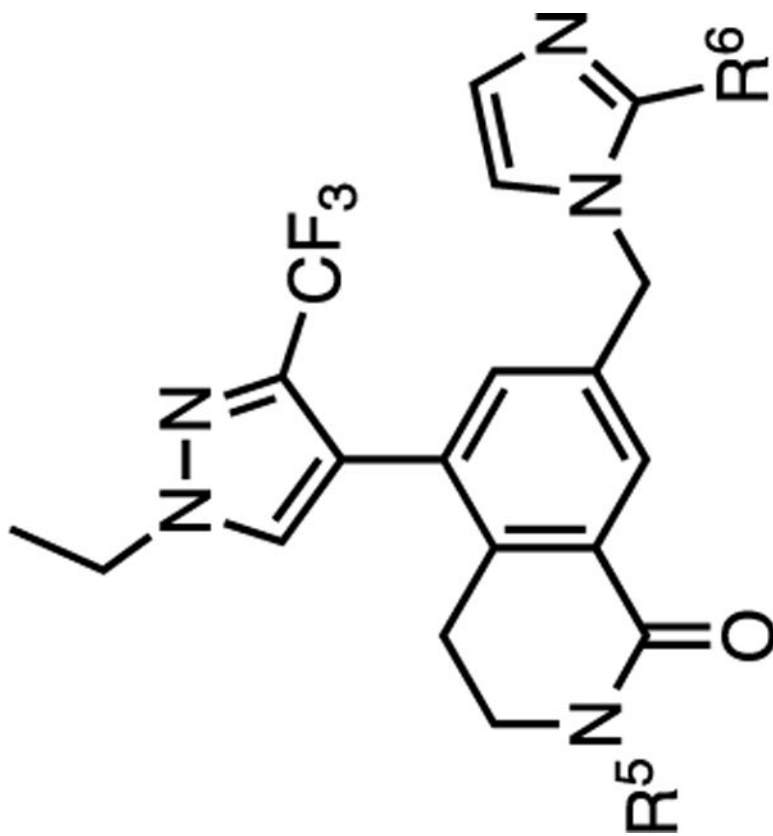
Author Manuscript

Author Manuscript

TR-FRET K_i and cell proliferation GI50 values represent four independent replicate determinations \pm standard deviation.

ρ Selectivity is defined as GI50_{K562/GI50,MV4;11} and is used to generally distinguish between on- and off-target inhibition mechanisms.

Table 4.

SAR Profile of the α -Substituted 2-Pyridyl Series WDR5 Inhibitors

34 – 41

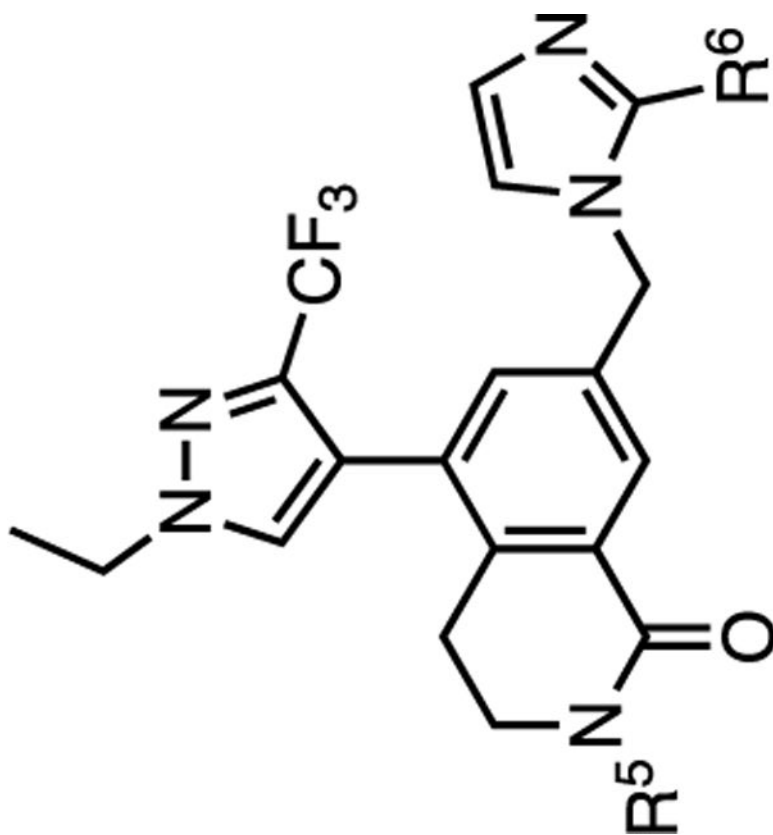
compnd	R ⁵ =	cLogP	Kinetic Solubility (μ M)	K _i (nM) TR-FRET ^d	Cell Proliferation Assays GI ₅₀ (nM) ^d			Selectivity ^b K562/MV4:11
					WDR5	MV4:11	MOLM-13	

Author Manuscript

Author Manuscript

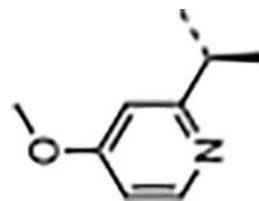
Author Manuscript

Author Manuscript



34 – 41

compnd	R ⁵ =	R ⁶ =	cLogP	Kinetic Solubility (μM)	K _i (nM) TR-FRET ^d		Cell Proliferation Assays GI ₅₀ (nM) ^a			Selectivity ^b K562/MV4:11
					WDR5	MV4:11	MOLM-13	K562		



34

11 ± 6.1

26 ± 8.8

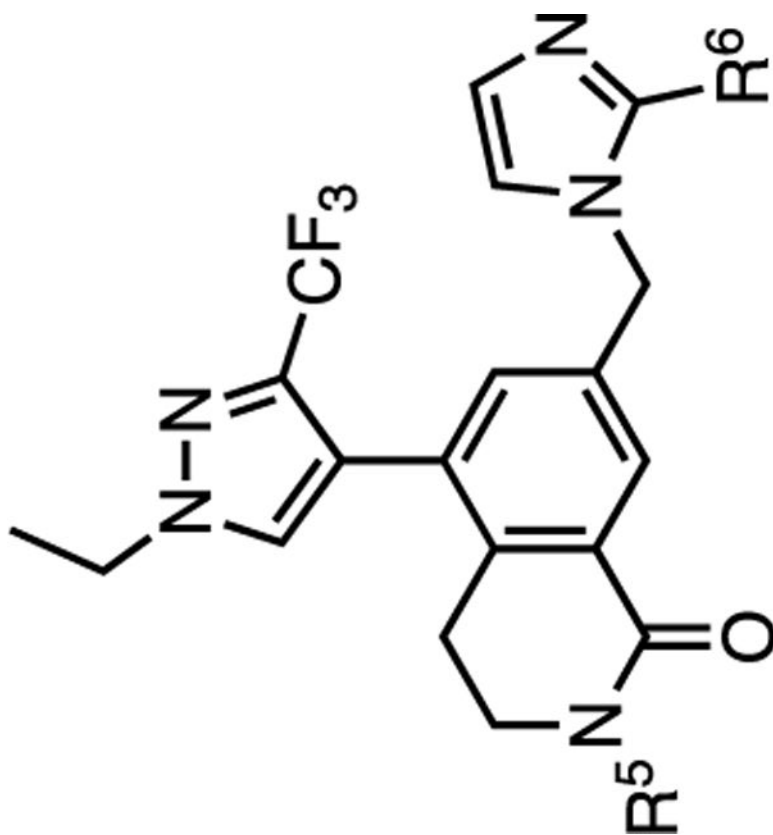
2200 ± 2300

200

80

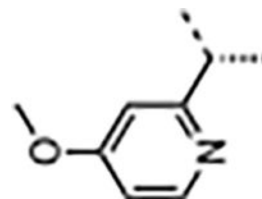
<0.02

2.6



34 – 41

compnd	R ⁵ =	R ⁶ =	cLogP	Kinetic Solubility (μ M)	K _i (nM) TR-FRET ^d	Cell Proliferation Assays GI ₅₀ (nM) ^a			Selectivity ^b
						WDR5	MV4:11	MOLM-13	



35

200

7800 ± 2700

110 ± 23

39 ± 9.0

0.029 ± 0.002

n.d.

2.6

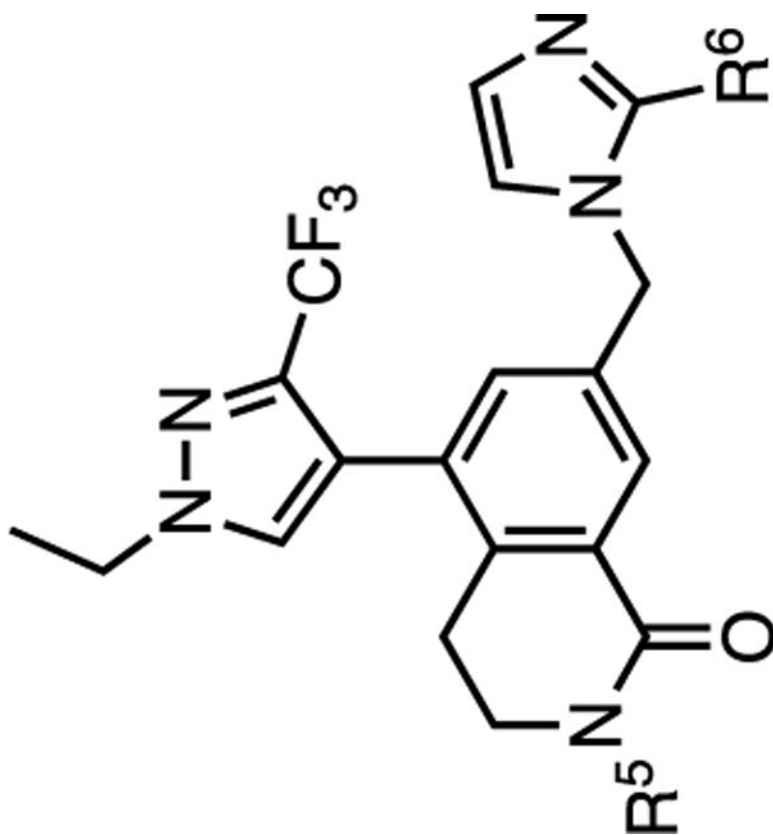
Me

Author Manuscript

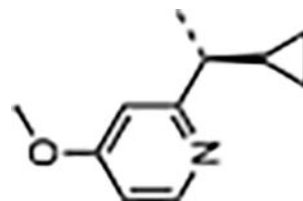
Author Manuscript

Author Manuscript

Author Manuscript

**34 – 41**

compnd	R ⁵ =	R ⁶ =	cLogP	Kinetic Solubility (μ M)	K _i (nM) TR-FRET ^d	Cell Proliferation Assays GI ₅₀ (nM) ^a			Selectivity ^b
						WDR5	MV4:11	MOLM-13	



36

170

2600 ± 1500

36 ± 11

15 ± 4.9

<0.02

65

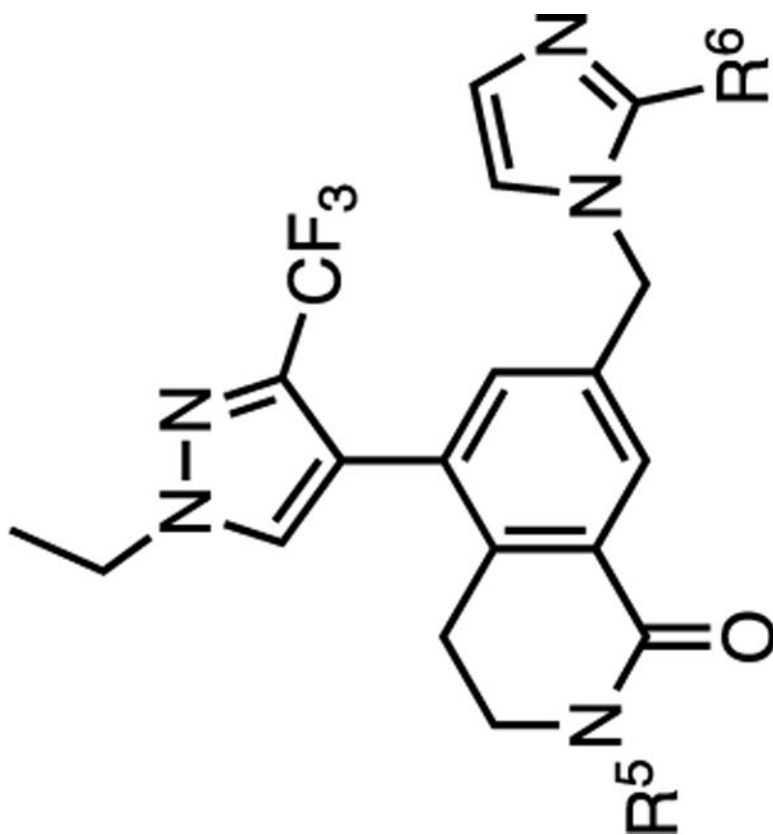
3.0

Author Manuscript

Author Manuscript

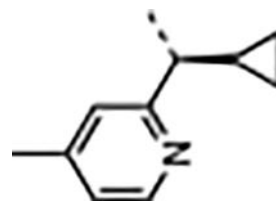
Author Manuscript

Author Manuscript



34 – 41

compnd	R ⁵ =	R ⁶ =	cLogP	Kinetic Solubility (μM)	K _i (nM) TR-FRET ^d		Cell Proliferation Assays GI ₅₀ (nM) ^a			Selectivity ^b K562/MV4:11
					WDR5	MV4:11	MOLM-13	K562		



37

Me

66

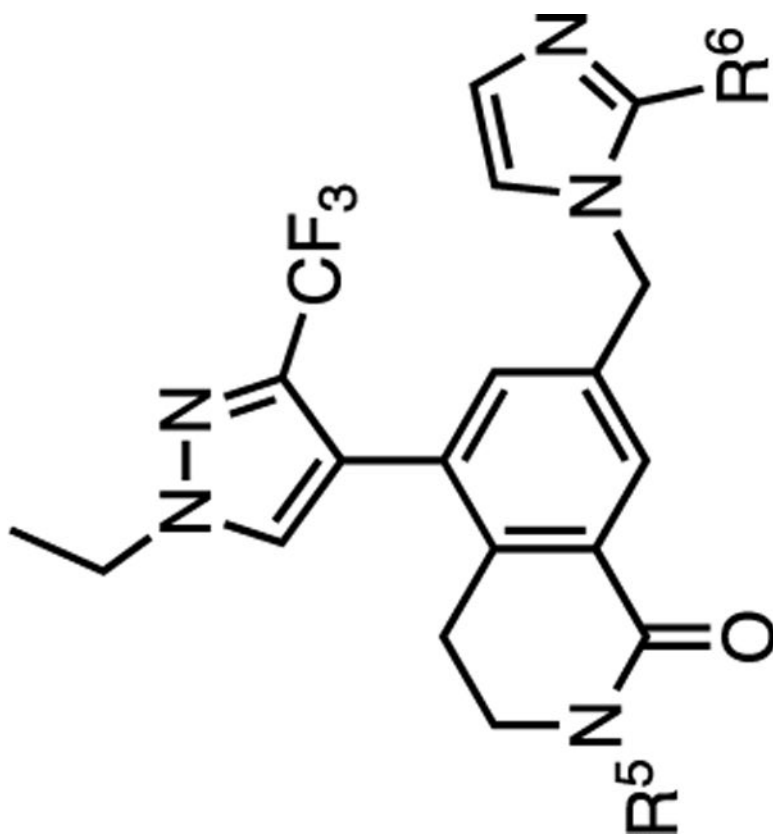
<0.02

17 ± 6.6

43 ± 9.0

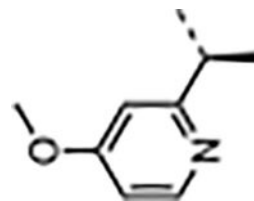
2500 ± 2100

150



34 – 41

compnd	R ⁵ =	R ⁶ =	cLogP	Kinetic Solubility (μ M)	K _i (nM) TR-FRET ^d	Cell Proliferation Assays GI ₅₀ (nM) ^a			Selectivity ^b K562/MV4:11
						MV4:11	MOLM-13	K562	



38

200

1900 ± 1800

19 ± 6.2

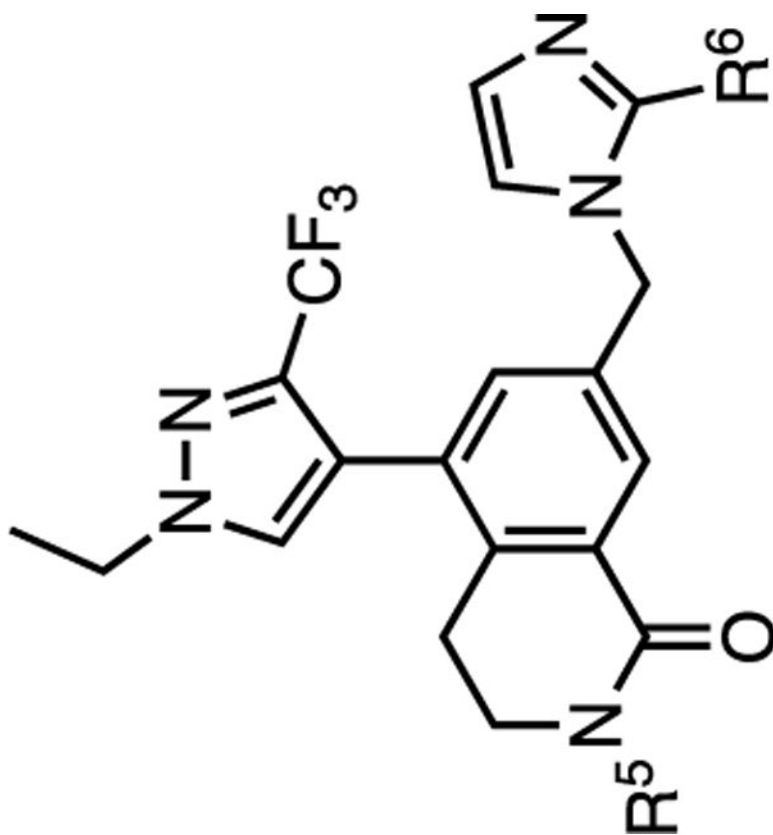
9.7 ± 5.6

<0.02

86

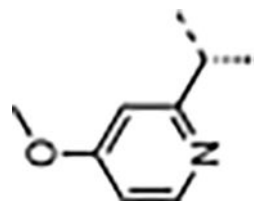
2.3

H



34 – 41

compnd	R ⁵ =	R ⁶ =	cLogP	Kinetic Solubility (μ M)	K _i (nM) TR-FRET ^d		Cell Proliferation Assays GI ₅₀ (nM) ^a			Selectivity ^b K562/MV4:11
					WDR5	MV4:11	MOLM-13	K562		



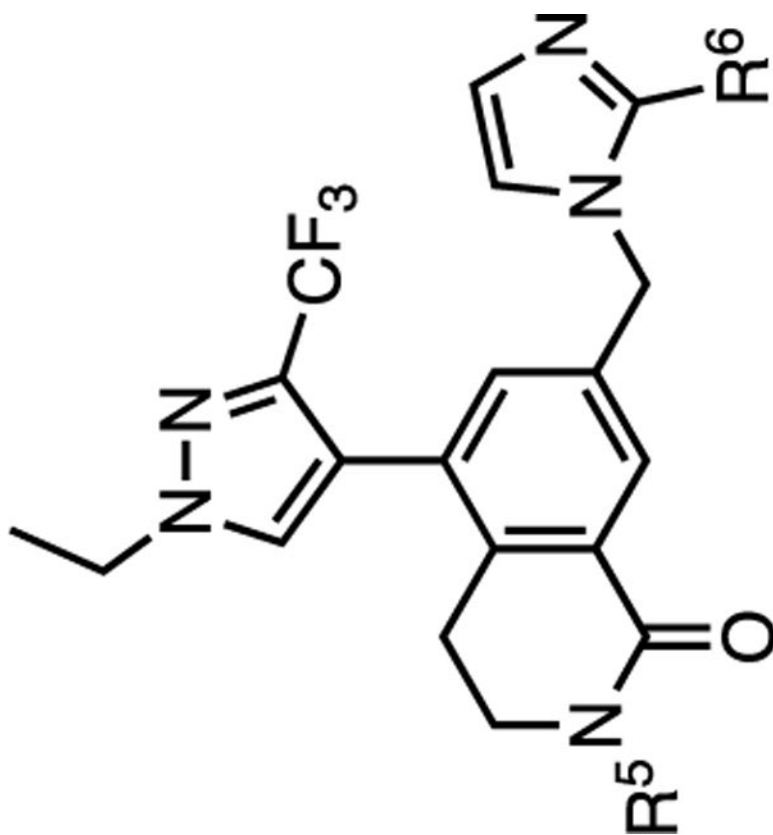
39	H	H	2.3	n.d.	0.028 ± 0.002	39 ± 7.4	100 ± 23	12000 ± 3600	310
----	---	---	-----	------	---------------	----------	----------	--------------	-----

Author Manuscript

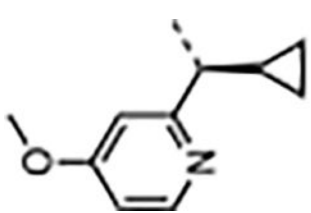
Author Manuscript

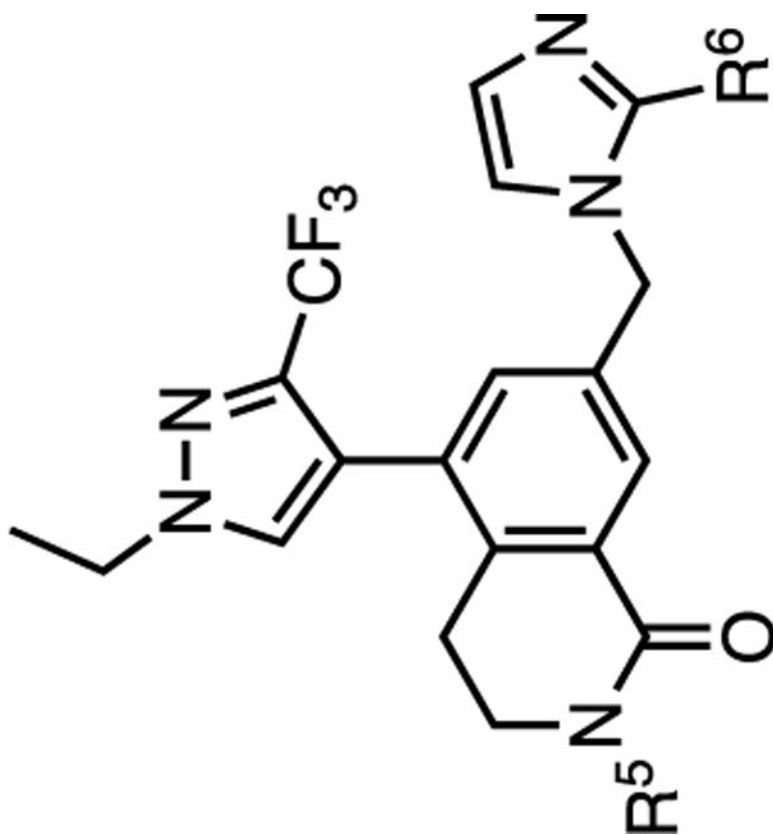
Author Manuscript

Author Manuscript



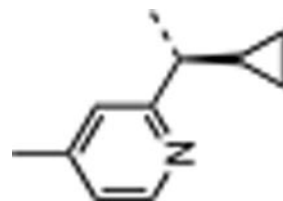
34 – 41

compnd	R ⁵ =	R ⁶ =	cLogP	Kinetic Solubility (μM)	K _i (nM) TR-FRET ^d			Cell Proliferation Assays GI ₅₀ (nM) ^a			Selectivity ^b K562/MV4:11
					WDR5	MV4:11	MOLM-13	MV4:11	MOLM-13	K562	
40		H	2.7	55	<0.02	19 ± 5.2	37 ± 8.1	1500 ± 860	79		



34 – 41

compnd	R ⁵ =	R ⁶ =	cLogP	Kinetic Solubility (μM)	K _i (nM) TR-FRET ^d		Cell Proliferation Assays GI ₅₀ (nM) ^a			Selectivity ^b K562/MV4:11
					WDR5	MV4:11	MOLM-13	K562		



41

13 ± 5.6

27 ± 4.5

3700 ± 3100

290

<0.02

60

3.3

H

q Selectivity is defined as GI₅₀,K562/GI₅₀,MV4;11 and is used to generally distinguish between on- and off-target inhibition mechanisms. Not determined = n.d.

q TR-FRET. K_i and cell proliferation GI₅₀ values represent four independent replicate determinations \pm standard deviation.

Author Manuscript

Author Manuscript

Author Manuscript

Author Manuscript

Table 5.

In Vivo PK Profile in CD-1 Mice^a

compnd	3 mg/kg iv			10 mg/kg po			F%
	CL (mL/min/kg)	AUC _{0-inf} (h·ng/mL)	V _{ss} (L/kg)	C _{max} (ng/mL)	AUC _{0-inf} (h·ng/mL)	t _{1/2} (h)	
1 ^b	78	642	16	n.c.	n.c.	n.c.	n.c.
34	118	429	3.8	279	397	1.2	28
36	41	1240	1.6	652	508	1.4	12
37	25	2075	1.1	1083	1000	1.2	15
38	76	707	2.3	2013	1712	1.2	73
40	20	2570	0.7	2767	3626	1.2	42
41	26	1951	1.6	2083	3984	1.3	61

^aPharmacokinetic parameter values represent the average of three animals.

^bThe iv PK parameter values are for one surviving animal due to the lethality of **1**. The oral exposure of **1** was below the limit of quantitation when administered orally at 3 mg/kg. Not calculated = n.c.